geodiversitas

2025 • 47 • 9

New data on archaic homodont odontocetes from the Early Miocene of Peru reveal a second species of *Chilcacetus* Lambert, Muizon & Bianucci, 2015 and a Southern Hemisphere record for a northeastern Pacific species

Olivier LAMBERT, Christian de MUIZON, Rebecca F. BENNION, Mario URBINA & Giovanni BIANUCCI

art. 47 (9) — Published on 5 June 2025
www.geodiversitas.com

PUBLICATIONS SCIENTIFIQUES

MUSÉUM NAL HIST NATURELLE

Couverture / *Cover*:
Vue dorsale du crâne de *Chilcacetus ullujayensis* n. sp. MUSM 2527.
Dorsal view of the skull of Chilcacetus ullujayensis *n. sp. MUSM 2527.*

Geodiversitas est indexé dans / Geodiversitas *is indexed in:*
– Science Citation Index Expanded (SciSearch®)
– ISI Alerting Services®
– Current Contents® / Physical, Chemical, and Earth Sciences®
– Scopus®

Geodiversitas est distribué en version électronique par / Geodiversitas *is distributed electronically by:*
– BioOne® (http://www.bioone.org)

Les articles ainsi que les nouveautés nomenclaturales publiés dans *Geodiversitas* sont référencés par /
Articles and nomenclatural novelties published in Geodiversitas *are referenced by:*
– ZooBank® (http://zoobank.org)

Geodiversitas est une revue en flux continu publiée par les Publications scientifiques du Muséum, Paris
Geodiversitas *is a fast track journal published by the Museum Science Press, Paris*

Les Publications scientifiques du Muséum publient aussi / *The Museum Science Press also publish:* ***Adansonia***, ***Zoosystema***, ***Anthropozoologica***, ***European Journal of Taxonomy***, ***Naturae***, ***Cryptogamie*** **sous-sections** ***Algologie***, ***Bryologie***, ***Mycologie, Comptes Rendus Palevol***

Diffusion – Publications scientifiques Muséum national d'Histoire naturelle
CP 41 – 57 rue Cuvier F-75231 Paris cedex 05 (France)
Tél. : 33 (0)1 40 79 48 05 / Fax : 33 (0)1 40 79 38 40
diff.pub@mnhn.fr / http://sciencepress.mnhn.fr

ISSN (imprimé / *print*) : 1280-9659/ ISSN (électronique / *electronic*) : 1638-9395

New data on archaic homodont odontocetes from the Early Miocene of Peru reveal a second species of *Chilcacetus* Lambert, Muizon & Bianucci, 2015 and a Southern Hemisphere record for a northeastern Pacific species

Olivier LAMBERT
D.O. Terre et Histoire de la Vie, Institut royal des Sciences naturelles de Belgique,
29 rue Vautier, B-1000 Brussels (Belgium)
olambert@naturalsciences.be (corresponding author)

Christian de MUIZON
Centre de recherche en paléontologie — Paris (CR2P), CNRS, MNHN, Sorbonne Université,
Département Origines et Évolution, Muséum national d'Histoire naturelle, case postale 38,
57 rue Cuvier, F-75231 Paris cedex 05 (France)
muizon@mnhn.fr

Rebecca F. BENNION
D.O. Terre et Histoire de la Vie, Institut royal des Sciences naturelles de Belgique,
29 rue Vautier, B-1000 Brussels (Belgium)
and Evolution & Diversity Dynamics Lab, UR Geology, Université de Liège,
14 Allée du 6 Août, B-4000 Liège (Belgium)
and Museum of North Craven Life, The Folly, Victoria Street, BD24 9EY Settle (United Kingdom)
rbennionpalaeo@gmail.com

Mario URBINA
Departamento de Paleontología de Vertebrados, Museo de Historia Natural-Universidad
Nacional Mayor de San Marcos, Avenida Arenales 1256, P-15072 Lima (Peru)
mariourbina01@hotmail.com

Giovanni BIANUCCI
Dipartimento di Scienze della Terra, Università di Pisa, via S. Maria 53, I-56126 Pisa (Italy)
giovanni.bianucci@unipi.it

Submitted on 22 April 2024 | accepted on 21 October 2024 | published on 5 June 2025

urn:lsid:zoobank.org:pub:35F944F3-E250-4840-8A70-18E704567FF7

Lambert O., Muizon C. de, Bennion R. F., Urbina M. & Bianucci G. 2025. — New data on archaic homodont odontocetes from the Early Miocene of Peru reveal a second species of *Chilcacetus* Lambert, Muizon & Bianucci, 2015 and a Southern Hemisphere record for a northeastern Pacific species. *Geodiversitas* 47 (9): 369-408. https://doi.org/10.5252/geodiversitas2025v47a9. http://geodiversitas.com/47/9

ABSTRACT
The systematic affinities of several homodont odontocetes (toothed whales) in the genera *Argyrocetus* Lydekker, 1893 and *Macrodelphinus* Wilson, 1935 from the Early Miocene of the northeastern Pacific and southwestern Atlantic have long been debated. The description of the longirostrine dolphin *Chilcacetus cavirhinus* Lambert, Muizon & Bianucci, 2015, based on two finely preserved skulls from the Early Miocene of Peru, revealed similarities with part of these taxa, but questions remained about their phylogenetic relationships. Two new specimens from the Burdigalian of the Chilcatay Formation

(East Pisco Basin, Peru) and recently rediscovered skull parts for the holotype of *C. cavirhinus* lead to the diagnosis of a new species of *Chilcacetus* Lambert, de Muizon & Bianucci, 2015, *Chilcacetus ullujayensis* n. sp., and the description of cranial regions previously unknown (or poorly known) for that genus, especially the ear bones. Another smaller skull from the Chilcatay Formation is referred here to *Amphidelphis bakersfieldensis* n. comb., a species previously only known from California whose palaeogeographic distribution is thus expanded across the equator. Rostral morphological features in the new specimen of *A. bakersfieldensis* n. comb. differ markedly from *Argyrocetus patagonicus* Lydekker, 1893, the Patagonian species that was earlier recognized as closely related to *A. bakersfieldensis* n. comb., and from Eurhinodelphinidae Abel, 1901, the family long proposed to have housed these two species. Finally, two other specimens from the Chilcatay Formation are identified as Odontoceti aff. *A. bakersfieldensis*. New phylogenetic analyses recover *Chilcacetus* spp. and *A. bakersfieldensis* n. comb. in a clade of longirostrine to hyper-longirostrine stem odontocetes, also including *Eoplatanista* Dal Piaz, 1916, *Macrodelphinus*, and eurhinodelphinids. The new records of *A. bakersfieldensis* n. comb. and *Chilcacetus* spp. presented here confirm the predominance of long-snouted species in the Burdigalian odontocete assemblages of the East Pisco Basin.

KEY WORDS
Miocene,
Burdigalian,
Chilcatay Formation,
Odontoceti,
Chilcacetus,
Argyrocetus,
East Pisco Basin,
phylogeny,
new combination,
new genus,
new species.

RÉSUMÉ
De nouvelles données sur les odontocètes archaïques homodontes du Miocène inférieur du Pérou révèlent une seconde espèce de Chilcacetus *Lambert, Muizon & Bianucci, 2015 et la présence dans l'hémisphère sud d'une espèce du Pacifique nord-est.*
Les affinités systématiques de plusieurs odontocètes homodontes (cétacés à dents) des genres *Argyrocetus* Lydekker, 1893 et *Macrodelphinus* Wilson, 1935, du Miocène inférieur du Pacifique nord-est et de l'Atlantique sud-ouest, ont longtemps été débattues. La description du dauphin longirostre *Chilcacetus cavirhinus* Lambert, Muizon & Bianucci, 2015, basée sur deux crânes bien préservés du Miocène inférieur du Pérou, a révélé des similitudes avec une partie de ces taxons, mais des questions subsistaient sur leurs relations phylogénétiques. Deux nouveaux spécimens du Burdigalien de la Formation Chilcatay (Bassin de Pisco, Pérou) et des parties de crâne récemment redécouvertes pour l'holotype de *C. cavirhinus* conduisent à la définition d'une nouvelle espèce de *Chilcacetus* Lambert, Muizon & Bianucci, 2015, *Chilcacetus ullujayensis* n. sp., et à la description de régions crâniennes jusqu'alors inconnues (ou mal connues) pour ce genre, en particulier les os de l'oreille. Un autre crâne plus petit de la Formation Chilcatay est rapporté ici à *Amphidelphis bakersfieldensis* n. comb., une espèce auparavant uniquement connue de Californie, dont la répartition paléogéographique s'étend ainsi au-delà de l'équateur. Les caractéristiques morphologiques du rostre du nouveau spécimen d'*A. bakersfieldensis* n. comb. diffèrent nettement de celles d'*Argyrocetus patagonicus* Lydekker, 1893, l'espèce patagonienne précédemment reconnue comme étroitement apparentée à *A. bakersfieldensis* n. comb., mais aussi de celles des Eurhinodelphinidae Abel, 1901, la famille longtemps proposée comme contenant ces deux espèces. Enfin, deux autres spécimens de la Formation Chilcatay sont identifiés en tant qu'Odontoceti aff. *A. bakersfieldensis*. De nouvelles analyses phylogénétiques placent *Chilcacetus* spp. et *A. bakersfieldensis* n. comb. dans un clade d'odontocètes longirostres à hyper-longirostres du groupe-souche, comprenant également *Eoplatanista* Dal Piaz, 1916, 1919, *Macrodelphinus*, et les eurhinodelphinidés. Les nouveaux signalements d'*A. bakersfieldensis* n. comb. et *Chilcacetus* spp. présentés ici confirment la prédominance des espèces à long museau dans les assemblages d'odontocètes burdigaliens du Bassin de Pisco.

MOTS CLÉS
Miocène,
Burdigalien,
Formation Chilcatay,
Odontoceti,
Chilcacetus,
Argyrocetus,
est du bassin de Pisco,
phylogénie,
combinaison nouvelle,
genre nouveau,
espèce nouvelle.

INTRODUCTION

During the last decade, palaeontological research in several fossil-bearing localities of the East Pisco Basin, on the southern coast of Peru, has yielded a rich odontocete (echolocating toothed whales) assemblage from Lower Miocene (Burdigalian) layers of the Chilcatay Formation; the main clades recorded are Eurhinodelphinidae Abel, 1901, Inticetidae Lambert, Muizon, Malinverno, Di Celma, Urbina & Bianucci, 2017, Kentriodontidae Slijper, 1936, Physeteroidea Gray, 1821, Platanistidae Gray, 1846, Squalodelphinidae Dal Piaz, 1917, and other Platanidelphidi Bianucci, Muizon, Urbina & Lambert, 2020 (Bianucci *et al.* 2018, 2020; Di Celma *et al.* 2019; Lambert *et al.* 2021; and references therein). Within this assemblage are two specimens of the longirostrine and homodont dolphin *Chilcacetus cavirhinus* Lambert, Muizon & Bianucci, 2015, which was tentatively placed in an unnamed clade of Early Miocene odontocetes, also including the southwestern Atlantic species *Argyrocetus patagonicus* Lydekker, 1893 and the northeastern Pacific '*Argyrocetus*' *bakersfieldensis* (Wilson, 1935), '*Argyrocetus*' *joaquinensis* Kellogg, 1932, and *Macrodelphinus kelloggi* Wilson, 1935 (Lambert *et al.* 2015). In this work, the content of the genus *Argyrocetus* Lydekker, 1893 was questioned, due to the fragmentary state of the

type material for the three referred species and the lack of synapomorphies, as also discussed in Lambert (2005a). In a subsequent phylogenetic analysis with a different character-taxon matrix, a clade including '*A.*' *bakersfieldensis*, *C. cavirhinus*, and *M. kelloggi* was also recovered, but with similarly low support values (Lambert *et al.* 2019). In the original description of *C. cavirhinus*, a number of anatomical differences were noted between the holotype and the referred specimen, leading to the statement that additional specimens were needed to test the attribution of these two skulls to the same species. Furthermore, the ear bones originally associated to the holotype cranium are lost and their initial description was based on preliminary drawings (Lambert *et al.* 2015). To reassess the content and diagnosis of the species *C. cavirhinus* and to further investigate its relationship, we studied a series of unpublished and newly collected odontocete specimens from the Chilcatay Formation, curated at the MUSM. In addition, undescribed parts of the holotype of *C. cavirhinus* recently rediscovered and prepared at the MNHN were added to the sample. Our comparison of this fossil material led to the definition of a new species in the genus *Chilcacetus* Lambert, Muizon & Bianucci, 2015, for which ear bones were described. We also identified for the first time the Californian species '*Argyrocetus*' *bakersfieldensis* in the Chilcatay Formation. New anatomical data on this species bring support for its referral to a new genus. Finally, the phylogenetic relationships of the studied taxa were investigated through a cladistic analysis.

MATERIAL AND METHODS

Institutional abbreviations

IRSNB	Institut royal des Sciences naturelles de Belgique, Brussels;
MGP	Museo di Geologia e Paleontologia dell'Università di Padova, Padova;
MLP	Museo de La Plata, La Plata;
MNHN	Muséum national d'Histoire naturelle, Paris;
MUSM	Museo de Historia Natural, Universidad Nacional Mayor de San Marco, Lima;
OU	Geology Museum, University of Otago, Dunedin;
YPM	Peabody Museum, Yale University, New Haven.

Anatomical terminology

We primarily follow Mead & Fordyce (2009) for the terminology of cranial parts and Evans & de Lahunta (2013) for postcranial bones.

Studied fossil material

The new specimens (or parts of them) described for the first time in this work all originate from the Chilcatay Formation, East Pisco Basin, southern coast of Peru (Fig. 1):

1) *Chilcacetus cavirhinus* MNHN.F.PRU11 (holotype): anterior portion of the rostrum and mandibles, rediscovered in the MNHN collection and recently prepared;

2) two new specimens of *Chilcacetus*, MUSM 4692 (cranium with a few teeth, associated partial right and left mandibles, atlas, and two sternum elements) and MUSM 2527 (cranium with two in situ periotics, detached left malleus, left tympanic bulla, several teeth, posterior part of mandibles, left humerus, three thoracic vertebrae, and rib fragments), from the localities of Ullujaya and Zamaca, respectively;

3) three new small odontocete partial crania, MUSM 602, MUSM 4961, and MUSM 4691, from the localities of Zamaca (MUSM 602) and Roca Negra (the two others).

Surface scanning

Textured 3D models of the skulls of MUSM 602, 2527, 4691, and 4692 were obtained using an Artec Eva structured-light scanner, and an untextured model of MUSM 1401 was obtained using a Creaform Go!Scan 20 (see Appendices 1-5).

Phylogenetic analyses

To investigate the phylogenetic relationships of the studied taxa, we modified the character-taxon matrix of Lambert *et al.* (2019), originating from the matrix of Geisler & Sanders (2003), in the following ways (Appendices 6; 7).

One character (199) was modified, with one derived state now divided into two:

199. Tubercule of the malleus. Unreduced (0); moderately reduced, making less than half the height of the malleus (1); highly reduced, almost indistinguishable from articular head (2).

Two new characters were added:

325. Edentulous premaxillary portion of rostrum: absent or very short (0); extended, making at least 20 % of rostrum length (1). In some specimens, the maxilla-premaxilla suture cannot be distinguished anteriorly, but the anteriormost alveoli are used as a proxy for the end of the maxilla.

326. Length of mandible: Roughly as long or slightly longer than rostrum (0); markedly shorter (1).

Four taxa were added: *Chilcacetus ullujayensis* n. sp., based on direct observations of MUSM 1401 and 2527 (holotype); *Eurhinodelphis cocheteuxi* du Bus, 1867, based on direct observations of IRSNB M.294 (holotype), M.295, M.299, and M.1856 (see also the 3D model for holotype cranium IRSNB M.294 using the link here); *Schizodelphis morckhoviensis* (du Bus, 1872), based on direct observations of IRSNB M.343, M.1859, USNM V 21291, 167676, and 187306; *Eoplatanista* spp., based on direct observations of *Eoplatanista italica* Dal Piaz, 1916 MGP 26150-3 (holotype), 26408, and 26411, and *Eoplatanista gresalensis* Dal Piaz, 1916 MGP 26169-71 (holotype), 26154, 26166, 26409, 26413, and 26435, complemented by photos and measurements from Pilleri (1985).

Several scores were added and modified for: *Chilcacetus cavirhinus*, based on direct observations of MNHN.F.PRU11 (holotype) and newly referred specimen MUSM 4692, as well as the removal of MUSM 1401 from that species; *Amphidelphis bakersfieldensis* n. comb., based on a cast of the facial region of the holotype YPM 13404 held at the IRSNB, new photos of this specimen taken by Advait Jukar, and direct observations of the newly referred specimen MUSM 4691; and *Xiphiacetus cristatus* (du Bus, 1872), based on direct observations of specimens IRSNB M.3234 (holotype) and 3241. The resulting matrix includes 114 taxa scored for 326 characters (Appendix 7).

As in past analyses with an earlier version of this matrix, the high volatility in preliminary tests of several taxa (*Auroracetus bakerae* Gibson & Geisler, 2009, *Brachydelphis jahuayensis* Lambert & Muizon, 2013, *Ischyrorhynchus vanbenedeni* Ameghino, 1891, *Lophocetus calvertensis* Harlan, 1842, *Meherrinia isoni* Geisler, Godfrey & Lambert, 2012, *Pithanodelphis cornutus* (du Bus, 1872), *Protophocaena minima* Abel, 1905, *Rudicetus squalodontoides* (Capellini, 1878), and *Stenasodelphis russellae* Godfrey & Barnes, 2008) only distantly related to the group of interest led us to remove these more fragmentarily known species, most of them lacking ear bones, from subsequent analyses. The parsimony analyses were performed with PAUP version 4.0 (Swofford 2003). *Bos taurus* Linnaeus, 1758, *Hippopotamus amphibius* Linnaeus, 1758, and *Sus scrofa* Linnaeus, 1758 were selected as outgroups. A constraint tree from Bayesian analysis of molecular data (McGowen *et al.* 2009, 2011; Geisler *et al.* 2011; Appendix 8) was used as a backbone to force relationships among extant cetaceans. All ordered multistate characters were scaled in a way that minimum length for each is 1 step, as for binary characters. The heuristic searches were performed with simple taxon addition, a tree-bisection-reconnection algorithm, and ACCTRAN optimization. Several heuristic searches were undertaken under equal and implied weights, using for the latter different values for K (3, 6, 9, and 12). Bootstrap and Jackknife analyses using 100 replicates were ran with the same settings as the ones yielding our preferred tree.

SYSTEMATIC PALAEONTOLOGY

Order CETACEA Brisson, 1762
Clade PELAGICETI Uhen, 2008
Clade NEOCETI Fordyce & Muizon, 2001
Suborder ODONTOCETI Flower, 1867
Family incertae sedis

Genus *Chilcacetus* Lambert, Muizon & Bianucci, 2015

TYPE SPECIES. — *Chilcacetus cavirhinus* Lambert, Muizon & Bianucci, 2015 by original designation.

OTHER REFERRED SPECIES. — *Chilcacetus ullujayensis* n. sp.

EMENDED DIAGNOSIS. — The differential diagnosis focuses primarily on differences with taxa that were found to be closely related to *Chilcacetus* in our phylogenetic analysis and comparison (other members of the *Chilcacetus* clade, Eoplatanistidae Muizon, 1988, Eurhinodelphinidae, and Squaloziphiidae (Muizon, 1991)). *Chilcacetus* is a medium-size (bizygomatic width ranging from about 240 to 280 mm), longirostrine (ratio between rostrum length and condylobasal length from 0.68 to 0.73), and homodont dolphin genus differing from all other odontocetes except *Eoplatanista* Dal Piaz, 1916, Eurhinodelphinidae, Physeteroidea, *Yaquinacetus* Lambert, Godfrey & Fitzgerald, 2019, and Ziphiidae Gray, 1850 in the tubercule of the malleus being shorter than the articular head; from all other odontocetes except '*Argyrocetus*' *joaquinensis*, *Ninoziphius* Muizon, 1983, *Olympicetus* Vélez-Juarbe, 2017, *Simocetus* Fordyce, 2002, *Squaloziphius* Muizon, 1991, and *Ziphiodelphis abeli* Dal Piaz, 1908 in having a finger-like posterior projection of the hamular process of the pterygoid; from all other odontocetes except *Amphidelphis bakersfieldensis* n. comb., '*Argyrocetus*' *joaquinensis*, *Crisocetus* Gaetán, Paolucci & Buono, 2023, *Dolgopolis* Viglino, Gaetán, Cuitiño & Buono, 2021, *Eoplatanista*, Eurhinodelphinidae, *Perditicetus* Nelson & Uhen, 2020, *Squaloziphius* and *Yaquinacetus* in the postglenoid process of the squamosal being anteroposteriorly long and transversely thick (this process being even anteroposteriorly longer in *Crisocetus*, *Dolgopolis*, *Squaloziphius*, and *Yaquinacetus*); from *Dolgopolis*, *Squaloziphius* and *Yaquinacetus* in the dorsal opening of the mesorostral groove being more gradual anterior to the bony nares; from most members of other longirostrine to hyper-longirostrine homodont extinct families (Allodelphinidae, Eoplatanistidae, Eurhinodelphinidae, and Platanistidae) in the absence of a deep lateral groove along the rostrum, the posterior process of the periotic being elongated in a posterolateral direction and transversely broad, and in the absence of ankylosis for the symphysis of the mandibles.
It further differs from Eurhinodelphinidae in lacking an extended edentulous anterior premaxillary portion of the rostrum, in the mandible being roughly as long as the rostrum, in the nasals partly overhanging the bony nares, in the more anteriorly elongated zygomatic process of the squamosal (ratio between the length and the height of the process ≥ 1.10), in the neurocranium being distinctly longer than wide, in the lesser transverse widening of the occipital shield (ratio between maximum width of supraoccipital at the lateral corners of the nuchal crest and postorbital width < 0.70), in the posterior margin of the postorbital process being vertical, in the top of the temporal fossa being nearly as high as the nuchal crest, in the palatines being separated anteromedially for a long distance at rostrum base, and in the longer and more laterally directed posterior process of the periotic.
It differs from Eoplatanistidae in the premaxillary foramen being roughly at the level of the antorbital notch, in the thinner and flatter antorbital process, in the acute anterior margin of the nasal partly overhanging the bony nares, in the transversely concave and less anteriorly projected anterodorsal portion of the supraoccipital shield, in the deep anterior bullar facet of the periotic, and in bearing a conspicuous median furrow on the tympanic bulla.
It differs from *Argyrocetus patagonicus* in the premaxillae being transversely wider at rostrum base, in lacking a wide dorsal opening of the mesorostral groove, in the premaxillary foramen being roughly at the level of the antorbital notch, in the angle formed by the basioccipital crests in ventral view < 50°, in the top of the temporal fossa being nearly as high as the nuchal crest, and in the absence of ankylosis for the symphysis of the mandibles. It differs from *Amphidelphis bakersfieldensis* n. comb. in its larger size, in lacking a deep sulcus anterior to the main dorsal infraorbital foramen at rostrum base, and in the palatines being separated anteromedially for a long distance at rostrum base. It differs from '*Argyrocetus*' *joaquinensis* in the dorsal opening of the mesorostral groove anterior to the rostrum base being narrower than the premaxilla, in the presence of more than one dorsal infraorbital foramen at rostrum base, in lacking a deep sulcus anterior to the main dorsal infraorbital foramen at rostrum base, in the proportionally shorter and wider nasal, in the nasal partly overhanging the bony nares, in the wide exposure of the frontal on the vertex, in the posterior margin of the postorbital process being vertical, in the palatines being separated anteromedially for a longer distance at rostrum base, and in the ventral margin of the postglenoid process of the squamosal being approximately at the same level as the ventral margin of the exoccipital in lateral view. It differs from *Caolodelphis* Godfrey & Lambert, 2023 in its larger size, the frontals not being separated anteromedially on the vertex, and the basioccipital crests being transversely thinner. It differs from *Macrodelphinus* in its smaller size, in the premaxillary portion of the rostrum making less than 10 % of its total length, in the premaxillary foramen being roughly at the level of the antorbital notch, in the nasal proportionally longer compared to the frontal on the vertex, in the palatines being separated anteromedially for a longer distance at rostrum base. It differs from *Perditicetus* in in the premaxillary foramen being roughly at the level of the antorbital notch

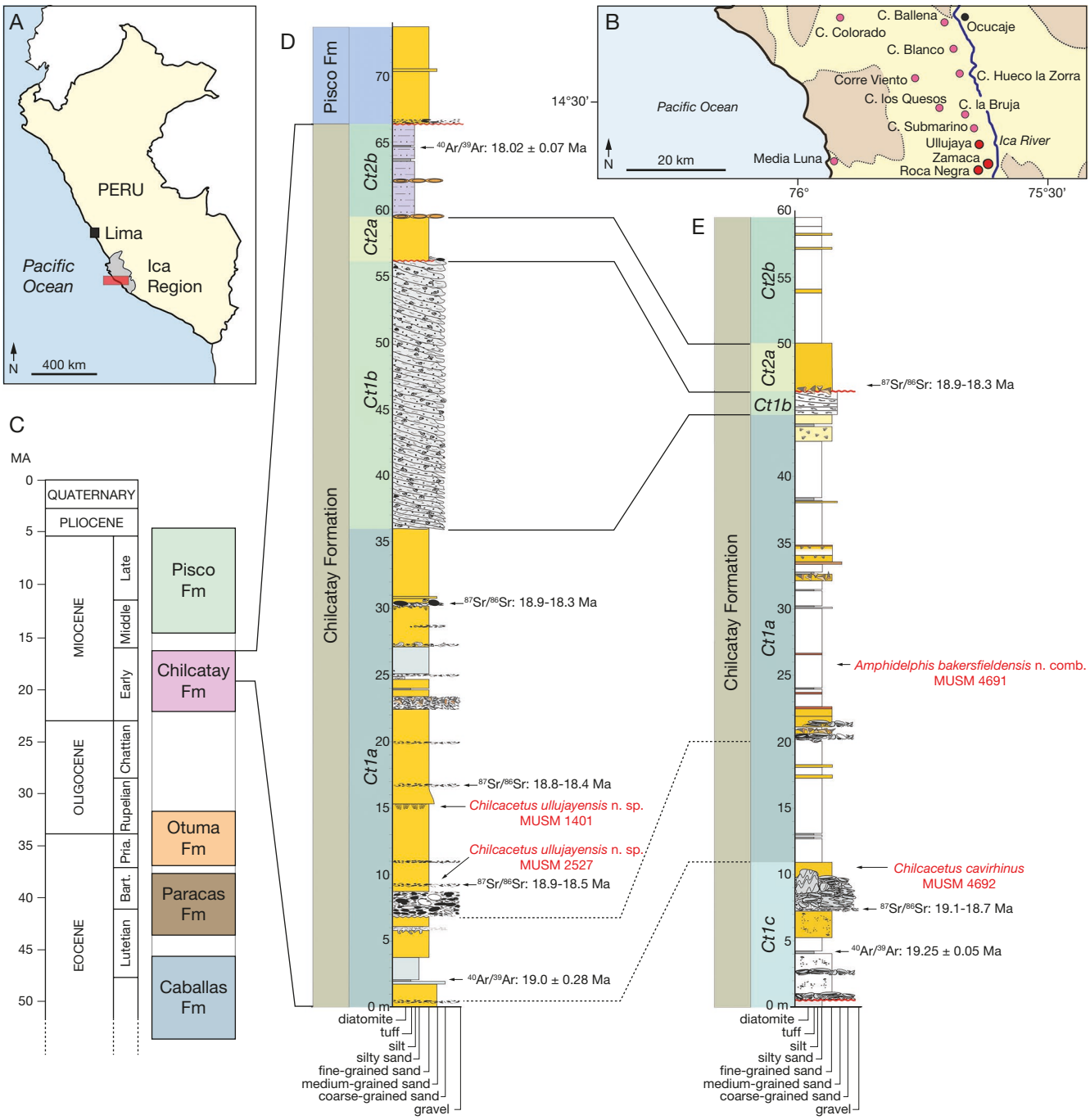

FIG. 1. — Geographic and geological setting: **A**, location of the main outcrops of the Chilcatay Formation along the southern coast of Peru; **B**, simplified map providing the position of Ullujaya (the type locality of *Chilcacetus ullujayensis* n. sp.), Roca Negra, and Zamaca (the localities of several other odontocetes described here) alongside other highly fossiliferous sites of the Ica desert; **C**, schematic stratigraphic column of the Cenozoic succession exposed in the East Pisco Basin; **D**, simplified stratigraphic section of the Chilcatay Formation in Ullujaya, showing the exact position of the two specimens of *Chilcacetus ullujayensis* n. sp. in the Ct1 allomember, *Ct1a* facies association; **E**, simplified stratigraphic section of the Chilcatay Formation in Roca Negra and Zamaca, showing the exact position of *Chilcacetus cavirhinus* Lambert, Muizon & Bianucci, 2015 MUSM 4692 in the Ct1 allomember, *Ct1c* facies association, and of *Amphidelphis bakersfieldensis* n. comb. MUSM 4691 in the Ct1 allomember, *Ct1a* facies association. Both sections **D** and **E** include positions of ash layers dated with $^{40}Ar/^{39}Ar$ and shell-rich beds dated with $^{87}Sr/^{86}Sr$ along with the corresponding age estimates (after Bosio *et al.* 2020a, b, 2022). Maps and sections modified from Bianucci *et al.* (2018), Di Celma *et al.* (2018, 2019), Bosio *et al.* (2020b, 2022), and Lambert *et al.* (2023).

and the zygomatic process of the squamosal being dorsoventrally more slender. It differs from *Papahu* Aguirre-Fernández & Fordyce, 2014 in the rostrum being proportionally dorsoventrally thicker in its proximal part, in the single premaxillary foramen being roughly at the level of the antorbital notch, in the dorsal exposure of the premaxilla being wider than the dorsal exposure of the maxilla at rostrum base, in the proportionally wider ascending process of the premaxilla, in the anterodorsal elevation of the dorsal surface of the nasal, in the posterolateral projection of the nasal, in the elongate postorbital process of the frontal, in the longer and deeper anterior bulla facet of the periotic, and in the posterior elevation of the dorsal margin of the mandible being progressive.

Chilcacetus cavirhinus
Lambert, Muizon & Bianucci, 2015
(Figs 2-4)

Chilcacetus cavirhinus Lambert, Muizon & Bianucci, 2015: 81.

TYPE MATERIAL. — **Holotype. Peru** • 1 specimen (nearly complete cranium with the associated mandibles and the manubrium; the anterior portion of the rostrum and of the right mandible, and the left mandible were re-discovered in the MNHN collection after the initial publication of this specimen); East Pisco Basin; 14°34'40"S, 75°38'40"W; Chilcatay Formation; Burdigalian (late Early Miocene); MNHN.F.PRU11.

TYPE LOCALITY. — Precise locality unknown, but close to Ullujaya, East Pisco Basin, Peru. Approximate geographic coordinates: 14°34'40"S, 75°38'40"W (Fig. 1A, B).

TYPE HORIZON AND AGE. — In Ullujaya, cetacean fossil remains only occur, abundantly, in the widely exposed Lower Miocene Chilcatay Formation. More specifically, all cetaceans originate from the *Ct1a* facies association, a sub-horizontal 36 m package of interbedded sandstones, sandy siltstones, and siltstones punctuated by conglomerate levels (Bianucci *et al.* 2018; Di Celma *et al.* 2018). The age of the entire Chilcatay Formation exposed at Ullujaya can be restricted between 19.28 and 17.95 Ma (Burdigalian) based on radiometric dating of two volcanic ash layers positioned respectively 1.6 m below the contact between the Chilcatay and overlying Pisco Formation ($^{40}Ar/^{39}Ar$: 18.02 ± 0.07 Ma) and 2 m above the base of the exposed section ($^{40}Ar/^{39}Ar$: 19.0 ± 0.28 Ma) (Di Celma *et al.* 2018; Bosio *et al.* 2020b) (Fig. 1D). This age is consistent with the $^{87}Sr/^{86}Sr$ stratigraphy and silicoflagellate and diatom biostratigraphy (Di Celma *et al.* 2018; Bosio *et al.* 2020a, 2022).

REFERRED SPECIMEN. — MUSM 4692, nearly complete cranium including a few teeth in situ with the associated partial right and left mandibles, the atlas, and two sternum elements. This specimen was reported in the geological map of Zamaca provided by Di Celma *et al.* (2019) with the field number ZM 12 and referred to *Chilcacetus cavirhinus*. Geographic coordinates: 14°38'20.2"S, 75°38'26.1"W. Zamaca is a locality a few kilometers south of Ullujaya where the same Burdigalian Chilcatay Formation is extensively exposed (Fig. 1B). In detail, the MUSM 4692 skeleton was collected 10.7 m above the contact with the underlying Otuma Formation, near the top of the of the *Ct1c* facies association (sandstones and conglomerate beds) of the Ct1 allomember (Fig. 1E). The age of *Ct1c* is well defined by two dates: 1) a 19.25 ± 0.05 Ma $^{40}Ar/^{39}Ar$ radiometric dating of a volcanic ash layers near the base of *Ct1c* (Di Celma *et al.* 2018); and 2) a 19.1-18.7 Ma $^{87}Sr/^{86}Sr$ dating obtained with the Strontium Isotope Stratigraphy analyzing oyster shells collected a few meters below the MUSM 4692 skeleton (Bosio *et al.* 2020a, 2022). Therefore, the age of MUSM 4692 is roughly 19 Ma (lower Burdigalian).

EMENDED DIAGNOSIS. — *Chilcacetus cavirhinus* differs from *Chilcacetus ullujayensis* n. sp. in its slightly smaller size (bizygomatic width < 260 mm); the rostrum being proportionally shorter (ratio between rostrum length and condylobasal length ≤ 0.7 and ratio between preorbital width and rostrum length > 0.4); 34 maxillary teeth per side; the mesorostral groove being dorsally open for a shorter distance (dorsomedial contact between premaxillae > 190 mm long); the vertex of the cranium being proportionally anteroposteriorly longer and narrower; the occipital shield being transversely broader (minimum posterior distance between temporal fossae clearly higher than width of premaxillae in facial region); the long axis of the zygomatic process of the squamosal being closer to the horizontal plane; and the higher number of alveoli (10) in the post-symphyseal region of the mandible.

COMMENTS
The specimen MUSM 1401 was originally referred to *Chilcacetus cavirhinus*, but several differences with the holotype were already noted (Lambert *et al.* 2015). With the addition of two new *Chilcacetus* specimens in the sample, some of these differences were observed between two subsets of specimens, leading to the proposal that two species of *Chilcacetus* are recorded in the Chilcatay Formation. Interestingly, the two specimens referred to *Chilcacetus ullujayensis* n. sp. originate from close levels of the Ct1 allomember of the Chilcatay Formation, both in the facies association *Ct1a*, while *C. cavirhinus* MUSM 4692 was collected in a lower level, from facies association *Ct1c* (Fig. 1). The latter can thus be considered geologically older. These considerations support the hypothesis that the two *Chilcacetus* species were not sympatric, with *C. cavirhinus* preceding *C. ullujayensis* n. sp. Such scenario would require that the holotype of *C. cavirhinus*, whose exact locality and stratigraphic provenance are unknown, also came from the oldest layers of the Chilcatay Formation exposed in the Ullujaya-Zamaca area.

BRIEF DESCRIPTION
This description focuses on the skull parts of the holotype MNHN.F.PRU11 recently re-discovered at the MNHN, as well as on some diagnostic regions of the newly referred specimen MUSM 4692.

Ontogenetic stage
Both MNHN.F.PRU11 and MUSM 4692 have robust cranial and mandibular bones, and neither display detached cranial elements or broadly open cranial sutures. Altogether, these observations point to subadult to adult individuals.

Cranium
The addition of the anterior part of the rostrum to the cranium of the holotype (MNHN.F.PRU11; Fig. 2) allows for the measurement of the condylobasal length (cbl) and rostrum length (rl) (Table 1). With a rl/cbl ratio of 0.7, corresponding to a longirostrine condition (see McCurry & Pyenson 2019; Lambert & Goolaerts 2022), the holotype has a rostrum proportionally slightly shorter than in *Chilcacetus ullujayensis* n. sp. MUSM 2527 (0.73) and MUSM 1401 (0.72). With a ratio estimated to 0.68, MUSM 4692 (Fig. 3) has a similarly shorter rostrum, as confirmed by the ratio between postorbital width and rl (0.48 and 0.49 for the holotype and MUSM 4692, respectively), which is greater than in MUSM 2527 (0.42). On the complete rostrum of the holotype, 41 alveoli are counted on the left side, a number that falls in the estimated range of *C. ullujayensis* n. sp. The premaxilla-maxilla suture is visible on both lateral surfaces of the holotype's rostrum, reaching the lateral margin of the alveolar groove at 65 mm from the tip of the rostrum. The premaxillary part thus makes 12.5 % of the rostrum length, a ratio that is close to that of MUSM 1401 (see Lambert *et al.* 2015). Seven well-defined alveoli are counted on each side of this premaxillary portion.

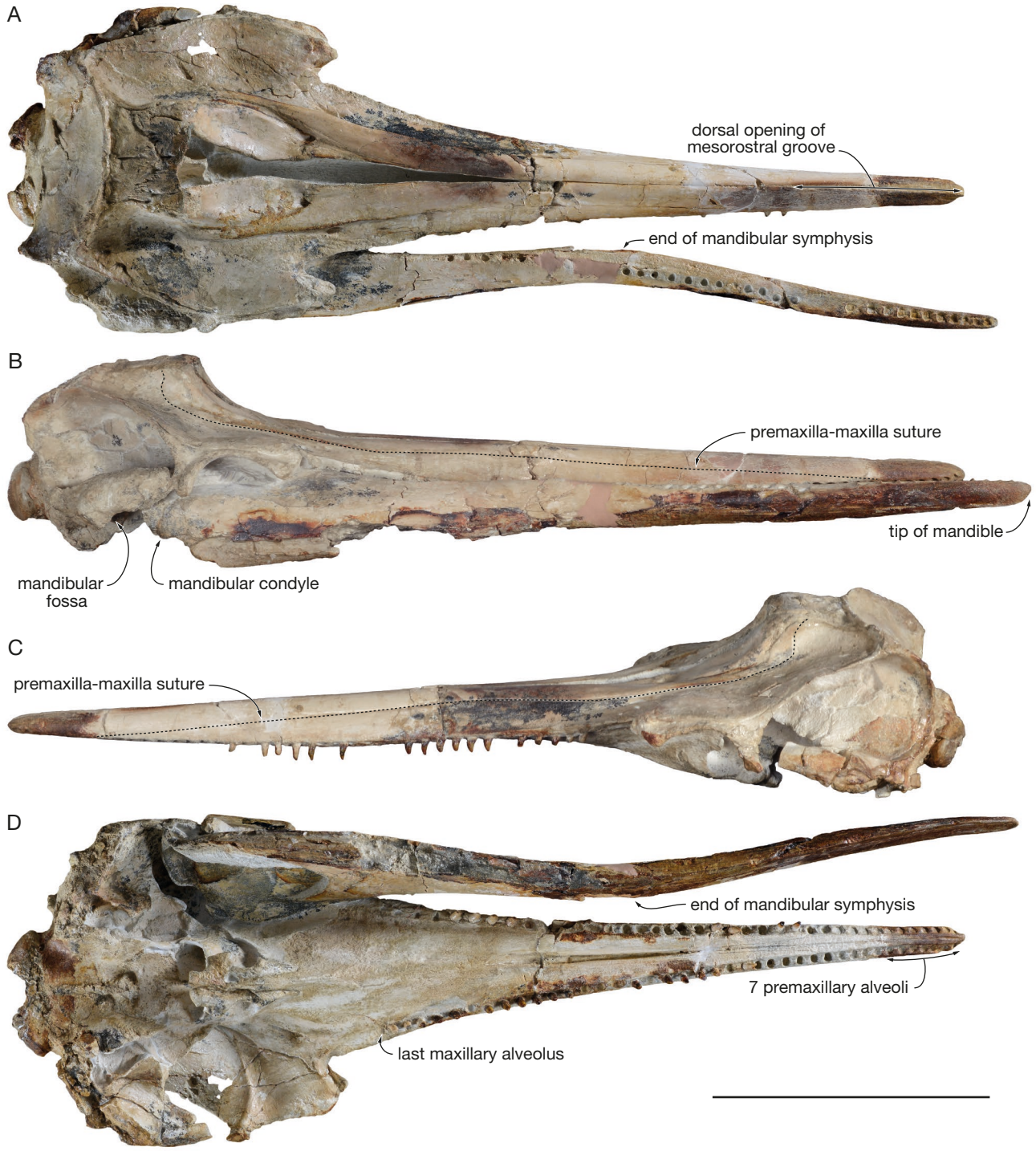

Fig. 2. — Cranium and right mandible of *Chilcacetus cavirhinus* Lambert, Muizon & Bianucci, 2015 MNHN.F.PRU11 (holotype, Chilcatay Formation, East Pisco Basin, Peru) in dorsal (**A**), right lateral (**B**), left lateral (**C**), and ventral (**D**) view. The mandible is shifted slightly anteriorly relative to the mandibular fossa on the cranium, which gives the wrong impression of some degree of underbite. Scale bar: 200 mm. Photos by Philippe Loubry and Lilian Cazes.

In both the holotype and MUSM 4692, the mesorostral groove is dorsally open on a shorter distance in the anterior part of the rostrum (Figs 2; 3; Appendix 1) when compared to specimens of *C. ullujayensis* n. sp. Previously observed in the holotype, the relatively long region of contact between the two premaxillae above the mesorostral groove is confirmed in MUSM 4692 (at least 200 mm). As for the holotype, the bony nares of MUSM 4692 are narrower than in *C. ullujayensis* n. sp. MUSM 2527 and MUSM 1401. The posterior apex of each premaxilla reaches farther along the nasal in MUSM 4692 compared to MUSM 1401, but no clear difference is noted with MUSM 2527. Due to the incompleteness of the anterior part of the nasals and the complex topology of the nasal-frontal sutures (see below), proportions of the vertex

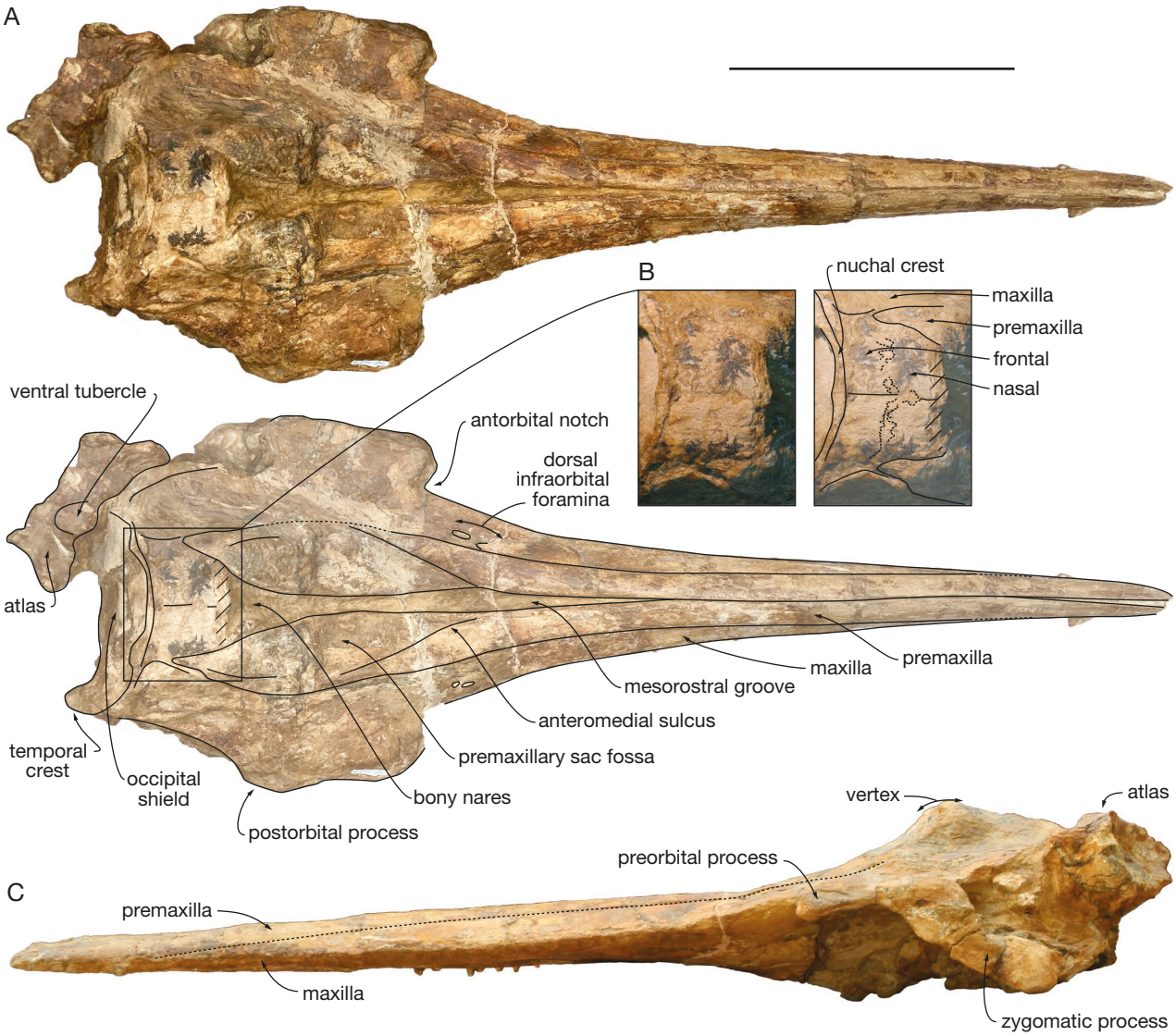

FIG. 3. — Cranium and atlas of *Chilcacetus cavirhinus* Lambert, Muizon & Bianucci, 2015 MUSM 4692 (Chilcatay Formation, East Pisco Basin, Peru) in dorsal view (**A**) with corresponding line drawing, detail of the vertex of the cranium in dorsal view (**B**) with corresponding line drawing, and left lateral view (**C**). Hatching for main break surfaces; **dashed lines on line drawing** for more tentative interpretations of sutures and edges; **dashed lines on photo** for maxilla-premaxilla suture. Scale bar: 200 mm. Photos by Olivier Lambert.

in MUSM 4692 cannot be precisely quantified. Still, it was originally proportionally anteroposteriorly longer than in *C. ullujayensis* n. sp. MUSM 2527 and MUSM 1401, with longer nasals, as in the holotype. Sutures between nasals and frontals appear to be interdigitated in MUSM 4692, with many longitudinal grooves and ridges, as in the holotype. The interpretation of the outline of these sutures is complex, as several lines are observed that may correspond to the suture lines (see Fig. 3B), a condition reminiscent of the holotype of *Yaquinacetus meadi* Lambert, Godfrey & Fitzgerald, 2019, where two different interpretations were provided for the nasal-frontal suture outline (Lambert *et al.* 2019). The challenging interpretation of vertex sutures in various groups of odontocetes could be partly due to the complex evolutionary and developmental history of the bones making this region (Roston *et al.* 2023). Noteworthily, several ziphiids have been described with an unusual configuration of vertex bones, sometimes showing extreme ossification (Bianucci *et al.* 2013) and in other cases including a prominent medial bone identified as the interparietal (e.g., Bianucci *et al.* 2007). The upper part of the occipital shield of MUSM 4692 is transversely and dorsoventrally concave. The temporal crests are robust and project far posteriorly, more so than in *C. ullujayensis* n. sp. MUSM 2527.

Mandible

With the anterior tip now added to the previously described posterior portion, the right mandible of the holotype is preserved on its whole length (Fig. 2A, B, D). The mandibular condyle is shifted about 30 mm anterior to its original position in the mandibular fossa, and the anterior tip of the mandible reaches about 40 mm more anterior than the rostrum.

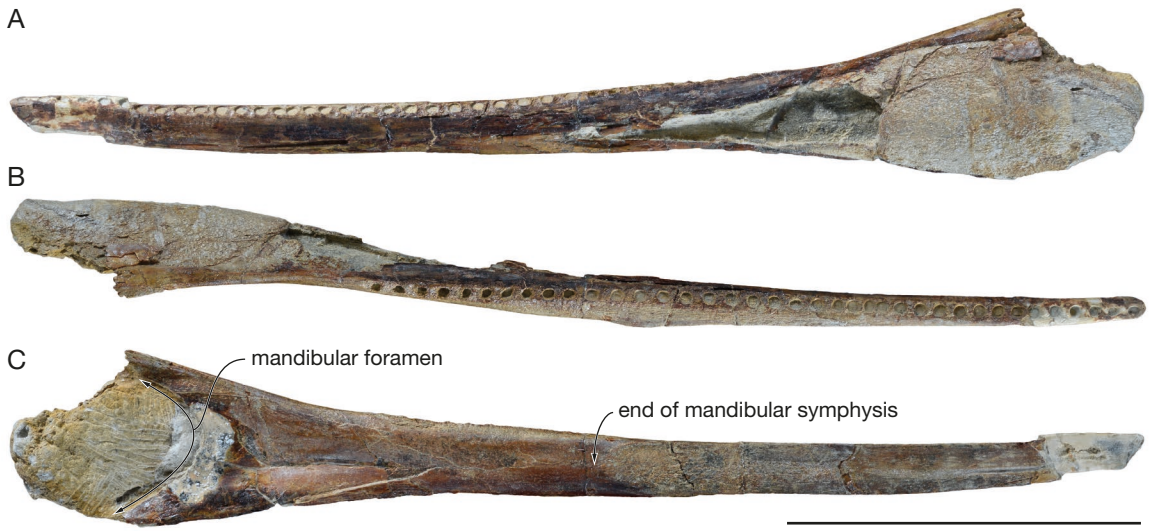

FIG. 4. — Partial left mandible of *Chilcacetus cavirhinus* Lambert, Muizon & Bianucci, 2015 MNHN.F.PRU11 (holotype, Chilcatay Formation, East Pisco Basin, Peru) in lateral (**A**), dorsal (**B**), and medial (**C**) view. Scale bar: 200 mm. Photos by Olivier Lambert.

The rostrum was thus not longer than the mandible, a major difference with the eurhinodelphinids for which a mandible was found associated to the rostrum (e.g., Kellogg 1925; Pilleri 1985). Thirty-eight alveoli are counted on the nearly complete left mandible of the holotype (Fig. 4); the total count was most likely close to the upper count. As in the holotype, the mandible of MUSM 4692 bears 10 alveoli in the post-symphyseal region, a number that is higher than in *Chilcacetus ullujayensis* n. sp. MUSM 2527. The symphysis is not ankylosed in MUSM 4692, a feature shared with the holotype.

Atlas

Preserved upside down attached to the left side of the occipital shield, the atlas of MUSM 4692 is 118 mm wide, 73 mm high, and 30.5 mm long on the ventral side along the sagittal plane (Fig. 3). There is no indication of an ankylosis, even partial, with the axis, a difference with most, but not all, ziphiids (Ramassamy *et al.* 2018). The lower transverse process is moderately elongated posterolaterally. The base of the ventral tubercle is broad, but this process only extends for a short distance posterior to the ventral edge of the posterior articular facets. The ventral tubercle is for example longer in the eurhinodelphinids *Xiphiacetus cristatus* and *Ziphiodelphis sigmoideus* Pilleri, 1985 (Pilleri 1985; Lambert 2005a) and several early platanistoids (Tanaka & Fordyce 2015; Kimura & Barnes 2016; Bianucci *et al.* 2020).

Chilcacetus ullujayensis n. sp.
(Figs 5-15)

urn:lsid:zoobank.org:act:7CFE27F3-EDC1-4572-B5DD-F1662483258D

TYPE MATERIAL. — **Holotype. Peru** • 1 specimen (nearly complete cranium including the two in situ periotics, the detached left malleus, left tympanic bulla, and several teeth, the posterior part of mandibles, the left humerus, three thoracic vertebrae, and a few rib fragments; this specimen has been previously attributed to *Chilcacetus cavirhinus*, in a paper including a field photo of the specimen, as well as photos of one rib and the humerus (Bianucci *et al.* 2018: figs 8, 13)); East Pisco Basin, Ullujaya locality; 14°34'2.2"S, 75°38'54.8"W; Chilcatay Formation; Burdigalian (late Early Miocene); MUSM 2527.

TYPE LOCALITY. — Ullujaya, East Pisco Basin, Peru (Fig. 1A, B). Geographic coordinates: 14°34'2.2"S, 75°38'54.8"W. This specimen was reported in the geological map of Ullujaya provided by Di Celma *et al.* (2018) with the field number O5.

TYPE HORIZON AND AGE. — Lower Miocene Chilcatay Formation. More precisely, the holotype MUSM 2527 was collected 9.7 m above the base of the exposed section in the sandstones of the *Ct1c* facies association of the Ct1 allomember (Fig. 1E). The age of the type horizon is constrained to the 18.9-18.5 Ma interval based on the $^{87}Sr/^{86}Sr$ values calculated from barnacle and pectinid samples collected just below the holotype skeleton (Bosio *et al.* 2020a, 2022). This dating is consistent with the roughly 19-18 Ma age interval for the whole Chilcatay Formation exposed at Ullujaya as indicated by $^{40}Ar/^{39}Ar$ radiometric dating, $^{87}Sr/^{86}Sr$ stratigraphy, and silicoflagellate and diatom biostratigraphy (Di Celma *et al.* 2018; Bosio *et al.* 2020a, b, 2022).

REFERRED SPECIMEN. — MUSM 1401, nearly complete cranium with associated fragments of both mandibles, eight partly preserved vertebrae, and rib fragments. This specimen was previously tentatively attributed to *Chilcacetus cavirhinus* (Lambert *et al.* 2015). It was reported in the geological map of Ullujaya provided by Di Celma *et al.* (2018) with the field number O6 (see also Bianucci *et al.* 2018: table 1, fig.13). Geographic coordinates: 14°34'36.00"S, 75°38'38.30"W. MUSM 1401 was collected 15 m above the base of the exposed section and 5.3 m above the level of the holotype of *Chilcacetus ullujayensis* n. sp., in the same sandstones of the *Ct1c* facies association of the Ct1 allomember of the Lower Miocene Chilcatay Formation (Fig. 1D). Two meters above MUSM 1401, sampled barnacles and oyster shells gave a $^{87}Sr/^{86}Sr$ dating between 18.8 Ma and 18.6 Ma (Bosio *et al.* 2020a, 2022). Therefore, both the holotype and referred specimen of *C. ullujayensis* n. sp. fall in the 18.9-18.4 age interval, i.e. lower Burdigalian.

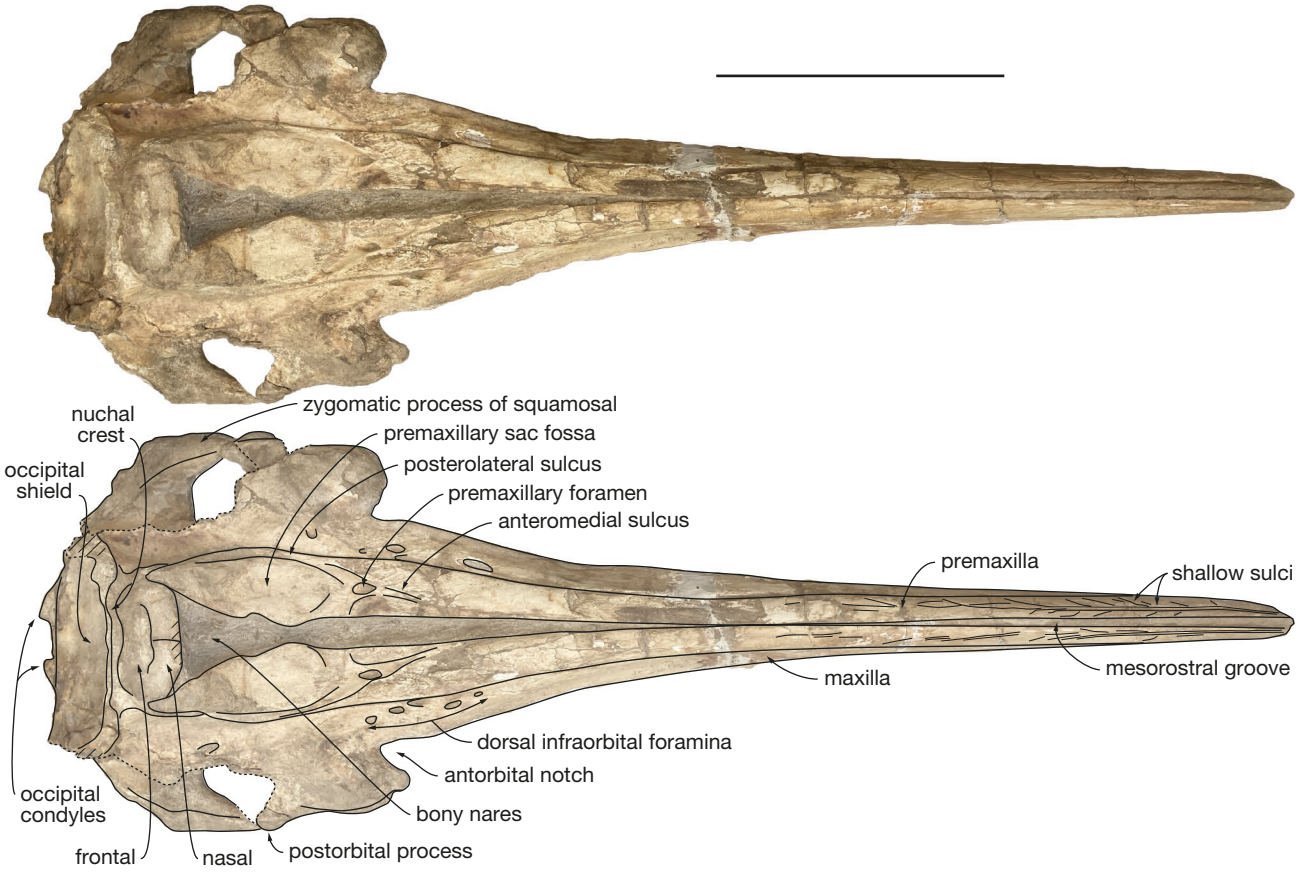

FIG. 5. — Cranium of *Chilcacetus ullujayensis* n. sp. MUSM 2527 (holotype, Chilcatay Formation, East Pisco Basin, Peru) in dorsal view with corresponding line drawing. Hatching for main break surfaces; **dashed lines** for incomplete parts. Scale bar: 200 mm. Photos by Olivier Lambert.

DIAGNOSIS. — *Chilcacetus ullujayensis* n. sp. differs from *Chilcacetus cavirhinus* in its slightly greater size (bizygomatic width > 270 mm); the rostrum being proportionally longer (ratio between rostrum length and condylobasal length > 0.71 and ratio between preorbital width and rostrum length < 0.4); 37-39 maxillary teeth per side; the mesorostral groove being dorsally open for a longer distance (dorsomedial contact between premaxillae absent to very short); the vertex of the cranium being proportionally anteroposteriorly shorter and wider; the occipital shield being transversely narrower (minimum posterior distance between temporal fossae approximates maximum width of premaxillae in facial region); the long axis of the zygomatic process of the squamosal being farther to the horizontal plane; and the lower number of alveoli (8) in the post-symphyseal region of the mandible.

ETYMOLOGY. — The species name refers to the East Pisco Basin fossil-rich locality of Ullujaya, where both the holotype MUSM 2527 and referred specimen MUSM 1401 of this new species were collected.

DESCRIPTION

This description is mostly based on the holotype MUSM 2527, focusing on parts that are not preserved or differently shaped in the previously described MUSM 1401 (Lambert *et al.* 2015; at that time referred to *Chilcacetus cavirhinus*).

Ontogenetic stage

All epiphyses of the three preserved thoracic vertebrae and left humerus of MUSM 2527 are fully ankylosed, indicating an adult individual (Galatius & Kinze 2003; Moran *et al.* 2015). A similar interpretation was proposed for MUSM 1401, based on a series of 8 vertebrae (Lambert *et al.* 2015). This is in agreement with the robustness of cranial and mandibular parts in these two specimens.

General cranial features

Displaying a complete rostrum and well-preserved facial region as in MUSM 1401, the cranium of MUSM 2527 is slightly more damaged on the roof of the temporal fossae, and its temporal crests are lost (Figs 5-11; Appendix 2). Compared to MUSM 1401 (Appendix 3), it has better-preserved orbits and ventral region in general, including well-defined maxillary and premaxillary alveoli, and complete hamular processes and jugals. Its in situ periotics as well as one detached tympanic bulla, one malleus, and teeth, are other parts not preserved in MUSM 1401 (and any other *Chilcacetus* spp. specimen with regards to the ear bones). Apart from a somewhat longer rostrum, cranial dimensions of MUSM 2527 are remarkably similar to MUSM 1401 (Table 1). The robust rostrum makes 73 % of the condylobasal length, a proportion that is slightly higher than in MUSM 1401, and the postorbital width is greater than in the two specimens of *Chilcacetus cavirhinus*. As in other *Chilcacetus* spp. specimens, the temporal fossa is anteroposteriorly longer than high, and its posterior part was not fully dorsally covered by the

TABLE 1. — Cranial and mandibular measurements (in mm) of specimens of *Chilcacetus cavirhinus* Lambert, Muizon & Bianucci, 2015 and *Chilcacetus ullujayensis* n. sp. (Chilcatay Formation, East Pisco Basin, Peru). Abbreviations: **e**, estimate; **r**, right side; **l**, left side; **+**, incomplete; **–**, no data.

	Chilcacetus cavirhinus		***Chilcacetus ullujayensis* n. sp.**	
	MNHN.F.PRU11 (holotype)	**MUSM 4692**	**MUSM 2527 (holotype)**	**MUSM 1401**
Condylobasal length	740	e770	872	852
Rostrum length	518	525	639	611
Width of rostrum at mid-length	45.5	52	51	–
Height of rostrum at mid-length	38	–	48	–
Width of premaxillae at mid rostrum length	32.5	36	37	–
Maximum width of mesorostral groove on the rostrum	20	–	–	17
Width of rostrum at base	146	e156	152	158
Width of premaxillae at rostrum base	89	87	92	92
Width of mesorostral groove at rostrum base	19.5	–	–	16.5
Distance between anterior tips of right and left premaxillary foramina	48.5	–	–	60.5
Preorbital width	221	233	240	e228
Postorbital width	250	255	268	–
Minimum distance between premaxillae anterior to bony nares	10	–	–	14
Distance between first posterior alveolus and antorbital notch	45.5	–	60	68
Length of upper tooth row	463	–	585 (r)/580 (l)	–
Number of dental alveoli per upper row	41 (l)	–	43 (r)/42 (l)	e41 (r)
Number of maxillary alveoli per row	34	–	37-39	–
Maximum width of premaxillae on cranium	109	e106	109	108.5
Width of right premaxillary sac fossa	45	45	47	47
Width of left premaxillary sac fossa	48	e46	49.5	45
Width of bony nares	42.5	42	46	46
Maximum width of nasals	63	–	74	61
Length of medial suture of nasals	+15.5	–	+15.5	19
Distance between lateral margins of premaxillae on vertex	84	–	–	77
Minimum distance between maxillae across vertex	64	e70	–	53.5
Maximum length of frontals on vertex	e37	–	–	25
Distance between anteromedial point of nasals and posterior margin of nuchal crest	+52	54	+44	+43
Bizygomatic width	e246	–	274	+271
Width between posterodorsal corners of temporal fossae	152	–	–	154
Minimum posterior distance between temporal fossae	131	–	118	106
Length of right orbit	78	–	81	–
Length of left orbit	e76	76	75	–
Height of right postorbital process of frontal	38	–	–	–
Height of right temporal fossa	77	–	e84	89
Height of left temporal fossa	75	–	e83	91
Length of right temporal fossa	e121	–	e125	–
Length of left temporal fossa	126	–	–	–
Width of occipital condyles	95	–	87	93
Height of right occipital condyle	47	–	50.5	+41
Width of right occipital condyle	28	–	–	29
Width of foramen magnum	e43	–	34	e44
Maximum distance between basioccipital crests	+98	–	e117	+109
Maximum distance between lateral margins of exoccipitals	+207	–	e209	241
Longitudinal distance between anterior apex of left palatine and level of left antorbital notch	35	–	–	–
Distance between anterior apex of left palatine and apex of left pterygoid	49	–	–	–
Distance between anterior apex of left pterygoid and apex of left hamular process	79	–	–	–
Maximum width of hamular processes	e48	–	–	–
Length of anterior process of periotic	–	–	11 (r)/11.5 (l)	–
Length of pars cochlearis (to anterior margin of fenestra rotunda)	–	–	14 (r)	–
Total length of left tympanic bulla	–	–	39	–
Maximum width of left tympanic bulla	–	–	22	–
Maximum height of left tympanic bulla (at sigmoid process)	–	–	26	–
Maximum height of involucrum	–	–	14	–
Height of left malleus in posteromedial view	–	–	5.7	–
Width of left malleus in posteromedial view	–	–	3.5	–
Length of mandible	657	–	–	–
Length of mandibular symphysis	309	+325	e400	–
Height of mandible at posterior end of symphysis	33.5	37	37	–
Width of mandibles at posterior end of symphysis	e52.5 (2 × 26.3)	–	65	–
Distance between posterior end of symphysis and last posterior alveolus	145	–	135	–
Number of mandibular alveoli per row	+38 (left)	–	–	–

TABLE 1. — Continuation.

	Chilcacetus cavirhinus		*Chilcacetus ullujayensis* n. sp.	
	MNHN.F.PRU11 (holotype)	MUSM 4692	MUSM 2527 (holotype)	MUSM 1401
Number of alveoli posterior to symphysis	10	10	8	–
Distance between posterior end of symphysis and posterior surface of condyle	355	–	385	–
Height of mandibular condyle	51	–	56	–
Width of mandibular condyle	–	–	30	–
Distance from posterior surface of condyle to anterior margin of mandibular foramen	125	–	e150	–

frontal and maxilla. The vertex is only slightly shifted to the left side compared to the sagittal plane, indicating a minor degree of asymmetry.

Premaxilla

As for *Chilcacetus cavirhinus,* the premaxilla is alone on the anterior tip of the rostrum for a relatively short distance, about 50 mm (Fig. 6A). In MUSM 2527, this premaxillary portion held 4 to 5 teeth, and the corresponding alveoli have an anteroposterior diameter of 9 mm and interalveolar spaces of 2.5 mm (Fig. 7). The premaxilla-maxilla suture is distinct until its tip on the lateral surface of the rostrum. More posteriorly, this suture is not located in a broad lateral groove, though a narrow sulcus occupies the intermediate third of the rostrum, starting from a foramen that is located along the suture. As in all other *Chilcacetus* spp. specimens, the dorsolateral surface of the premaxilla is marked along the anterior half of the rostrum by numerous shallow and sinuous sulci, leaving from a main longitudinal sulcus that start at the tip of the rostrum (Fig. 5). Right and left premaxillae contact each other above the mesorostral groove from a point at mid rostrum length, before diverging 200 mm anterior to the antorbital notch level. The premaxillary foramen is located at the level of this notch. The anteromedial sulcus is moderately long (about 80 mm) and the posteromedial sulcus is deep and broad; these two sulci define a roughly flat, dorsomedially sloping prenarial triangle. Each premaxillary sac fossa is transversely and anteroposteriorly concave. The left premaxillary sac fossa is only slightly wider than the right, while the opposite condition occurs in MUSM 1401, so no clear signal can be detected for the asymmetry of this region in *Chilcacetus ullujayensis* n. sp., as in *C. cavirhinus* MNHN.F.PRU11. No prominence is seen on the posterolateral corner of the thick ascending process of the premaxilla. The premaxilla contacts the anterolateral and lateral margin of the nasal for most of the length of the latter. The presence of a contact between premaxilla and frontal could not be assessed due to uncertainties about the lateral extent of the nasal-frontal suture on both sides of the vertex.

Maxilla

Five and four dorsal infraorbital foramina are observed in the area anteromedial to the antorbital notch of MUSM 2527, on the right and left sides, respectively (Fig. 5). This count does not differ much from MUSM 1401. At least one additional foramen is found on the left side, 35 mm posteromedial to the notch. Only the right posteriormost foramen is preserved, level to the posterior edge of the bony nares and 18 mm lateral to the premaxilla-maxilla suture. Better preserved in MUSM 2527 than in MUSM 1401, the antorbital notches are deep and wide, slightly more anterolaterally open than in *Chilcacetus cavirhinus* MNHN.F.PRU11. As in the latter, the right notch is narrower than the left, due to a more anteriorly projected antorbital process, reaching a level 12 mm anterior to the preorbital process of the frontal. The dorsal surface of the right antorbital process makes an oblique, prominent blade as in MNHN.F.PRU11. Along the vertex, the raised medial wall of the maxilla is distinctly shorter than in MUSM 1401 and, to an even greater extent, than in the two specimens of *C. cavirhinus*, corresponding to an anteroposteriorly shorter posterior part of the vertex.

With a total count of 42 to 43 upper alveoli per row, MUSM 2527 had 37 to 39 maxillary teeth per row (Fig. 7), a count that is higher than in *C. cavirhinus* MNHN.F.PRU11 (34). The alveolar groove ends 60 mm anterior to the level of the antorbital notch, and the last alveoli are shifted slightly medially compared to the lateral margin of the rostrum. Most maxillary alveoli have an anteroposterior diameter of 9 to 10 mm, with a slight decrease in posteriormost alveoli. Interalveolar spaces range from 2.5 mm anteriorly to 7 mm at mid rostrum length, 11 mm at 3/4 of rostrum length, and 3-4 mm between posteriormost alveoli.

170 mm from the rostrum tip, the vomerine trough widens and deepens backwards with a V-shaped cross section, until 420 mm from tip, where it starts shallowing. A first pair of palatine foramina is located 500 mm from rostrum tip, each followed anteriorly by a well-defined sulcus. A second pair of smaller foramina is observed 15 mm more posteriorly, and a third pair is along the anteromedial border of the palatines, at 70-80 mm from the level of the antorbital notches.

Palatine and pterygoid

The anteromedial part of the palatine-maxilla suture is visible on both sides of the deeply keeled rostrum base, until a level 25 mm posterior to the last pair of palatine foramina (Fig. 7). The pterygoid is much shorter anteriorly, not reaching the level of the antorbital notch. The anteriorly short pterygoid sinus fossa is laterally defined by a low lateral lamina of the pterygoid. This lamina is directed posterolaterally, but remains

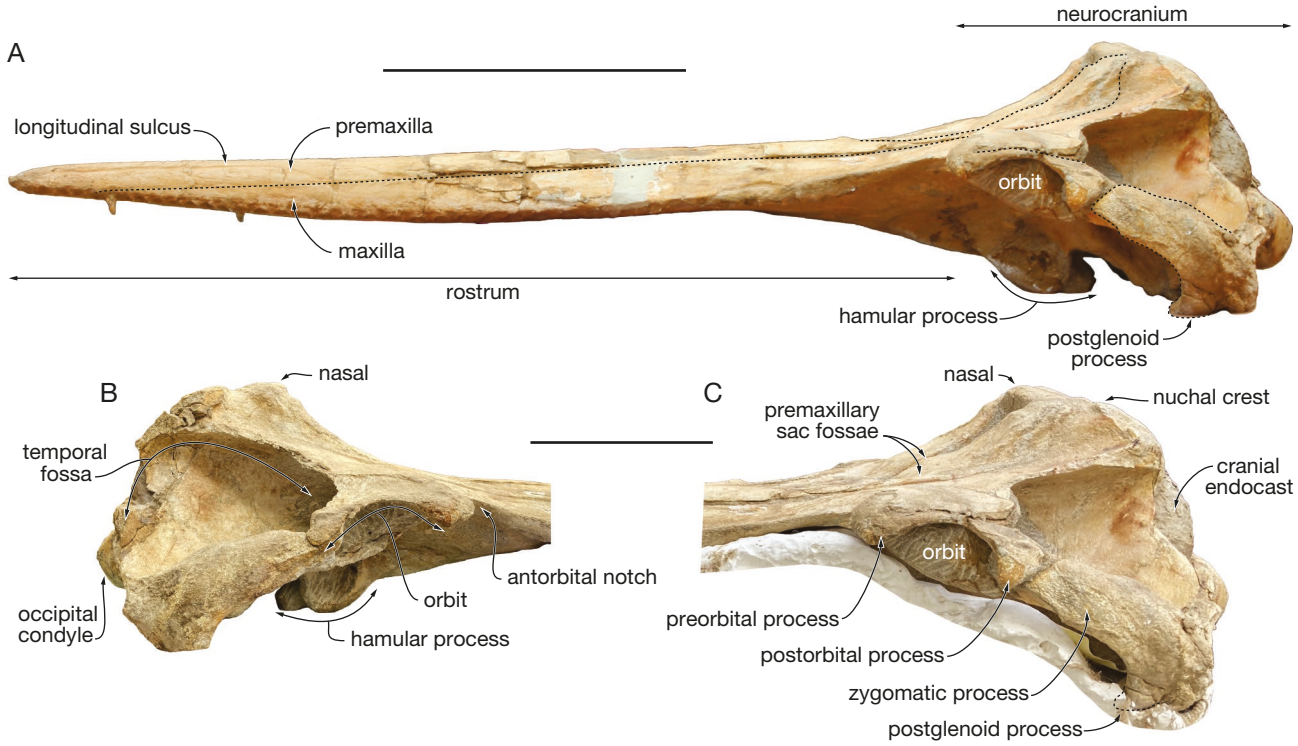

Fig. 6. — Cranium of *Chilcacetus ullujayensis* n. sp. MUSM 2527 (holotype, Chilcatay Formation, East Pisco Basin, Peru) in left lateral view (**A**), detail of the neurocranium in right (**B**) and left (**C**) lateral view. **Dashed lines** for main sutures and some bone outlines. Scale bars: A, 200 mm; B, C, 100 mm. Photos by Olivier Lambert.

low before disappearing anterior to the path for the mandibular nerve V3. This lamina does not contact the falciform process of the squamosal, a condition already proposed for *Chilcacetus cavirhinus* MNHN.F.PRU11 and, for example, also observed in *Squaloziphius emlongi* Muizon, 1991 and *Waipatia maerewhenua* Fordyce, 1994 (Muizon 1991; Fordyce 1994). The medial wall of the pterygoid thickens both transversely and dorsoventrally in posterior direction, more gradually than in *C. cavirhinus* MNHN.F.PRU11, making a robust hamular process with a ventrolateral edge that is keeled anteriorly and more rounded posteriorly (Figs 6-8). Right and left processes are separated by a deep V-shaped valley. The main body of the hamular process is distinguished from its long, finger-like posteromedial projection by a broad notch that is ventral to the choana. Right and left projections do not contact each other (8 mm apart), and are 9.5 mm broad and 25 mm long. They are broadly similar, though shorter, than in '*Argyrocetus*' *joaquinensis*, *Simocetus rayi* Fordyce, 2002, and *Olympicetus thalassodon* Velez-Juarbe, 2023 (Kellogg 1932; Fordyce 2002; Velez-Juarbe 2023), similar but more distant to each other than in *Ziphiodelphis abeli* (Pilleri 1985; plates 39, 40), longer than in *C. cavirhinus*, and more posteriorly directed than in *S. emlongi*. The medial lamina of the pterygoid thickens gradually towards the posterior region of the basioccipital basin, ending 60 mm from the posterior tip of the basioccipital crest.

Nasal

Though the anteromedial margin of each nasal is abraded in MUSM 2527, considering the better-preserved anterolateral margins the anterior outline of the nasals did most likely not differ much from MUSM 1401, displaying a smoothly rounded outline and a short projection above the bony nares (Figs 5; 6; 11B). The dorsal surface of the joined nasals is transversely convex. The nasal-frontal sutures are difficult to follow laterally, but they indicate that each nasal is transversely wider than medially long and that medially each nasal is shorter than the corresponding frontal. As in MUSM 1401, each nasal sends a posterolateral projection, whose full extent cannot be assessed here. There is no indication of interdigitated nasal-frontal sutures in both MUSM 2527 and MUSM 1401, a possible difference with *Chilcacetus cavirhinus*.

Frontal

On the vertex, the anteromedial part of the frontals is slightly prominent, as in *C. cavirhinus* MNHN.F.PRU11, reaching dorsally the same height as the highest preserved medial portions of nasals. From there, the dorsal surface of the frontals slopes posteroventrally to a narrow depression just anterior to the nuchal crest.

In lateral view (Fig. 6), the preorbital process is moderately thickened, as in *Chilcacetus cavirhinus*. The orbit roof is highly arched, with a maximum depth of 21 mm on the right side. Better preserved on the left side, the postorbital process is robust and roughly vertical.

Lacrimojugal complex

The lacrimojugal complex makes the ventrolateral wall of the antorbital notch, as a thin oblique plate along the anteroventral margin of the preorbital process of the frontal (Figs 7; 8), with no major difference with *C. cavirhinus*

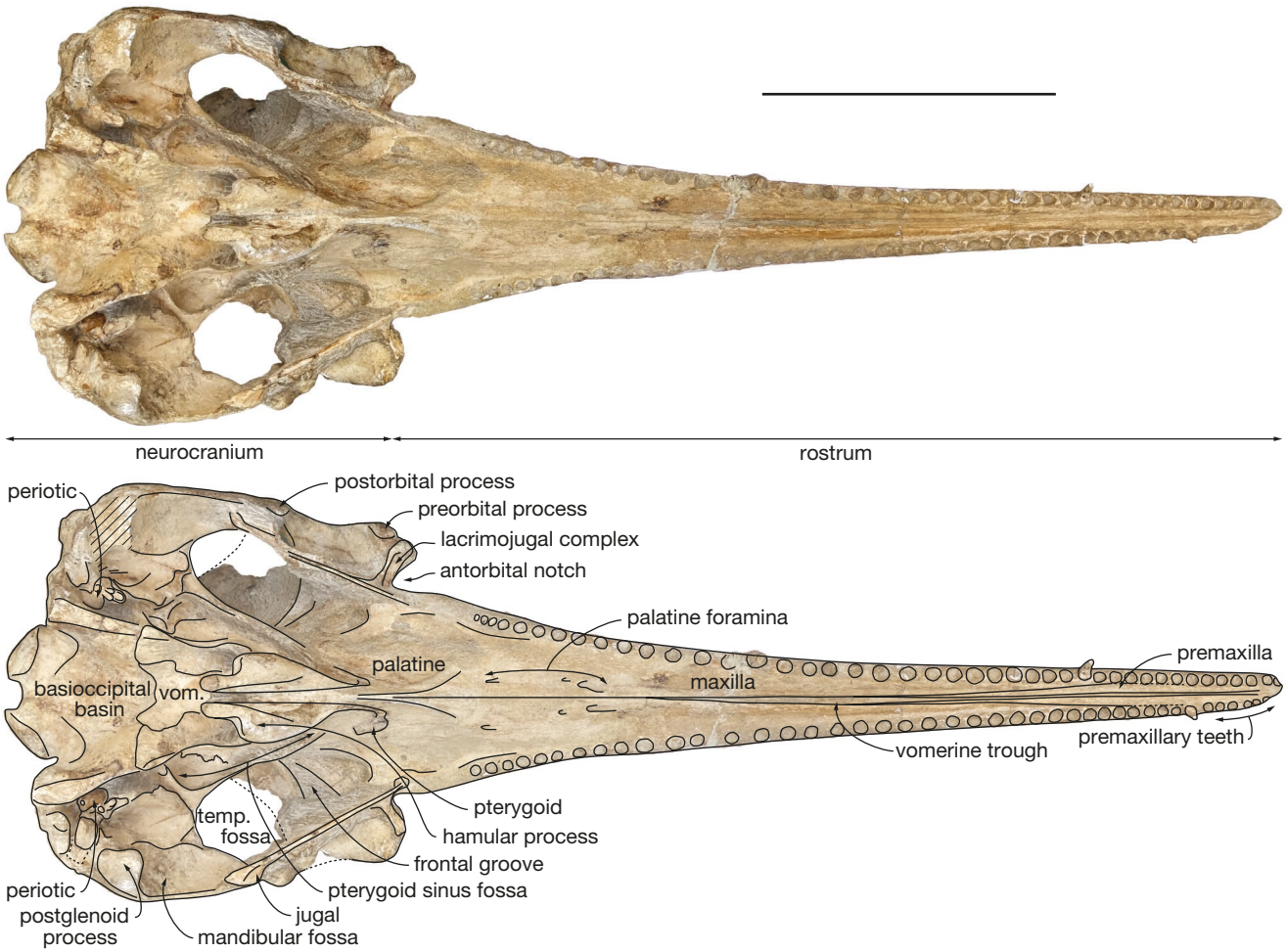

FIG. 7. — Cranium of *Chilcacetus ullujayensis* n. sp. MUSM 2527 (holotype, Chilcatay Formation, East Pisco Basin, Peru) in ventral view with corresponding line drawing. Hatching for main break surfaces; **dashed lines** for reconstructed parts and tentative outline of the posterior process of the left periotic. Scale bar: 200 mm. Photos by Olivier Lambert.

MNHN.F.PRU11. The base of the styliform process of the jugal extends at least 15 mm more anteromedially than the bottom of the antorbital notch. The styliform process remains thin (transverse thickness 3 mm) for most of its length, only expanding a short distance before the contact with the zygomatic process of the squamosal (better seen on the left side).

Supraoccipital

The nuchal crest is thin anteromedially, but it thickens considerably towards the dorsolateral corners of the occipital shield (Figs 5; 11A), as in *C. cavirhinus* MNHN.F.PRU11 and *Macrodelphinus kelloggi*, reaching a maximum thickness of 15 mm, measured on the left side, which is greater than in MUSM 1401. In posterior view, most of the outline of the nuchal crest is horizontal, as in MUSM 1401 and *C. cavirhinus* MNHN.F.PRU11. The occipital shield is moderately transversely concave and its dorsal region is slightly dorsoventrally concave, while more ventrally a broad sagittal groove is present. The ventrolateral parts of the occipital shield being lost, the cranial endocast is visible, with the outer surface better preserved on the left side.

Exoccipital

The exoccipital does not reach as far laterally as the squamosal (Fig. 11A). The region of the paroccipital process is too damaged on both sides to allow for a description of this area, as well as of the details of the narrow jugular notch. The occipital condyles are slightly mediolaterally narrower and dorsoventrally higher than in *Chilcacetus cavirhinus* MNHN.F.PRU11, with a transversely narrower foramen magnum. The condylar neck is well defined (Figs 6; 7), and the dorsal, condyloid fossa is broad and deep (Fig. 11A).

Alisphenoid

The anterior portion of the ventral exposure of the alisphenoid is excavated by the broadest part of the pterygoid sinus fossa, the latter being laterally margined by a moderately developed subtemporal crest (Figs 7; 8). Posterior to the sinus fossa, the path for the mandibular nerve V3 extends obliquely from the foramen ovale.

Squamosal

The zygomatic process of the squamosal is long and robust, pointing anterodorsally (Fig. 6). Its preserved position com-

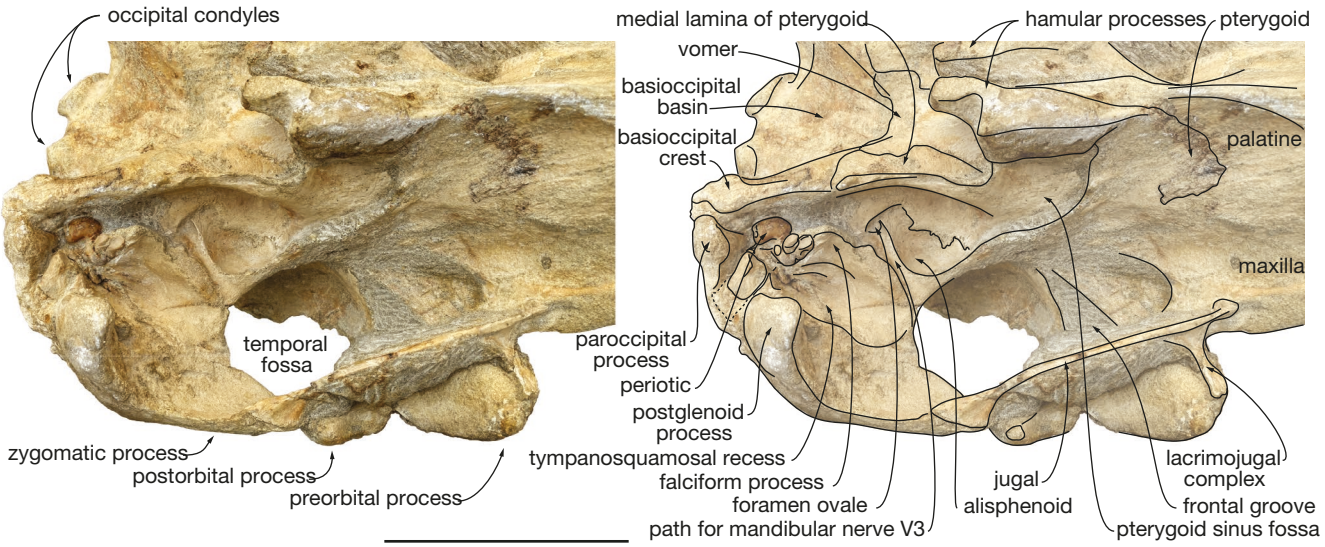

Fig. 8. — Cranium of *Chilcacetus ullujayensis* n. sp. MUSM 2527 (holotype, Chilcatay Formation, East Pisco Basin, Peru). Detail of the left side of the neurocranium in ventrolateral view with corresponding line drawing. **Dashed line** for tentative outline of the posterior process of the left periotic. Scale bar: 100 mm. Photos by Olivier Lambert.

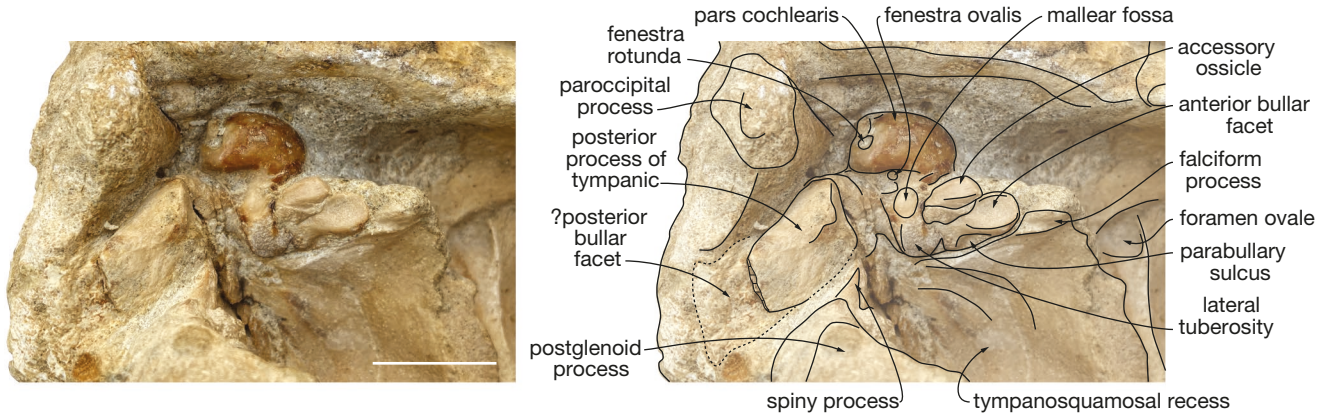

Fig. 9. — In situ left periotic of *Chilcacetus ullujayensis* n. sp. MUSM 2527 (holotype, Chilcatay Formation, East Pisco Basin, Peru) in ventral view with corresponding line drawing. **Dashed line** for tentative outline of the posterior process of the left periotic. Scale bar: 20 mm. Photos by Olivier Lambert.

pared to the postorbital process of the frontal on both sides suggests either a long, oblique contact between the two bones, or a near contact. The dorsal margin of the zygomatic process is moderately convex in lateral view, and this margin thickens transversely posteriorly. The contact facet with the jugal is best seen on the left side, as a 23 mm long concave portion of the ventral margin, defined posteroventrally by a low tuberosity. From this point, the concave ventrolateral margin of the zygomatic process remains thin until the base of the robust postglenoid process. Not preserved in *C. cavirhinus* MNHN.F.PRU11 and MUSM 1401, the latter is anteroposteriorly long (29 mm from the anterior meatal crest to its anterior margin) and transversely thick in MUSM 2527, similar to the condition in eurhinodelphinids, *Eoplatanista* spp., *Amphidelphis bakersfieldensis* n. comb., '*Argyrocetus*' *joaquinensis*, *Caolodelphis milleri* Godfrey & Lambert, 2023, and *Perditicetus yaconensis* Nelson & Uhen, 2020, but anteroposteriorly shorter than in squaloziphiids and possible relatives *Crisocetus lydekkeri* Gaetán, Paolucci & Buono, 2023, *Dolgopolis kinchikafifforo* Viglino, Gaetán, Cuitiño & Buono, 2021, *Squaloziphius emlongi*, and *Yaquinacetus meadi*, as well as in *Enigmatocetus posidoni* Godfrey & Lambert, 2023 (Muizon 1991; Lambert *et al.* 2019; Nelson & Uhen 2020; Viglino *et al.* 2021; Gaetán *et al.* 2023; Godfrey & Lambert 2023); it reaches ventrally the same level as the basioccipital crest and the exoccipital. One main sternocephalicus fossa is best seen on the right side, not extending much along the zygomatic process (ending before the level of the anterior margin of the postglenoid process).

As in *C. cavirhinus* MNHN.F.PRU11, the tympanosquamosal recess is not clearly separated from the mandibular fossa (Figs 7; 8). The recess excavates the base of the postglenoid process' medial surface and extends anteriorly until the anterior limit of the mandibular fossa, thus not reaching farther along the zygomatic process. Probably complete on both sides of MUSM 2527, the falciform process is pointing ventrally just

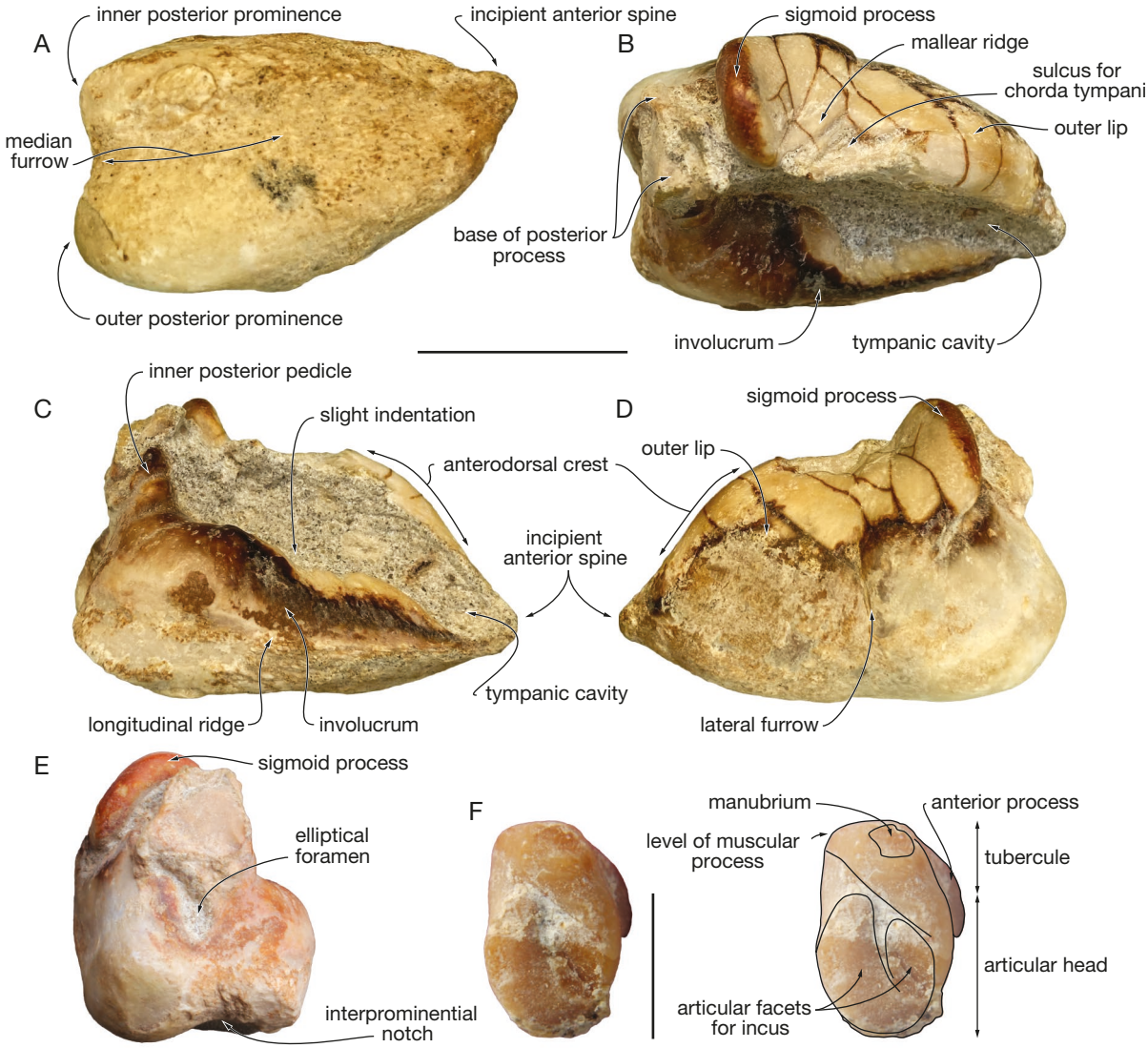

Fig. 10. — Left tympanic and left malleus of *Chilcacetus ullujayensis* n. sp. MUSM 2527 (holotype, Chilcatay Formation, East Pisco Basin, Peru). Tympanic in ventral (**A**), dorsal (**B**), medial (**C**), lateral (**D**), and posterior (**E**) view; malleus in posteromedial view (**F**) and corresponding line drawing. Scale bars: A-E, 20 mm; F, 0.5 mm. Photos by Olivier Lambert.

anterior to the periotic, but extends distally (in the ventral direction) less than in *C. cavirhinus* MNHN.F.PRU11. The falciform process lowers abruptly until the posterior margin of the path for the mandibular nerve V3, where it disappears (Figs 8; 9).

Basioccipital

Better preserved on the left side of MUSM 2527, each basioccipital crest is thickened along its posteromedial surface (Figs 7; 8), but not to the extent of *Caolodelphis milleri*. Right and left crests draw an angle of 35° in ventral view. A curved ridge runs from the base of each basioccipital crest towards the medial region of the basioccipital basin.

Periotic

Both periotics of the holotype (MUSM 2527) are preserved in situ (Figs 7-9), with the anterior process closely appressed to the corresponding falciform process of the squamosal and with the posterior process displaying a long dorsal contact with the exoccipital and squamosal. Anatomical details are thus only available for the ventral and ventrolateral regions. The anterior process is short (Table 1) and bears a shallow but transversely broad (4.5 to 5 mm wide) anterior bullar facet. This condition differs from the narrower facet seen in an interpretive drawing of the now lost periotic of the holotype of *Chilcacetus cavirhinus* MNHN.F.PRU11 (Lambert *et al.* 2015). Part of a well-defined parabullary sulcus can be seen on the medial surface of the anterior process of the left periotic (Fig. 9), along the falciform process of the squamosal. It is much closer to the anterior bullar facet than in *Yaquinacetus meadi*, and is more similar to *Perditicetus yaconensis* (Nelson & Uhen 2020), though the latter shares with *Y. meadi* an anterior bullar facet that is shifted distinctly medially compared to the lateral margin of the anterior process (condition unknown in MUSM 2527, the lateral margin being hidden by the falciform process).

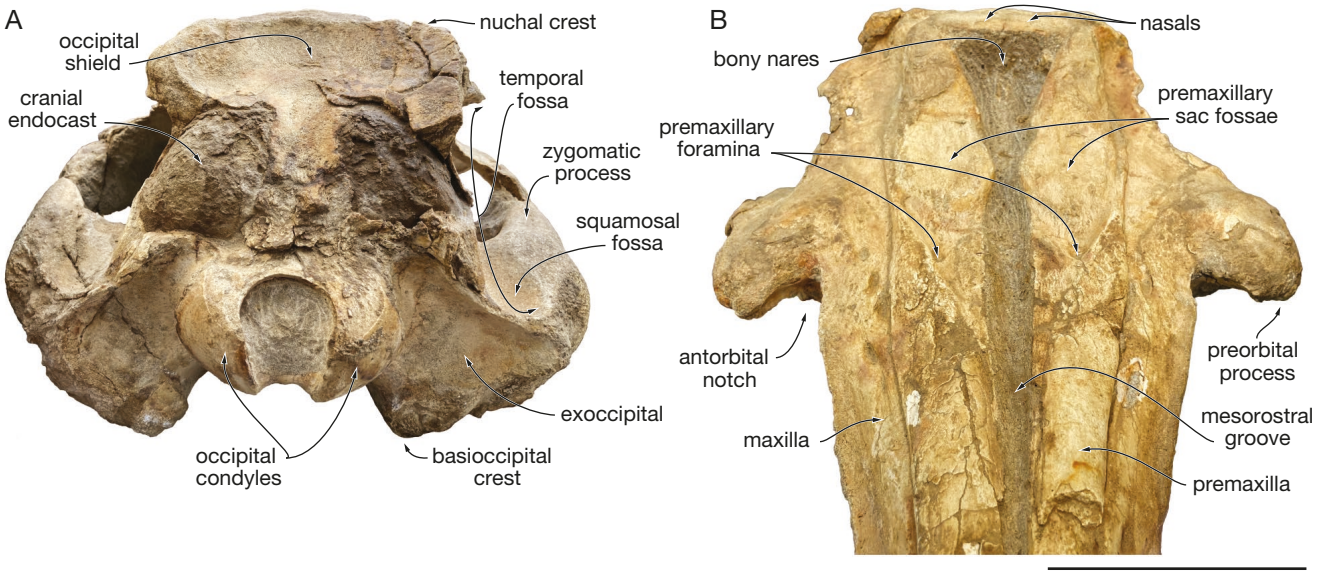

FIG. 11. — Cranium of *Chilcacetus ullujayensis* n. sp. MUSM 2527 (holotype, Chilcatay Formation, East Pisco Basin, Peru) in posterior (**A**) and anterodorsal (**B**) view. Scale bar: 100 mm. Photos by Olivier Lambert.

A medium-size accessory ossicle is preserved in situ on both sides, differing from the right periotic of MNHN.F.PRU11. The anteromedial outline of the pars cochlearis is rounded, while the posteromedial corner is marked by a prominence just medial to the fenestra rotunda. The lateral tuberosity is large, with a ventromedial surface that is broader than the mallear fossa, extending far laterodorsally and anteriorly defining a deep and narrow hiatus epitympanicus. Though being partly hidden by the posterior process of the tympanic bulla on the left side and by sediment and bone fragments on the left right side, the posterior process is tentatively interpreted as long (estimated length 35 mm), nearly reaching the posterior margin of the exoccipital in a posterolateral direction. It retains a considerable breadth for most of its visible/preserved portion, a condition that is reminiscent of the outline proposed in ventral view for MNHN.F.PRU11. A transverse break surface tentatively observed in ventral and medial view on the left periotic of *P. yaconensis* (Nelson & Uhen 2020: fig. 7) may indicate a similarly elongated posterior process. The exposed proximal surface of the right posterior bullar facet is concave along an oblique axis.

Tympanic bulla

In ventral view, the finely preserved left tympanic of MUSM 2527 is olive-shaped, with the inner posterior prominence being slightly shorter than the outer prominence, and the latter being markedly transversely broader (Fig. 10A-E). The ventral surface of the inner prominence is moderately keeled, and the keel extends anteriorly for 21 mm. The median furrow is wide but shallow posteriorly, vanishing anteriorly before mid-length of the tympanic. The anterior spine is incipient, barely thickened, associated with an inconspicuous anterolateral notch. In medial view the posterior part of the involucrum is 14 mm thick. After 5 mm the dorsal surface slopes gradually down to a slight indentation, followed by a second plateau before a more abrupt descent towards the anterior opening of the tympanic cavity. The medial surface of the tympanic is crossed at about mid-height by an anteroposteriorly directed ridge, presumably marking the ventral limit of the peribullary sinus. In dorsal view the sigmoid process is slightly obliquely directed, hiding the conical process in lateral view. The lateral furrow is narrow and nearly vertical. The anterodorsal crest is moderately convex in lateral view. The elliptical foramen is 2.5 mm wide and at least 4 mm high. Preserved in situ in the basicranium, the posterior process of the left tympanic lacks its thin distal part (Figs 7; 8), indicating that this process was long and sub rectangular in outline, as proposed for the posterior process of the periotic. Except for the somewhat more swollen outer posterior prominence, the ventral and medial views of this tympanic are highly similar to these views in *Chilcacetus cavirhinus* MNHN.F.PRU11. Strong similarities are also noted with *Yaquinacetus meadi* and eurhinodelphinids, though these generally display a deeper and anteriorly longer median furrow (see Muizon 1988a; Lambert 2005a, b). An even shallower, nearly indistinct median furrow is seen in *Eoplatanista* spp. (Muizon 1988a).

Malleus

The left malleus of USNM 2527 displays an articular head that makes 70 % of the height of the bone in posteromedial view, corresponding to a markedly shortened tubercule (Fig. 10F), as seen in eurhinodelphinids, *Inticetus* Lambert, Muizon, Malinverno, Di Celma, Urbina & Bianucci, 2017, *Eoplatanista*, *Yaquinacetus*, physeteroids, and ziphiids (Muizon 1988a; Lambert 2005b; Bianucci *et al.* 2010; Lambert *et al.* 2018, 2019). On the tubercule, which is longer than in physeteroids and most ziphiids, the manubrium is approximately at the same height as the low muscular process; the manubrium is considerably less prominent than in eurhinodelphinids and *Inticetus*, closer to *Eoplatanista* and *Yaquinacetus*. The anterior

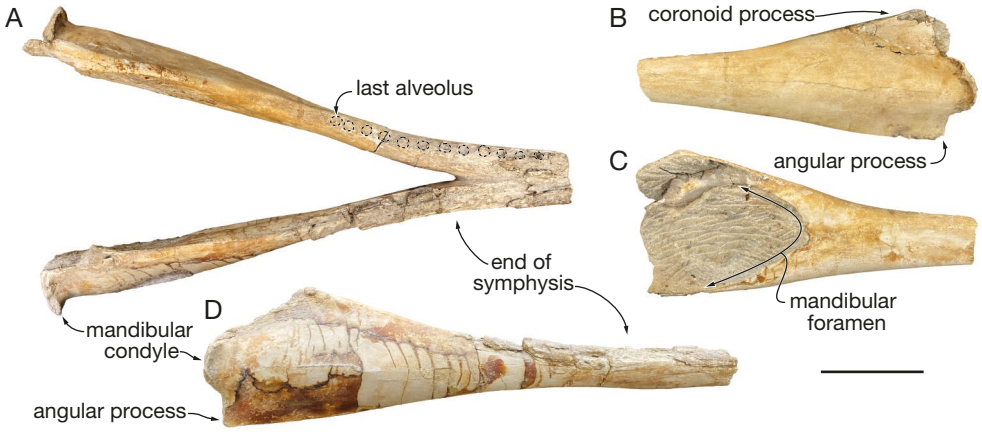

Fig. 12. — Partial mandibles of *Chilcacetus ullujayensis* n. sp. MUSM 2527 (holotype, Chilcatay Formation, East Pisco Basin, Peru) in dorsal view (**A**); partial left mandible in lateral (**B**) and medial (**C**) view; partial right mandible in lateral view (**D**). Scale bar: 100 mm. Photos by Olivier Lambert.

Fig. 13. — Three detached teeth of *Chilcacetus ullujayensis* n. sp. MUSM 2527 (holotype, Chilcatay Formation, East Pisco Basin, Peru), the two first still partly embedded in sediment. Scale bar: 20 mm. Photos by Olivier Lambert.

facet for the incus does not project outside the articular head, drawing a general outline in posteromedial view that is more regularly rounded than in *Eoplatanista italica* MGP 26166 (Muizon 1988a: fig. 12).

Mandible

As the mandible of *Chilcacetus ullujayensis* n. sp. is poorly preserved in MUSM 1401 (see Lambert *et al.* 2015), our description is mostly based on MUSM 2527 (Fig. 12). The latter only preserves a short (110 mm) posterior part of the symphyseal region. The anterior cross section is semi-circular to subtriangular, with no indication of a lateral groove, as in other *Chilcacetus* spp. specimens. While the two dentaries remain attached to each other, the suture line is visible dorsally, ventrally, and in cross section, indicating that no strong ankylosis occurred along the symphysis. At the level of the posterior end of the symphysis, alveoli have an anteroposterior diameter of 10 mm, with interalveolar spaces of 8 to 10 mm. This is in the range of MUSM 1401, with alveoli larger than in *Chilcacetus cavirhinus* MNHN.F.PRU11 and MUSM 4692. Eight alveoli are posterior to the symphysis; the last alveolus is 135 mm posterior to the end of the symphysis and 255 mm anterior to the posterior end of the mandibular condyle. There is no precoronoid crest and the dorsal margin of the coronoid crest flattens and widens in the posterior direction, with thin longitudinal ridges along the medial and lateral edges of the process. Neither of the coronoid processes are complete in MUSM 2527. The angular process draws an angle of about 90°. The mandibular condyle is laterally convex and slightly medially concave, with a dorsoventral height that is slightly greater than in *C. cavirhinus* MNHN.F.PRU11. The condyle is in line with most of the alveolar groove, the last alveolus being roughly at the same dorsoventral level as the upper edge of the condyle. The mandibular foramen has a regularly rounded anterior outline, similar to *C. cavirhinus* MNHN.F.PRU11, but ending farther anteriorly, 150 mm from the mandibular condyle.

Teeth

Four teeth were found detached along the skull of MUSM 2527 (Fig. 13). Total length ranges between 27 and 35 mm, with a crown length between 8.7 and 10.9 mm, a maximum diameter at the base of the crown between 4.5 and 5.7 mm, and a maximum diameter of the root between 7.2 and 9.2 mm. These dimensions are close to those of the posterior upper teeth of *Chilcacetus cavirhinus* MNHN.F.PRU11. Each crown is moderately curved lingually, is slightly labio-lingually flattened, and bears barely discernible mesial and distal carinae, lacking any accessory denticle, as observed in *C. cavirhinus*. The enamel is thin, with a nearly smooth surface only marked by very low apicobasal ridges. The crown apex is complete, with no apical wear visible on any of the four teeth. No clear occlusion facet could be identified along the prepared surfaces (but see below for one in situ tooth). The root is somewhat inflated in all teeth, with a slight to moderate curvature along a plane perpendicular to the curvature of the crown. The surface of the root along the root-crown boundary is smoothened, possibly corresponding to the part emerging from the alveolus, where some degree of hydrowear or acid corrosion may

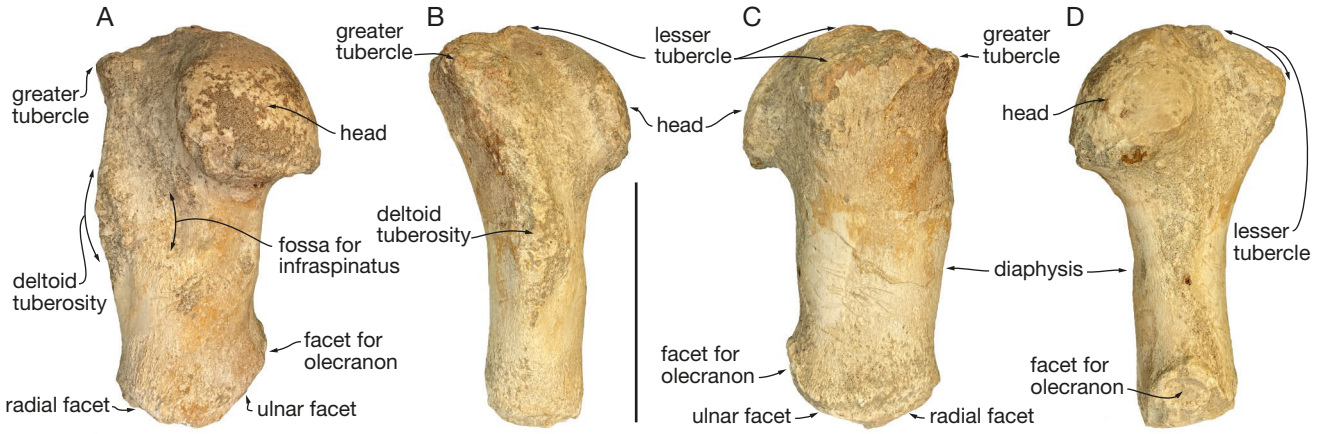

Fig. 14. — Left humerus of *Chilcacetus ullujayensis* n. sp. MUSM 2527 (holotype, Chilcatay Formation, East Pisco Basin, Peru) in lateral (**A**), anterior (**B**), medial (**C**), and posterior (**D**) view. Scale bar: 100 mm. Photos by Olivier Lambert.

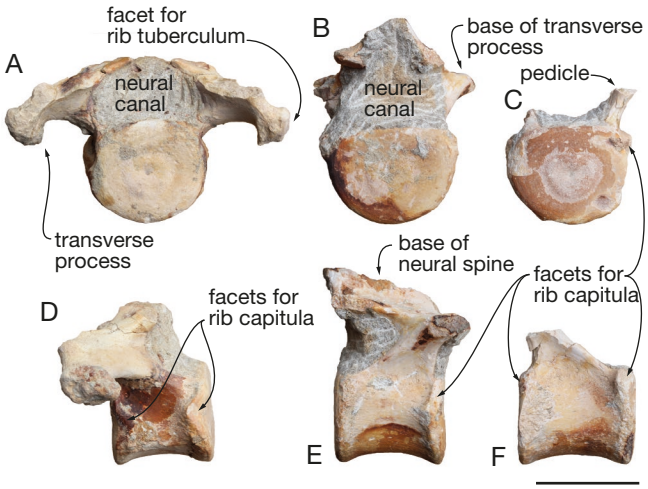

Fig. 15. — Three thoracic vertebrae of *Chilcacetus ullujayensis* n. sp. MUSM 2527 (holotype, Chilcatay Formation, East Pisco Basin, Peru). **Ta** in anterior (**A**) and left lateral (**D**) view; **Tb** in posterior (**B**) and right lateral (**E**) view; and **Tc** in anterior (**C**) and left lateral (**F**) view. Scale bar: 50 mm. Photos by Olivier Lambert.

have occurred (see Marx *et al.* 2023). A couple of anterior maxillary teeth are preserved in situ. One of them displays a long but shallow occlusal surface along the distal surface.

Humerus

Previously figured to highlight shark bite marks (Bianucci *et al.* 2018: fig. 13b, c), the complete left humerus of MUSM 2527 (Fig. 14) has a total length of 149 mm, a maximum diameter of the humeral head of 62 mm, a minimum mediolateral width of the diaphysis of 36.7 mm, an anteroposterior length of the distal epiphysis of 60 mm, and a mediolateral width of the distal epiphysis of 38 mm. The large, posterolaterally facing head is prominent, with a well-defined neck. The attachment area for the supraspinatus on the greater tubercle reaches proximally as far as the head. The lesser tubercle extends slightly more proximally, but not to the extent seen in *Amphidelphis bakersfieldensis* n. comb. YPM 13406 (see below), the humerus YPM 13437 attributed to *Macrodelphinus kelloggi*, and *Xiphiacetus bossi* (Kellogg, 1925) USNM 8842 (Kellogg 1925: pl. 12), where the lesser tubercle extends farther proximomedially (better seen in posterior view). The diaphysis is rectilinear in lateral view, while in anterior/posterior view its long axis is not as curved as in *A. bakersfieldensis* n. comb., being more similar to *M. kelloggi*. The narrow (9 mm), proximodistally elongated (21 mm), and well-defined fossa for the infraspinatus is located 15 mm anterodistal to the head. The moderately anteriorly thickened, 20 mm mediolaterally wide deltoid tuberosity is located at about mid-length of the bone, as in *A. bakersfieldensis* n. comb., *M. kelloggi*, and *Eurhinodelphis cocheteuxi* IRSNB M.299 (Abel 1931: pl. 28, fig. 12: collection number 3403). The tuberosity is located more distally in *X. bossi*. A distinct constriction marks the posterior margin of the diaphysis just before the distal epiphysis. Separated by a rectilinear ridge, the radial and ulnar facets are 31 and 28 mm long, respectively. The latter is followed by a distinct, 10 mm long facet for the olecranon.

Table 2. — Measurements (in mm) of three thoracic vertebrae of *Chilcacetus ullujayensis* n. sp. MUSM 2527 (holotype, Chilcatay Formation, East Pisco Basin, Peru). Abbreviations: **e**, estimate; **–**, no data.

	Ta	Tb	Tc
Centrum length	48	55	58
Anterior width of centrum	54	62	+57
Anterior height of centrum	48	46.5	47
Posterior width of centrum (excl. facet for rib)	62	62	62
Posterior height of centrum	47	e49	48
Maximum width of vertebra	127	–	–

Thoracic vertebrae

Three partial anterior thoracic vertebrae, corresponding to bicipital ribs, were found associated with MUSM 2527 (Fig. 15). They are listed from Ta to Tc based on the increase of centrum length, ranging from 48 to 58 mm (Table 2), but marked differences in the height of the transverse process, especially between Ta and Tc, suggest that intermediate thoracics could be missing. The three thoracics have a centrum that is wider

than long, and while Ta has anterior and posterior heights that are roughly equal to its length, Tb and Tc are proportionally longer. Only Ta has moderately well-preserved transverse processes, projecting anterolateroventrally and each bearing a robust facet for the rib tuberculum. The articulation facets for the rib capitula on the anterior epiphysis are located slightly below mid centrum height; facets on posterior epiphysis are just above mid height. Only the pedicles, base of the neural spine, and base of transverse processes are preserved on Tb, defining a pentagonal neural canal. The posterior epiphysis of this vertebra bears facets for ribs on the dorsolateral corner of the epiphysis that are much more developed than the barely visible facets on the anterior epiphysis. On Tc, in addition to the centrum only part of the left pedicle is preserved. The facets for ribs are similarly located on the dorsolateral corner of the posterior epiphysis.

Ribs

As for the humerus, one of the ribs of MUSM 2527 was figured in Bianucci *et al.* (2018: fig. 13a) to illustrate shark bite marks. In the same paper, a transverse thin section of a rib from that specimen was also figured, showing sediment infilling in cancellous bone (Bianucci *et al.* 2018: fig. 11e).

Genus *Amphidelphis* n. gen.

urn:lsid:zoobank.org:act:888073F3-FD61-422F-BE20-36B7FCDF7991

TYPE SPECIES. — *Amphidelphis bakersfieldensis* (Wilson, 1935) n. comb.

DIAGNOSIS. — Same as for the only species, *Amphidelphis bakersfieldensis* n. comb.

ETYMOLOGY. — From ancient Greek "ἀμφί" (amphi, from both sides), in reference to the distribution of this taxon in both the Northern and Southern hemispheres (California and Peru), and "delphis", the Latin word for dolphin.

Amphidelphis bakersfieldensis n. comb.
(Wilson, 1935)
(Figs 16-20)

Acrodelphis bakersfieldensis Wilson, 1935: 58.

Argyrocetus bakersfieldensis – Barnes 1976: 325.

'*Argyrocetus*' *bakersfieldensis* – Lambert 2005a: 224.

TYPE MATERIAL. — **Holotype. United States** • 1 specimen (partial cranium lacking the anterior part of the rostrum, most of the occipital shield, the right side of the basicranium, and the ear bones, with two associated cervical vertebrae and the left humerus); California, Kern County, southwest of Woody; undifferentiated sediments from Freeman Silt and Jewett Sand; Aquitanian to early Burdigalian (Early Miocene); YPM 13406.

TYPE LOCALITY. — Approximately eight km southwest of the small town of Woody, Kern County, California, United States, the same locality as the holotype of *Macrodelphinus kelloggi*, and a short distance from the type locality of the allodelphinid *Allodelphis pratti* Wilson, 1935 (Wilson 1935; Kimura & Barnes 2016).

TYPE HORIZON AND AGE. — Undifferentiated sediments from the Freeman Silt and Jewett Sand, 50 feet (about 15 m) lower in the section than the holotype of *Allodelphis pratti*, Woody Local Fauna, Early Miocene (Aquitanian to early Burdigalian), Saucesian benthic foraminifera stage, Arikareean North American Land Mammal age (Wilson 1935; Barnes 1976; Shimada *et al.* 2014; Kimura & Barnes 2016).

NEWLY REFERRED SPECIMEN FROM THE EAST PISCO BASIN. — MUSM 4691, partial cranium lacking the occipital shield and basicranium, with associated partial right mandible. This specimen was found at Roca Negra, a locality close to Zamaca (Fig. 1B). Geographic coordinates: 14°38'59.5"S, 75°38'51.8"W. This cranium was reported in the geological map of Zamaca provided by Di Celma *et al.* (2019) with the field number ZM 36 and referred there to Odontoceti indet. It was collected 25.9 m above the contact with the underlying Otuma Formation in the *Ct1a* facies association (sandstones and conglomerate beds) of the Ct1 allomember of the Lower Miocene Chilcatay Formation (Fig. 1E). The age of *Ct1a* in the Roca Negra-Zamaca areas is constrained between 19.1 and 18.3 Ma (early Burdigalian), based on a Strontium Isotope Stratigraphy analysis of oyster shells collected in the underlying *Ct1c* facies association and shark teeth in the overlying Ct2a facies association, respectively (Bosio *et al.* 2020a, 2022).

DIAGNOSIS. — The differential diagnosis focuses primarily on differences with taxa that were found to be closely related to *Amphidelphis* in our phylogenetic analysis and comparison (other members of the *Chilcacetus* clade, Eoplatanistidae, Eurhinodelphinidae, and Squaloziphiidae). *Amphidelphis bakersfieldensis* n. comb. is a small (bizygomatic width estimated at 174 mm in the holotype), longirostrine, and homodont dolphin species differing from *Argyrocetus patagonicus* in its smaller size, in the rostrum being proportionally considerably shorter (ratio between preorbital width and rostrum length estimated at 0.5), and lacking an extended premaxillary portion, in the dorsal opening of the mesorostral groove being narrower than the premaxilla at rostrum base, in the premaxillary foramen being roughly at the level of the antorbital notch, and in the absence of ankylosis for the symphysis of the mandibles; from '*Argyrocetus*' *joaquinensis* in its smaller size, in the dorsal opening of the mesorostral groove being narrower than the premaxilla at rostrum base, in the presence of more than one dorsal infraorbital foramen at rostrum base, in the proportionally shorter and wider nasals, and in the nasals partly overhanging the bony nares; from *Chilcacetus* in its smaller size, in the rostrum being proportionally shorter, in possessing a deep sulcus anterior to the main dorsal infraorbital foramen at rostrum base, and in the palatines not being separated anteromedially for a long distance at rostrum base; from *Perditicetus* in its smaller size, in the premaxillary foramen being roughly at the level of the antorbital notch, and in the zygomatic process of the squamosal being dorsoventrally more slender; from *Caolodelphis* in its smaller size, the frontals not being separated anteromedially on the vertex, and the basioccipital crests being transversely thinner; from *Macrodelphinus* in its much smaller size, in the rostrum being proportionally shorter and lacking an extended premaxillary portion, in the premaxillary foramen being roughly at the level of the antorbital notch, and in the exposure of the frontals on the vertex being shorter and narrower.
It differs from *Crisocetus*, *Dolgopolis*, *Squaloziphius*, and *Yaquinacetus* in the postglenoid process of the squamosal being significantly shorter anteroposteriorly, and from *Dolgopolis*, *Squaloziphius*, and *Yaquinacetus* in the dorsal opening of the mesorostral groove being more gradual anterior to the bony nares. It differs from most members of other longirostrine to hyper-longirostrine homodont extinct families (including Eoplatanistidae and Eurhinodelphinidae) in the absence of a deep lateral groove along most of the rostrum and in the absence of ankylosis for the symphysis of the mandibles. It further differs from Eurhinodelphinidae in lacking an extended

TABLE 3. — Cranial measurements (in mm) of *Amphidelphis bakersfieldensis* n. comb. YPM 13406 (holotype, Kern County, California, United States) and MUSM 4691 (Chilcatay Formation, East Pisco Basin, Peru), Odontoceti aff. *Amphidelphis bakersfieldensis* MUSM 602 and 4961 (Chilcatay Formation, East Pisco Basin, Peru), compared to *'Argyrocetus' joaquinensis* Kellogg, 1932 USNM 11996 (holotype, Kern County, California, United States). Measurements of YPM 13406 are partly taken from Wilson (1935) and measurements of USNM 11996 are taken from Kellogg (1932). Abbreviations: **c**, taken on a IRSNB cast; **e**, estimate; **+**, incomplete; **–**, no data.

	***Amphidelphis bakersfieldensis* n. comb.**		**Odontoceti aff. *A. bakersfieldenis***		***'Argyrocetus' joaquinensis***
	YPM 13406 (holotype)	**MUSM 4691**	**MUSM 602**	**MUSM 4961**	**USNM 11996 (holotype)**
Total length as preserved	260	438	370	226	370
Rostrum length	+155	e322	+210	–	–
Width of rostrum at mid-length	–	35	–	–	–
Width of premaxillae at mid rostrum length	–	22	–	–	–
Rostrum width at base	e84 (c)	93	e114	e108	108
Width of premaxillae at rostrum base	51 (c)	41	52	e53	–
Maximum opening of mesorostral groove	12	13	–	3	–
Maximum width of premaxillae	64.7	71	72	74	85
Width of right premaxillary sac fossa	25	33	31	–	–
Width of left premaxillary sac fossa	26.6	33.5	34	–	–
Width of bony nares	31.5 (c)	30.5	26	29.5	–
Preorbital width	e145 (c)	165	166	152	176
Orbit length	+45	–	50	46	–
Length of temporal fossa	–	–	–	e71	–
Height of temporal fossa	–	–	–	48	–
Postorbital width	–	–	180	170	e204
Bizygomatic width	e174	–	182	172	e210
Anteroposterior length of nasals along sagittal plane	12	–	+15.5	e18	35
Maximum anteroposterior length of nasal	19	e13	–	–	–
Distance between posterior side of nuchal crest and anteromedial tip of nasal	32 (c)	e36	+33	35	–
Minimum distance between maxillae across vertex	34.6	e45	47	53	–
Minimum distance between temporal crests across occipital shield	–	–	e80	e94	–
Width of occipital condyles	–	–	65	e66	74
Oblique height of right condyle	–	–	34	–	–
Oblique height of left condyle	35	–	33.5	–	44
Oblique width of right condyle	–	–	22	–	–
Oblique width of left condyle	23.6	–	22	–	33
Width of foramen magnum	–	–	29	–	35

edentulous anterior premaxillary portion of the rostrum and in the nasals partly overhanging the bony nares. It further differs from Eoplatanistidae in the premaxillary foramen being roughly at the level of the antorbital notch, in the thinner and flatter antorbital process, in the acute anterior margin of the nasal partly overhanging the bony nares, and in the less anteriorly projected supraoccipital shield.

Remark on the taxonomy and systematics of *Acrodelphis* Abel, 1900 and *Argyrocetus*

Originally placed in the genus *Acrodelphis* as *Acrodelphis bakersfieldensis* n. comb. by Wilson (1935), this species was later referred to the genus *Argyrocetus* by Barnes (1976), together with the type species *Argyrocetus patagonicus* and the other Californian species '*Argyrocetus*' *joaquinensis*. Later, due to the fragmentary state of the type specimens and the lack of synapomorphies for this genus, the referral of the two Californian species to this genus was questioned (Lambert 2005a; Lambert *et al.* 2015). The description of the new specimen MUSM 4691 allows for the identification of major differences with *A. patagonicus*, further supporting the removal of '*Argyrocetus*' *bakersfieldensis* from the genus *Argyrocetus*. The original genus, *Acrodelphis*, has been previously identified by Muizon (1988a) as a junior synonym of *Champsodelphis* Gervais, 1848, and the latter has been regarded in the same work as an incertae sedis, restricted to the type specimen (a partial mandible) of its type species, *Champsodelphis macrogenius* (Fischer, 1829). A new genus name is thus proposed here for '*Argyrocetus*' *bakersfieldensis*.

Description and comparison of the newly referred specimen MUSM 4691 with notes on the holotype

A detailed description of the holotype YPM 13406 is to be found in Wilson (1935), together with interpretive line drawings of the cranium in dorsal and left lateral view. This description is complemented here with photos of the cranium in two pieces (partial rostrum with facial region and detached left portion of the basicranium), as well as of the left humerus and two cervical vertebrae.

General cranial features

Cranial dimensions of MUSM 4691 differ little from the holotype of *Amphidelphis bakersfieldensis* n. comb. YPM 13406 (Table 3; Wilson 1935), being smaller than in *Argyrocetus patagonicus* and '*A.*' *joaquinensis*. The roughly complete, pointed rostrum is moderately elongated (Fig. 16; Appendix 4), with a ratio between preorbital width and rostrum length estimated to 0.51. This ratio is considerably higher than in *Chilcacetus* spp.

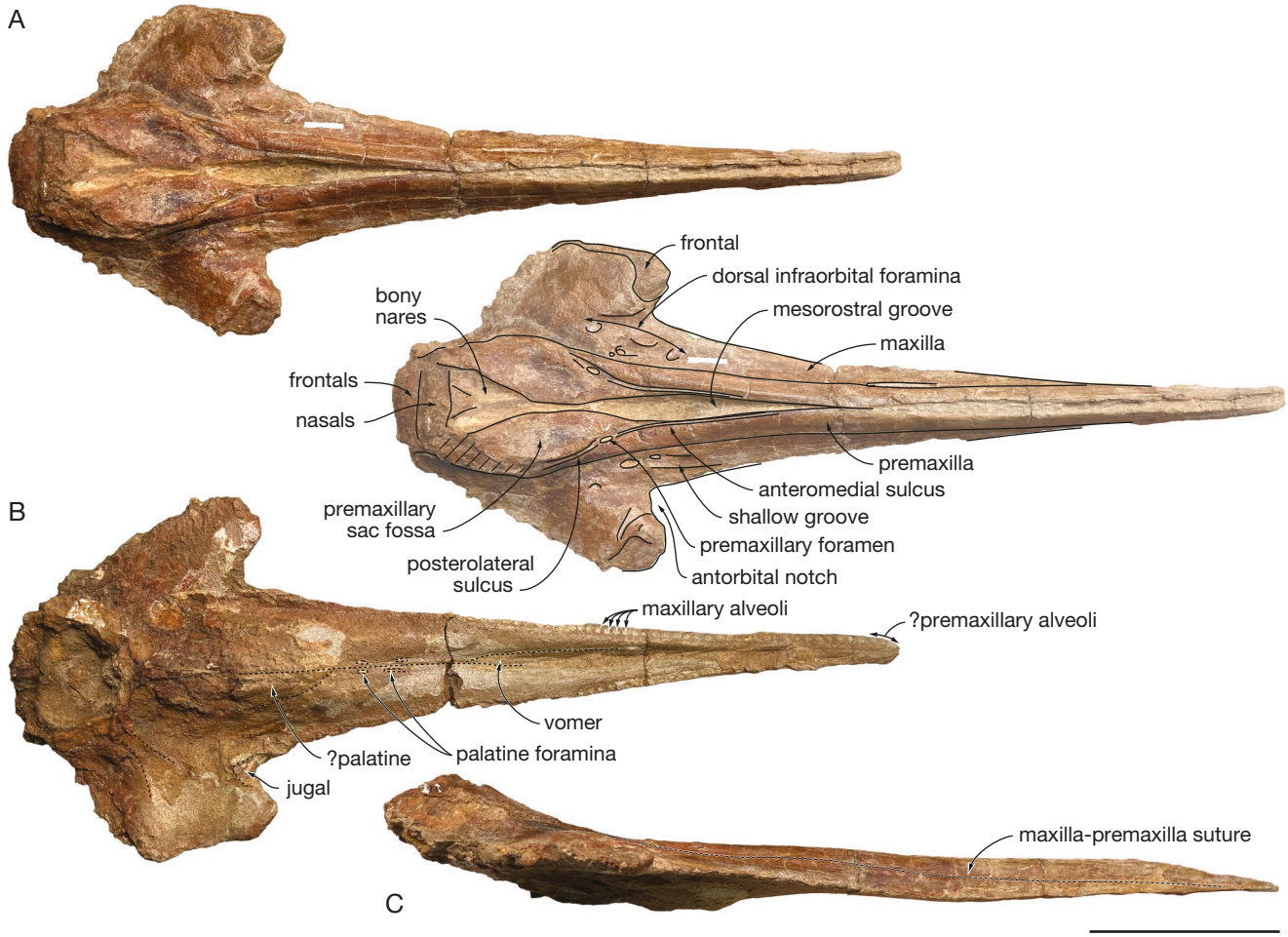

FIG. 16. — Partial cranium of *Amphidelphis bakersfieldensis* n. comb. MUSM 4691 (Chilcatay Formation, East Pisco Basin, Peru) in dorsal view (**A**) with corresponding line drawing, in ventral view (**B**), and in right lateral view (**C**). Hatching for main break surfaces; dashed lines on photo for maxilla-premaxilla suture. Scale bar: 200 mm. Photos by Olivier Lambert.

and, most likely, *Argyrocetus patagonicus*, corresponding to a proportionally shorter rostrum. Though the condylobasal length can only be estimated (between 465 and 480 mm), the rostral index (rostral length/condylobasal length) was most likely in the range of longirostrine odontocetes (between 0.6 and 0.78, see McCurry & Pyenson 2019). The antorbital notches are U-shaped and broadly anterolaterally open (more so on the right side), as in the holotype YPM 13406. The vertex is weakly elevated as seen in lateral view.

Premaxilla

The premaxilla-maxilla suture can be followed until near the anterior end of the maxilla (Fig. 16C), indicating that the premaxillary anterior portion of the rostrum was not as extended as in eurhinodelphinids. Based on the extent of the maxillary portion of the rostrum and the length of the mandible, Cabrera (1926) proposed for the type of *Argyrocetus patagonicus* MLP 5-7 a more than 200 mm-long premaxillary portion of the rostrum. He also suggested that this premaxillary portion was edentulous in the latter, as in eurhinodelphinids. The upper alveolar groove of *Amphidelphis bakersfieldensis* n. comb. MUSM 4691 reaches the tip of the rostrum (Fig. 16B), indicating that there was no edentulous premaxillary portion in this species. Premaxillae are incomplete dorsally in the anterior part of the rostrum. The dorsal opening of the mesorostral groove in this region is thus at least partly artificial. From a level 115 mm anterior to the antorbital notches, both premaxillae contact each other dorsomedially for 25 mm, before a broad, spindle-shaped dorsal opening of the mesorostral groove, as in YPM 13406 (Fig. 17A). The premaxillary foramen is 15 mm posterior to the antorbital notch on the right side and 25 mm posterior on the left side, while in YPM 13406 the right premaxillary foramen is only 7.5 mm posterior to the corresponding antorbital notch. The anteromedial sulcus is long (about 82 mm on the right side and at least 76 mm on the left side). The dorsal surface of the narrow prenarial triangle is approximately flat and horizontal. The relatively deep posterolateral sulcus runs until the anterior margin of the bony nares, as in YPM 13406, and the posteromedial sulcus is indistinct. As in YPM 13406, on the lateral edge of the transversely and anteroposteriorly concave premaxillary sac fossa, the premaxilla is dorsoventrally thick, forming a pedestal medial to the posterolateral sulcus. While the dorsal part of the ascending process is abraded on

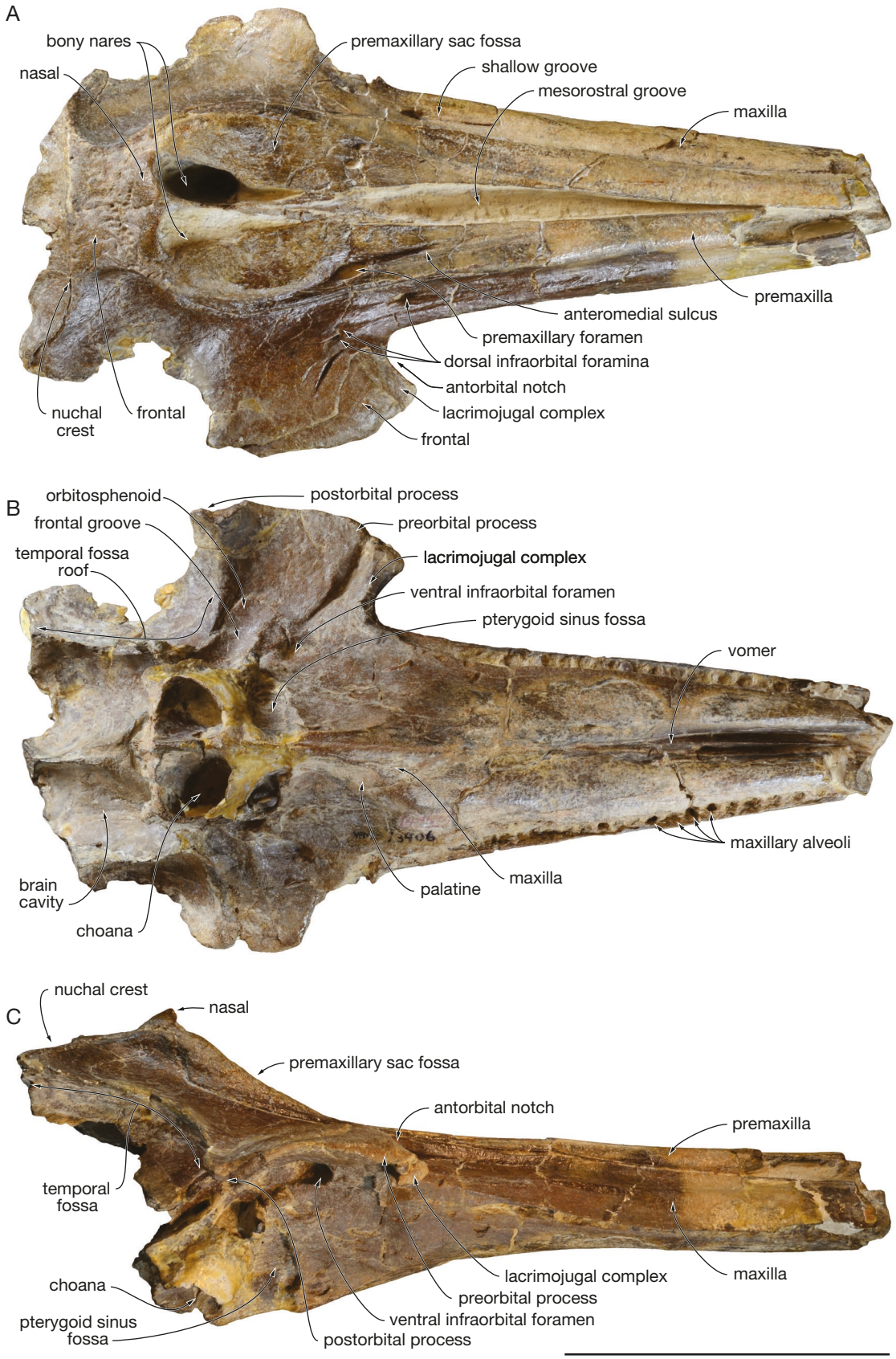

FIG. 17. — Partial cranium of *Amphidelphis bakersfieldensis* n. comb. YPM 13406 (holotype, Kern County, California, United States) in dorsal (**A**), ventral (**B**), and right lateral (**C**) view. Scale bar: 100 mm. Credits: Photos by Advait Jukar. Photos by Olivier Lambert.

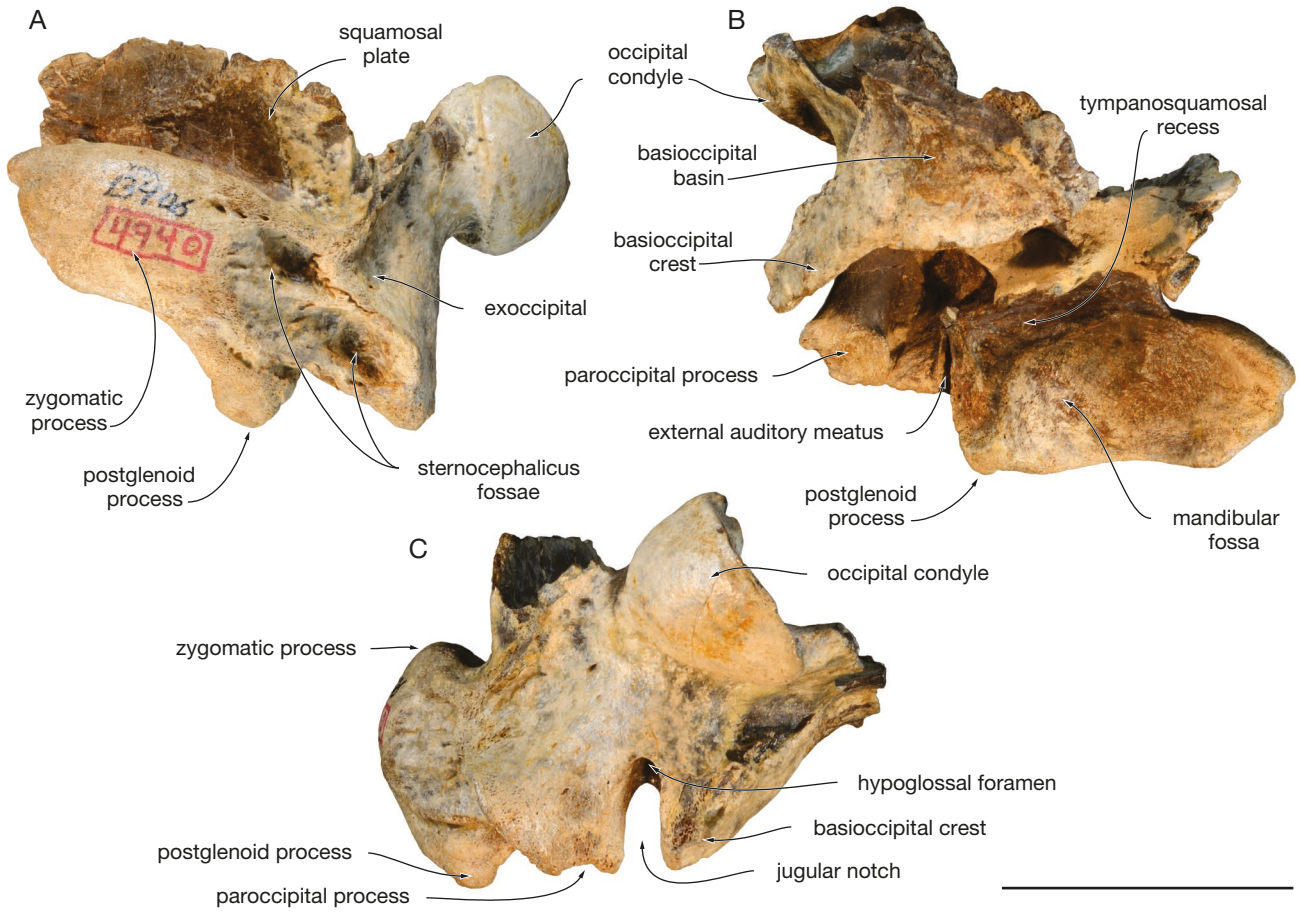

Fig. 18. — Detached left part of the basicranium of *Amphidelphis bakersfieldensis* n. comb. YPM 13406 (holotype, Kern County, California, United States) in lateral (**A**), ventral (**B**), and posterior (**C**) view. Scale bar: 50 mm. Credits: Photos by Advait Jukar. Photos by Olivier Lambert.

the right side, the roughly complete left side reveals a moderately pointed posterior end of the premaxilla, displaying an extensive contact with the corresponding nasal.

Maxilla

In dorsal view, the maxilla is wider than the premaxilla at the level of the antorbital notch (Fig. 16A), a condition that differs from YPM 13406. As noted by Wilson (1935), the maxilla of YPM 13406 is marked by a shallow and broad longitudinal groove extending on the maxilla, below the premaxilla-maxilla suture, for 100-120 mm anterior to the anteriormost dorsal infraorbital foramen. A similar groove extends forwards for only about 40 mm in MUSM 4691. In both specimens the groove is less developed than the deep lateral groove following the premaxilla-maxilla suture, on a much longer distance, in various clades of longirostrine to hyper-longirostrine odontocetes. On the right side, a small (transverse diameter 1.5 mm) dorsal infraorbital foramen is just anterior to the antorbital notch; a larger foramen (diameter 4.5 mm) is slightly posterior to the notch; and a smaller foramen (diameter 2 mm) is 25 mm posterior to the notch. Three dorsal infraorbital foramina are also observed on the left side: the first is posteromedial to the notch (diameter 4 mm); the second is just posteromedial (diameter 2.5 mm); and the third is posterolateral (diameter 3 mm). In the slightly dorsally domed antorbital region, the maxilla only partly covers the frontal, with a dorsal exposure of the latter that has an outline strikingly similar to YPM 13406 (Fig. 17A). As in the latter, a deep oblique groove directed towards the antorbital notch marks the dorsal surface of the right maxilla in this region.

In lateral view, the maxilla-premaxilla suture raises posterodorsally from about mid rostrum length, becoming slightly dorsally convex in the posterior part of the rostrum (Fig. 16C). The ventral surface of the rostrum is relatively flattened, and the alveolar groove is close to the lateral margin (Fig. 16B), a condition that is reminiscent of *Yaquinacetus meadi*. Part of the upper alveoli are preserved on both sides. As mentioned above, the anteriormost alveoli may correspond to premaxillary teeth, though most preserved alveoli are located in the maxilla. 31 small, circular alveoli with a diameter ranging from 2.5 to 3 mm are counted on a length of 155 mm, with interalveolar septa ranging from 2 to 3 mm in length. This corresponds to 20 alveoli for 100 mm, a number that is close to YPM 13406 (20 alveoli for 108 mm; Wilson 1935; Fig. 17B). One pair of tiny palatine foramina is located 65 mm anterior to the level of the antorbital notches, each followed anteriorly by a narrow sulcus; a second pair may be present 8 mm posteriorly, but the surface is too damaged for a clear identification.

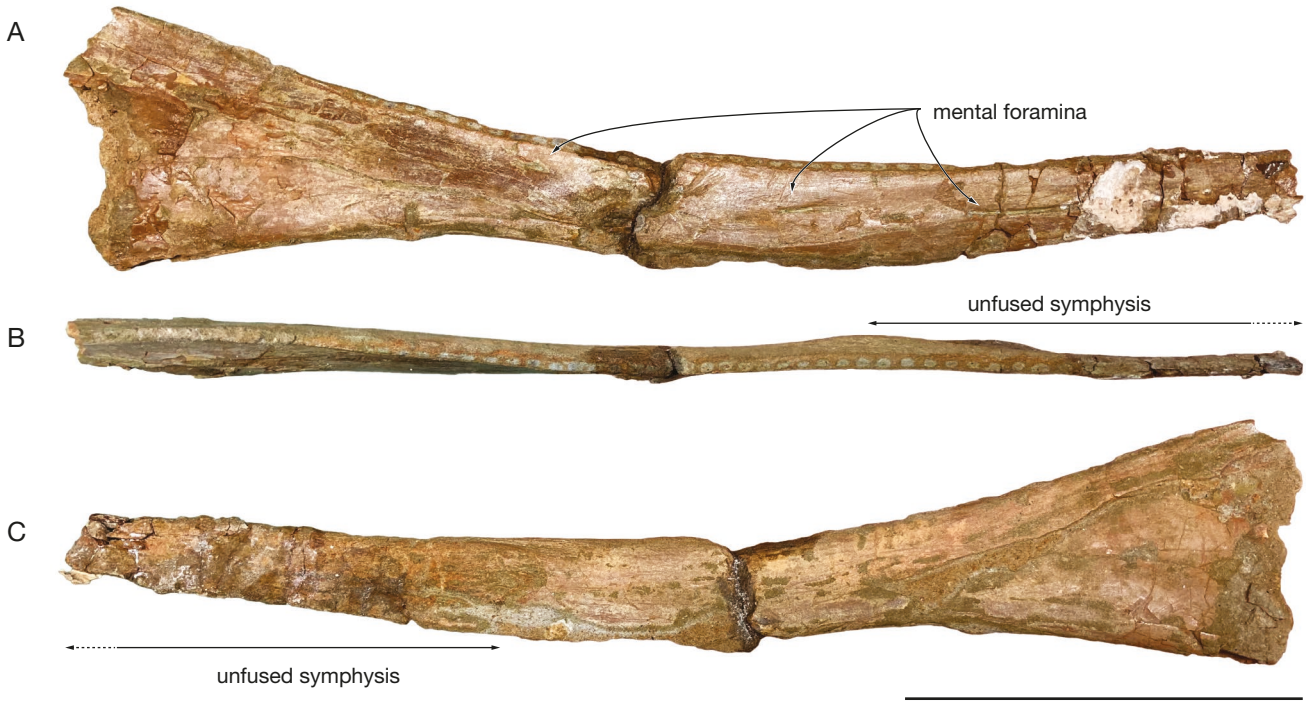

FIG. 19. — Partial right mandible of *Amphidelphis bakersfieldensis* n. comb. MUSM 4691 (Chilcatay Formation, East Pisco Basin, Peru) in lateral (**A**), dorsal (**B**), and medial (**C**) view. Scale bar: 100 mm. Photos by Olivier Lambert.

Nasal
The nasal extends dorsally higher than the frontal, making the top of the cranium. The anterodorsal portion of each nasal is strongly abraded, indicating that it may have been as dorsally elevated as in YPM 13406 (Fig. 17C) and *Argyrocetus patagonicus* (nasals of the type MLP 5-7 are now lost, but original illustrations of the skull by Lydekker (1893: plate 5) reveal anterodorsally elevated nasals).

Frontal
The frontal-supraoccipital suture is possibly preserved, 10 mm anterior to the preserved posterior edge of the specimen (Fig. 16A); if correct, this interpretation indicates a 10 mm-long frontal exposure on the vertex, with a smooth, slightly transversely convex dorsal surface. In lateral view, the preorbital process is dorsoventrally thin, as in YPM 13406 (Fig. 17C). Both postorbital processes are missing, and the preserved lateral margin of the orbit roof is slightly ventrally concave in lateral view.

Jugal
Only the preserved base of the styliform process is visible posteromedial to the antorbital notch (Fig. 16B).

Squamosal
Not preserved in MUSM 4691, the squamosal displays a relatively short and dorsoventrally high zygomatic process with a distinctly convex dorsal outline in the holotype YPM 13406 (Fig. 18A). The irregular outline of its anterior tip both in ventral and lateral view suggests that it may be incomplete. Two deep sternocephalicus fossae extend to a level slightly anterior to the ventral tip of the postglenoid process. Both fossae are visible in posterior view, not being hidden by the exoccipital. The postglenoid process is moderately anteroposteriorly thickened, with a rounded ventral outline in lateral view. Its medial wall is invaded by the posterolateral part of the tympanosquamosal recess (Fig. 18B). The latter extends anteriorly along the medial side of the broad mandibular fossa, ending approximately at the level of the anterior margin of the squamosal fossa.

Exoccipital/basioccipital
In the holotype, the left paroccipital process is separated from the transversely thin basioccipital crest by a deep and narrow jugular notch, in which the hypoglossal foramen is visible (Fig. 18C).

Mandible
The right mandible of MUSM 4691 is preserved on a length of 310 mm, including 114 mm of the posterior part of the symphyseal region (Fig. 19). The symphysis is not ankylosed, a major difference with eurhinodelphinids. This region is narrow, with height and width of the bone at the end of the symphysis being 27 and 10 mm, respectively. Posterior to the symphysis, the ventral margin of the bone is moderately concave in lateral view. Approximately 34 small alveoli (diameter between 3 and 3.5 mm) are counted on a length of 172 mm, with interalveolar septa 2 to 2.5 mm long. This count for lower alveoli matches well the upper count.

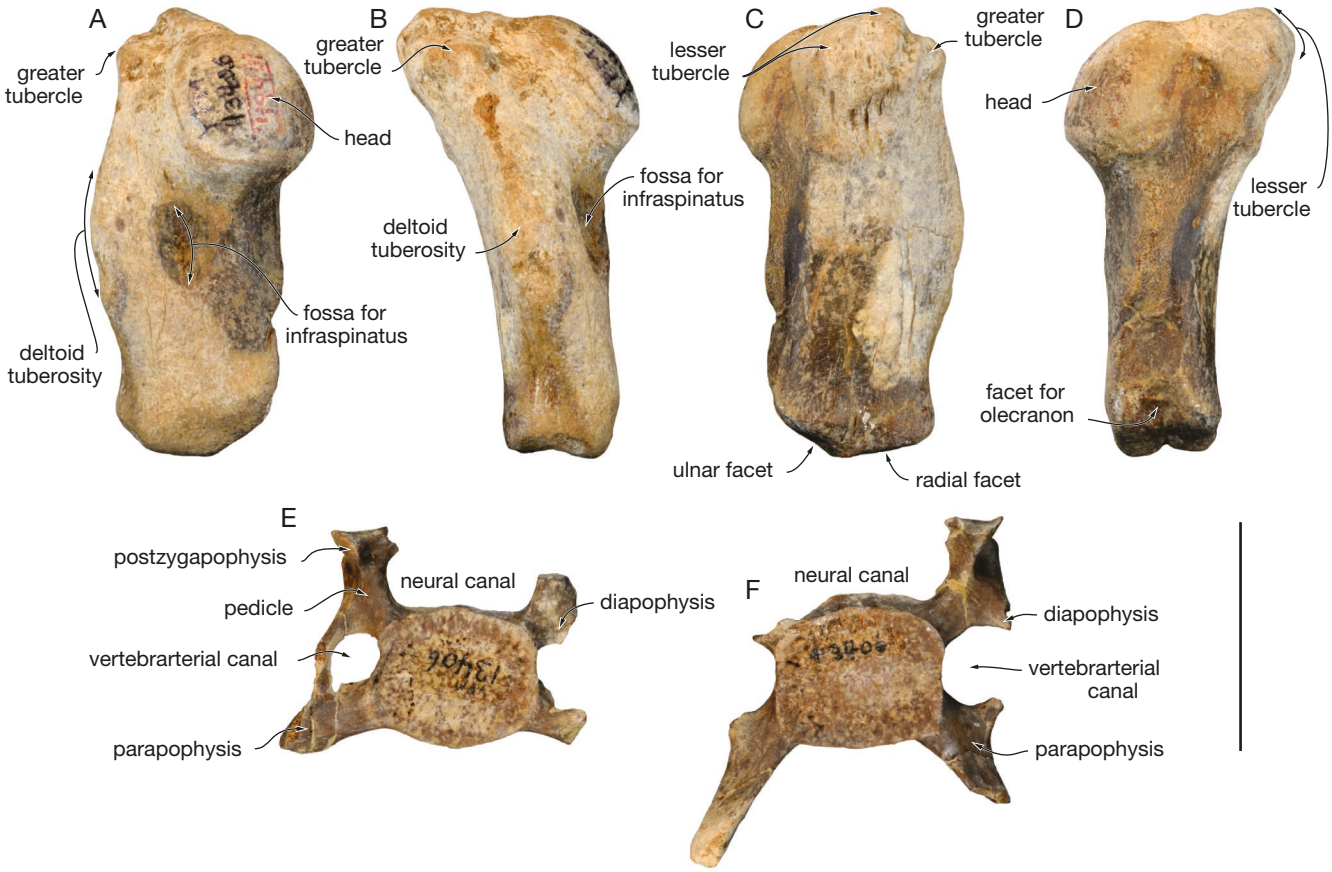

Fig. 20. — Left humerus and two cervical vertebrae of *Amphidelphis bakersfieldensis* n. comb. YPM 13406 (holotype, Kern County, California, United States). Humerus in lateral (**A**), anterior (**B**), medial (**C**), and posterior (**D**) view; ?4th cervical in posterior view (**E**); 6th cervical in posterior view (**F**). Scale bar: 50 mm. Credits: Photos by Advait Jukar.

Humerus

The left humerus of the holotype YPM 13406 (Fig. 20A-D) is characterized by a low greater tubercle which does not extend as far proximally as the robust lesser tubercle, a proximo-distally long but moderately prominent deltoid tuberosity that is centered at about mid-length of the diaphysis, a deep fossa for the infraspinatus, and a short facet for the olecranon (see comparison with humeri of *Chilcacetus ullujayensis* n. sp. and *Macrodelphinus kelloggi* above). Measurements are provided in Wilson (1935: 69).

Cervical vertebrae

A description and measurements of the two unfused cervical vertebrae of the holotype YPM 13406 (Fig. 20E, F), identified there as C4 and C6, are provided in Wilson (1935: 67, 68). Though the centra are described as anteroposteriorly short by Wilson (1935) (ratio between width and length without epiphyses = 3.9 in C4 and ratio between width and length with one epiphysis = 2.6 in C6), their proportions do not differ much from the cervicals of *Xiphiacetus cristatus*, comparable to the extant freshwater dolphins *Inia* Orbigny, 1834 and *Platanista* Wagler, 1830 (Lambert 2005a).

Comments

Despite a few minor differences with the holotype YPM 13406, including a slightly wider dorsal opening of the mesorostral groove, a relatively broader dorsal exposure of the maxilla at rostrum base, and a slightly more anterior premaxillary foramen, MUSM 4691 is morphologically similar enough to YPM 13406 to allow for its attribution to the same species, *Amphidelphis bakersfieldensis* n. comb. Differences between these two individuals may be explained by intraspecific variation; YPM 13406 represents for example a relatively young animal, as indicated by unfused epiphyses for two cervical vertebrae (Fig. 20E, F; Galatius & Kinze 2003)

The attribution of MUSM 4691 to *A. bakersfieldensis* n. comb. provides information on cranial regions that are not preserved in the holotype. The anterior portion of the rostrum is especially informative for the comparison with *Argyrocetus patagonicus* and eurhinodelphinids.

Odontoceti aff. *Amphidelphis bakersfieldensis* n. comb. (Figs 21-25)

Referred specimens from the East Pisco Basin. — MUSM 602, partial cranium lacking the anterior part of the rostrum, part of the roof of the temporal fossae, ear bones, and teeth, with the ventral surface of the basicranium and palate damaged. This specimen was collected in 1993 by M. Urbina in an undetermined level of the Lower Miocene Chilcatay Formation from the locality of Zamaca (Fig. 1B). MUSM 4961, partial cranium lacking most

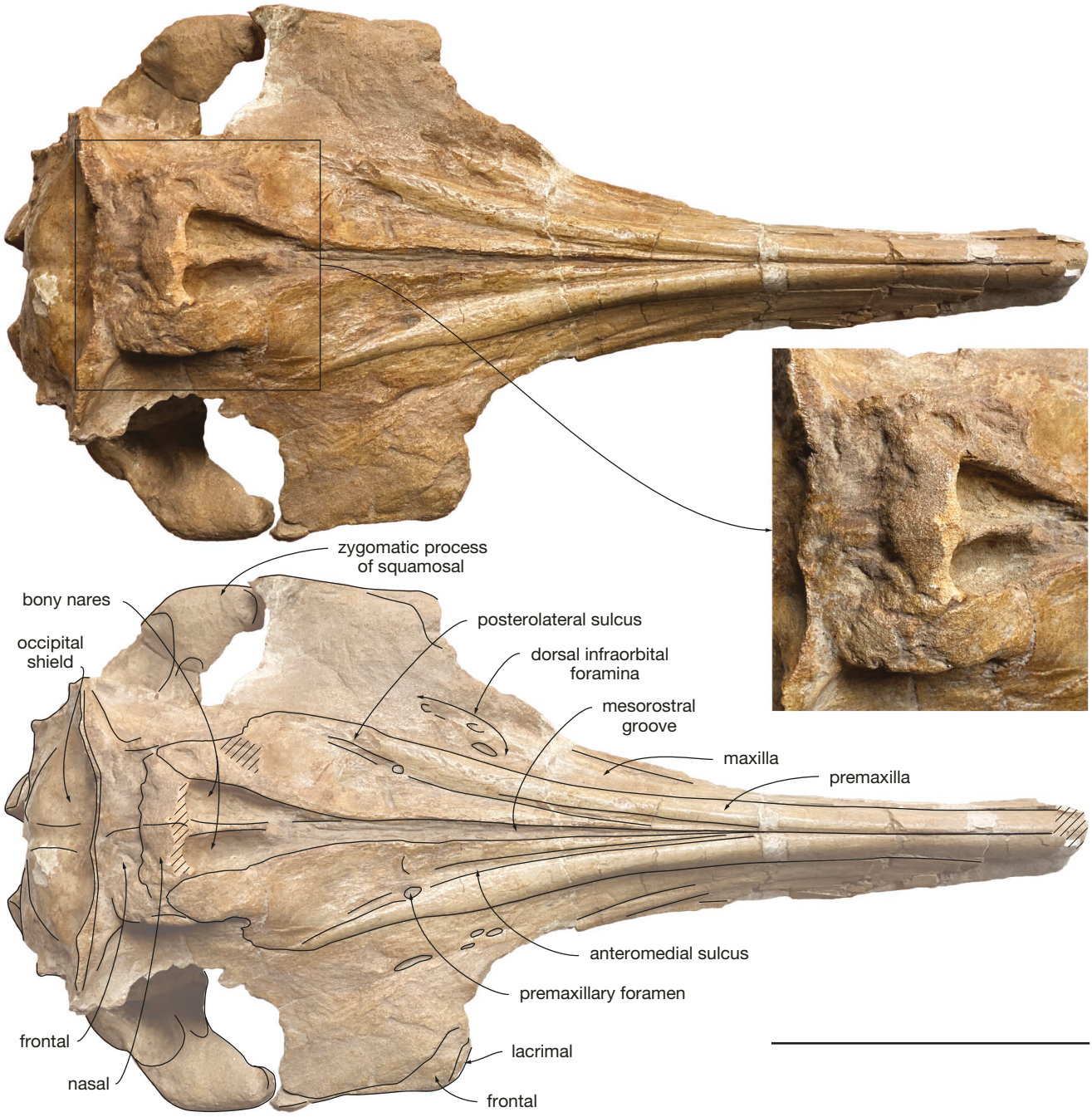

Fig. 21. — Partial cranium of Odontoceti aff. *Amphidelphis bakersfieldensis* MUSM 602 (Chilcatay Formation, East Pisco Basin, Peru) in dorsal view with corresponding line drawing and detail view of the vertex in dorsal view. Hatching for main break surfaces. Scale bar: 100 mm. Photos by Olivier Lambert.

of the rostrum, ear bones, and teeth, with superficial bone being either damaged or covered with a thin layer of hard sediment in many regions of the neurocranium. This specimen was collected at an unknown date by M. Urbina in an undetermined level of the Chilcatay Formation from the locality of Roca Negra (Fig. 1B; see Lambert *et al.* 2018). Considering the above-mentioned dates obtained through $^{40}Ar/^{39}Ar$ radiometric analyses and Strontium Isotope Stratigraphy, and in agreement with silicoflagellate and diatom biostratigraphy, the age of MUSM 602 can be restricted between 19.3 and 17.95 Ma and the age of MUSM 4961 between 19.3 and 18.3 Ma (both Burdigalian) (Lambert *et al.* 2018; Di Celma *et al.* 2019; Bosio *et al.* 2020b).

Description of referred specimens

Most of the description is based on the better-preserved cranium MUSM 602 (Figs 21-24), except for the few parts that are only preserved in MUSM 4961 (Fig. 25; Appendix 5), that differ between the two specimens, or that display shared differences with *Amphidelphis bakersfieldensis* n. comb. Both specimens have similar cranial dimensions, with MUSM 4961 being only slightly smaller. Except for the vertex of the cranium that is transversely broader than in YPM 13406, no marked differences are noted with specimens of *A. bakersfieldensis* n. comb.

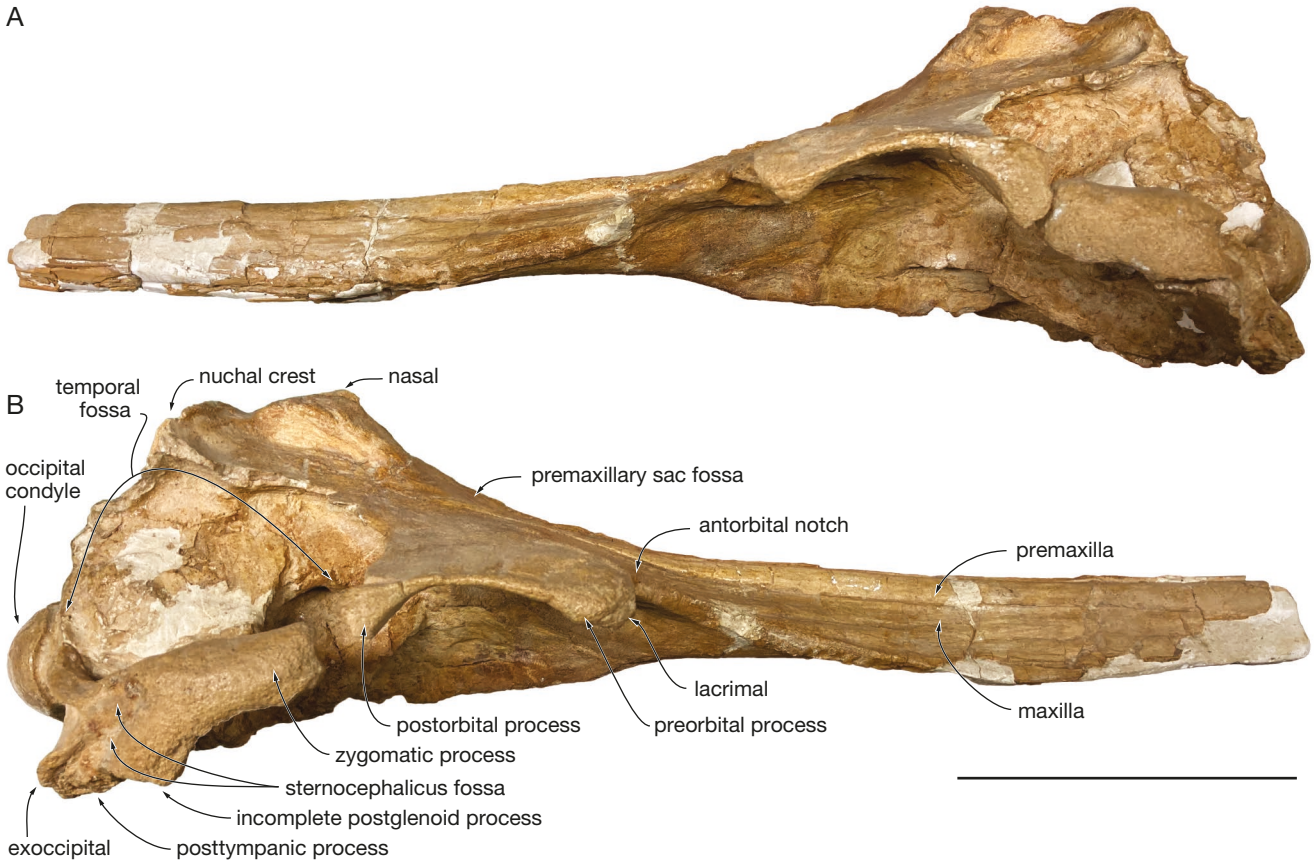

FIG. 22. — Partial cranium of Odontoceti aff. *Amphidelphis bakersfieldensis* MUSM 602 (Chilcatay Formation, East Pisco Basin, Peru) in left (**A**) and right (**B**) lateral view. Scale bar: 100 mm. Photos by Olivier Lambert.

Premaxilla

Though the rostrum of MUSM 602 appears to be slightly transversely crushed in its anterior portion, right and left premaxillae most likely contacted each other dorsomedially for at least 100 mm, before a gradual divergence of the medial margins towards the bony nares (Fig. 21). In both specimens, and to an even greater extent in MUSM 4961 (Fig. 25A), the resulting dorsal opening of the mesorostral groove is narrower than in MUSM 4691 and YPM 13406 (and also '*Argyrocetus*' *joaquinensis*, as well as squaloziphiids) and is not spindle-shaped. In MUSM 602, the premaxillary foramen is 15 mm posterior to the antorbital notch on the right side and 20 mm posterior on the left side. As in *Amphidelphis bakersfieldensis* n. comb., the anteromedial sulcus is long (110 mm on the right side and 120 mm on the left). At least in MUSM 602, the prenarial triangle is longer than in *A. bakersfieldensis* n. comb. The posteromedial sulcus is poorly defined, and the posterolateral sulcus is narrow, becoming nearly indiscernible before the anterior margin of the bony nares. The premaxillary sac fossae are generally less dorsally elevated in MUSM 602 (but not in MUSM 4961) than in *A. bakersfieldensis* n. comb.; they are transversely concave, with an anterior portion that is also longitudinally concave while the thicker posterior portion has a roughly flat surface. At the level of the anterior margin of the bony nares, the lateral margin of each premaxilla is laterally concave, with an abrupt posteromedial turn at mid length of the bony nares. Better preserved on the right side of MUSM 602, the ascending process of the premaxilla is narrower than in MUSM 4691 and YPM 13406, with parallel lateral and medial margins, a condition that is reminiscent of *Squaloziphius emlongi* and *Yaquinacetus meadi*. Posteromedially, each premaxilla broadly contacts the corresponding nasal. Due to the complex and not fully resolved outline of the nasal-frontal suture, the presence of a contact between premaxilla and frontal on the vertex cannot be assessed.

Maxilla

Along the rostrum base, the lateral margin of the maxilla is incomplete in MUSM 602. In MUSM 4961, this margin is directed more posterolaterally than in MUSM 4691 and YPM 13406, suggesting that both MUSM 602 and MUSM 4961 had a broader rostrum base compared to *A. bakersfieldensis* n. comb. In both MUSM 602 and 4961, the lateralmost portion of the dorsal surface of the maxilla is moderately thickened just anteromedial to the antorbital notch (maxillary flange). In both MUSM 602 and MUSM 4961, the antorbital notch is much more laterally open and shallow than in MUSM 4691 and YPM 13406; differing from the latter (and also *Chilcacetus* spp., *Macrodelphinus kelloggi*, *Perditicetus yaconensis*, *Squaloziphius emlongi*, and *Yaquinacetus meadi*), the antorbital region does not extend anterior to the bottom of the antorbital notch, in a way more similar to '*Argyrocetus*'

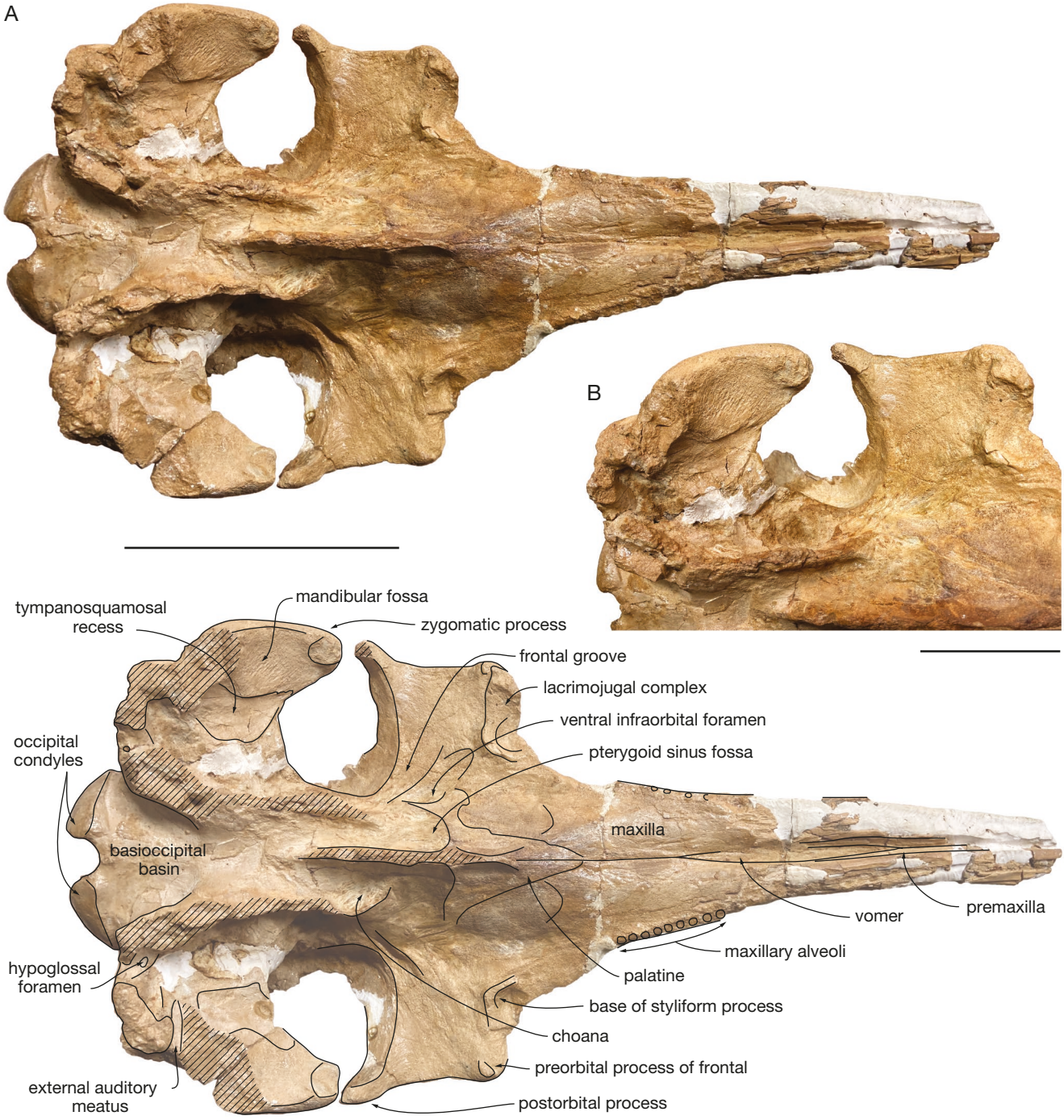

Fig. 23. — Partial cranium of Odontoceti aff. *Amphidelphis bakersfieldensis* MUSM 602 (Chilcatay Formation, East Pisco Basin, Peru) in ventral view (**A**) with corresponding line drawing and detail view of the right half of the basicranium in ventral view (**B**). Hatching for main break surfaces. Scale bars: A, 100 mm; B, 50 mm. Photos by Olivier Lambert.

joaquinensis. The dorsal surface of the maxilla is flat in this area. In MUSM 602, four dorsal infraorbital foramina are present in the right antorbital notch region and three in the left region. Along the vertex, the dorsomedial margin of the maxilla overhangs the more ventral part of the bone. Posteriorly, the maxilla similarly raises abruptly to contribute to the acute nuchal crest. Roughly rectilinear along the vertex, the nuchal crest turns moderately posterolaterally towards the posteriormost part of the roof of the temporal fossa. Roughly complete in MUSM 4961, the posterolateral corner of the maxilla is more medial than the postorbital process in dorsal view, indicating that the posterior part of the temporal fossa remained dorsally open to an extent similar to YPM 13406 (at least for the right side of the latter).

In ventral view, a few small maxillary alveoli are visible in the posterior portion of the alveolar groove (Fig. 23A). The first posterior alveolus is 50 mm anterior to the antorbital notch, but it cannot be excluded that a few more posterior alveoli

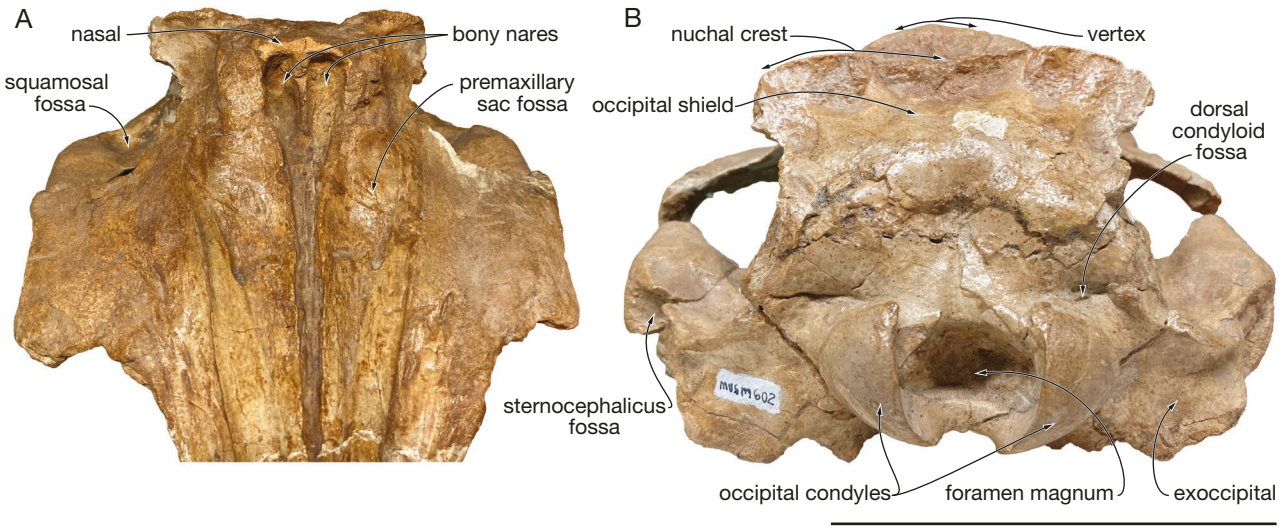

FIG. 24. — Partial cranium of Odontoceti aff. *Amphidelphis bakersfieldensis* MUSM 602 (Chilcatay Formation, East Pisco Basin, Peru) in anterodorsal (**A**) and posterior (**B**) view. Scale bar: 100 mm. Photos by Olivier Lambert.

have been abraded. The mean diameter of the preserved alveoli is 3 mm and interalveolar septa are short, 1-2 mm long, a condition that does not differ substantially from *Amphidelphis bakersfieldensis* n. comb.

Vomer

In MUSM 602, the vomer is exposed in the vomerine trough from a level 62 mm anterior to the antorbital notch (Fig. 23A).

Lacrimojugal complex

Better preserved on the right side of MUSM 602, the lacrimojugal complex sends a thin plate laterally, anteroventral to the preorbital process of the frontal (Fig. 23). A similar plate is instead directed anterolaterally in *Amphidelphis bakersfieldensis* n. comb. This plate thickens dorsoventrally in its lateralmost portion, up to 7 mm.

Palatine/pterygoid

The pointed anterior end of the joined palatines is 23 mm anterior to the level of the antorbital notch in MUSM 602. The palatine-maxilla suture gradually diverges posterolaterally for about 20 mm before abruptly turning towards the ventral infraorbital foramen. No parts of the pterygoid could be identified on any of the two specimens, except for part of the medial lamina along the pharyngeal crest. The pterygoid sinus fossa is anteriorly short, with an anterior margin 25 mm posterior to the level of the antorbital notch, a feature that is similarly seen in *Amphidelphis bakersfieldensis* n. comb., *Chilcacetus* spp., *Macrodelphinus kelloggi*, *Perditicetus yaconensis*, and *Yaquinacetus meadi*; the fossa is somewhat anteriorly longer in *Squaloziphius emlongi* and, to a greater extent, *Dolgopolis kinchikafiforo*.

Nasal

As in *Amphidelphis bakersfieldensis* n. comb., the top of the cranium is made by the nasals, with a dorsal surface sloping posteroventrally (Figs 21; 22; 24A). Their anterodorsal portion is damaged in MUSM 602; the break surface suggests that each nasal originally projected anterodorsally, as seen in YPM 13406, overhanging the bony nares for more than 4 mm, in a way similar to *Chilcacetus* spp. The outline of the nasal-frontal suture is complex and difficult to interpret, due to a series of deep grooves, as in YPM 13406, but also *Chilcacetus cavirhinus* and *Yaquinacetus meadi*. The nasals were either as long or longer than the frontals on the vertex. As preserved, the left nasal is wider than long.

Frontal

As in YPM 13406, the dorsal surface of the frontals on the vertex of MUSM 602 and MUSM 4961 is irregular, marked by a series of meandering grooves, pits, and crests, a feature also seen for example in *Chilcacetus cavirhinus* and *Macrodelphinus kelloggi*.

As in *Amphidelphis bakersfieldensis* n. comb., the preorbital process of the frontal is dorsally exposed. In lateral view (Fig. 22), it is only moderately thickened and anteroventrally margined by the lacrimal. Better preserved on the left side of MUSM 602 and right side of MUSM 4961, the postorbital process is robust and directed ventrally. Except for the right side of MUSM 602, the posterior surface of the postorbital process roughly contacts the similarly robust anterior margin of the zygomatic process of the squamosal. A slight degree of post-mortem deformation may have either separated the two bones on the right side of MUSM 602 or, less likely, brought these closer to each other on the left side of the latter and in MUSM 4961. In ventral view, the infratemporal crest is distinct from the tip of the postorbital process to the posterior wall of the frontal groove, as seen in YPM 13406.

Supraoccipital

The dorsomedial part of the occipital shield is anteroposteriorly concave, this depressed region being anteriorly defined by the high posterior wall of the nuchal crest (Figs 21; 22; 24A). From the nuchal crest, the surface of the shield leaves

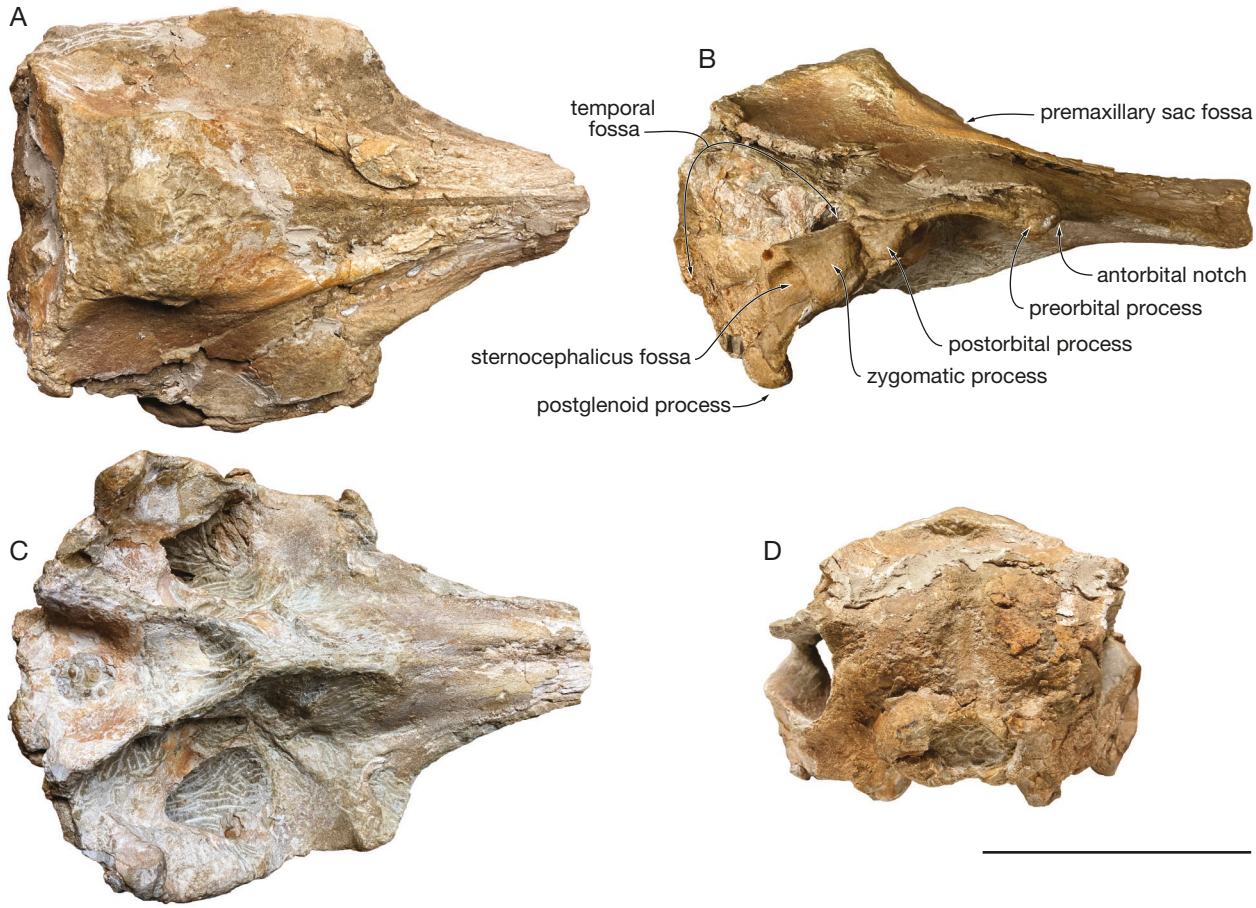

Fig. 25. — Partial cranium of Odontoceti aff. *Amphidelphis bakersfieldensis* MUSM 4961 (Chilcatay Formation, East Pisco Basin, Peru) in dorsal (**A**), right lateral (**B**), ventral (**C**), and posterior (**D**) view. Scale bar: 100 mm. Photos by Olivier Lambert.

in a nearly horizontal posterior direction, as in YPM 13406, before becoming markedly anteroposteriorly convex. A broad, longitudinal groove separates two posteriorly swollen regions corresponding to the right and left brain hemispheres. Only partly preserved in both specimens, the temporal crest was originally short but distinct, and directed posterolateroventrally.

Exoccipital

The occipital condyles protrude posterior to the rest of the exoccipital, with a well-defined condylar neck and moderately excavated dorsal condyloid fossae (Figs 22; 24B). The posterior surface of the exoccipital slopes more posteroventrally in MUSM 602 compared to MUSM 4961 and YPM 13406, but this may be the result of some post-mortem deformation. The jugular notch is too incomplete on the two specimens to be compared to the deep notch observed in *Amphidelphis bakersfieldensis* n. comb. YPM 13406.

Basioccipital

Only the dorsal part of the basioccipital crests is preserved in both specimens, defining a basioccipital basin that is narrow anteriorly (38 mm at about the posterior tip of the pterygoids in MUSM 602), with a gradual posterior widening (distance between the two crests reaching 45 mm at their posterior end). The medial surface of each crest is marked by a ridge that turns anterodorsally and dorsomedially.

Squamosal

The outline of the zygomatic process of the squamosal varies from one side to the other and from one specimen to the other (Figs 22; 25B). It is more slender, anteroposterioly elongated on the right side of MUSM 602 and markedly dorsoventrally thicker (22 mm) and shorter on the right side of MUSM 4961, with intermediary conditions on the left side of MUSM 602 and left side of MUSM 4961. The preserved right zygomatic process of *Amphidelphis bakersfieldensis* n. comb. YPM 13406 (Fig. 18A) is more similar to the left side of MUSM 4961. The anterior margin of the process is anteriorly concave in lateral view, with a shallow transverse groove at mid-height possibly corresponding to the surface of contact with the postorbital process of the frontal. The shape of the dorsal margin of the zygomatic process varies also markedly, from roughly rectilinear on the right side of MUSM 602 and left side of MUSM 4961 to concavo-convex on the other sides of these two specimens, with a specially dorsally bulging posterior part on the left side of MUSM 4961. Such a variation may be related to a highly variable development of the sternocephalicus fossa, which is much deeper and anteriorly extended on the right side of

MUSM 4961 and, probably, the left side of MUSM 602. Such an extent of morphological variation between the two sides of a single specimen should urge to remain cautious with the use of zygomatic process characters to diagnose new taxa. On the right side of MUSM 602, the sternocephalicus fossa is subdivided in two fossae by a thick oblique crest, a condition that is similarly observed in YPM 13406.

Only preserved in MUSM 4961 (Fig. 25B), the postglenoid process is ventrally long, reaching much farther than the posttympanic process, and slightly anteroposteriorly longer (more than 19.5 mm) than transversely thick (18 mm) on the left side. This process appears only slightly anteroposteriorly longer than in YPM 13406 and does not differ much from '*Argyrocetus*' *joaquinensis*, *Caolodelphis milleri*, *Chilcacetus ullujayensis* n. sp., and *Perditicetus yaconensis*. Based on the preserved proximal part, similar proportions of the postglenoid process can be proposed for MUSM 602. As for the corresponding zygomatic process, the right postglenoid process of MUSM 4961 displays unusual proportions, forming an oblique plate that is 10 mm thick and 22 mm long. It cannot be excluded that such a highly asymmetric condition is pathological.

In ventral view, the tip of the ventral surface of the zygomatic process displays a circular articulation surface for the jugal, with an anteroposterior diameter of 12 mm in MUSM 602 (Fig. 23). The mandibular fossa is broad (24 mm on the right side) and medially margined by a shallow tympanosquamosal recess. Separated from the mandibular fossa by a well-defined step, the latter extends anterolaterally for a short distance beyond the level of the anterior margin of the squamosal fossa, in a way similar to YPM 13406. The falciform process is not adequately preserved in any of the two specimens.

The squamosal fossa is shorter in MUSM 4961 compared to MUSM 602, lacking the anterior part with an anteroposteriorly convex floor seen in the latter.

Comments

These two crania are highly similar in both their dimensions and main cranial features. Several differences were noted above, and those mostly focus on the squamosal (zygomatic process, sternocephalicus fossa, and postglenoid process). Because strong differences are also noted between the left and right sides of one specimen for this region, their diagnostic value can be reasonably questioned. Therefore, it is proposed that MUSM 602 and MUSM 4961 belong to the same species. As they share several differences with *Amphidelphis bakersfieldensis* n. comb. MUSM 4691 and YPM 13406, including the outline of the rostrum base in dorsal view, the shape of the antorbital notch, and the extent of the dorsal opening of the mesorostral groove at rostrum base, it cannot be excluded that they correspond to another, closely related species. Furthermore, the lack of more anterior sections of the rostrum prevents from investigating the relative anterior extent of the premaxilla and maxilla, a key character to test for eurhinodelphinid affinities. Pending the discovery of more complete and better-preserved specimens to provide diagnostic characters, it is proposed to identify these two specimens as Odontoceti aff. *A. bakersfieldensis* n. comb.

PHYLOGENETIC ANALYSIS

When comparing the results between analyses with equal weights and implied weights (down-weighting homoplastic characters, with K = 3, 6, 9, and 12), in all analyses, both *Amphidelphis bakersfieldensis* n. comb. and *Chilcacetus* spp. are recovered as late branching stem odontocetes. In all analyses (Fig. 26; Appendix 9), they are part of a clade also including *Macrodelphinus kelloggi*, *Eoplatanista* spp. and a monophyletic Eurhinodelphinidae. In only part of the analyses (K = 3, 6), this clade also includes squaloziphiids (*Squaloziphius emlongi* and *Yaquinacetus meadi*), as well as, more surprisingly, the heterodont dolphin *Inticetus vertizi* Lambert, Muizon, Malinverno, Di Celma, Urbina & Bianucci, 2017 and the ziphiid *Ninoziphius platyrostris* Muizon, 1983. In other analyses, squaloziphiids form either a clade that is stem (k = 9, 12) or a paraphyletic group that is crown (equal weights) to the clade including *A. bakersfieldensis* n. comb., *Chilcacetus* spp., *Eoplatanista* spp., *M. kelloggi*, and Eurhinodelphinidae, *I. vertizi* is the earliest taxon to branch, and *N. platyrostris* is in the crown group, among ziphiids. Finally, *Chilcacetus cavirhinus* and *Chilcacetus ullujayensis* n. sp. are recovered as sister groups in two analyses (k = 12 and equal weights). The only analysis (k = 12) that recovers a monophyletic *Chilcacetus*, a monophyletic Squaloziphiidae including *S. emlongi* and *Y. meadi*, and *N. platyrostris* among Ziphiidae (time-calibrated tree in Fig. 26) is considered as the most convincing, considering the high level of morphological similarity between these couples of taxa (see Lambert *et al.* 2013; Lambert *et al.* 2019; this work), and further discussed here and below. The single most parsimonious tree has a consistency index (CI) of 0.15 and a retention index (RI) of 0.56, close to the values in Lambert *et al.* (2019). Both the bootstrap and Jackknife analyses yielded low support values for most nodes (only values > 50 are shown in Fig. 26). Among odontocetes, except for physeteroids, ziphiids, xenorophids, and some less inclusive delphinidan clades, higher values were only found for eurhinodelphinids (bootstrap value for the whole family of 55, and bootstrap and Jackknife values for *Eurhinodelphis cocheteuxi* + *Schizodelphis morckhoviensis* of 67 and 59, respectively. In this analysis, *A. bakersfieldensis* n. comb. is the first taxon to branch, followed by a clade including the two species of *Chilcacetus* and *M. kelloggi*, and then *Eoplatanista* and the Eurhinodelphinidae.

DISCUSSION

Because of the fragmentary state of most specimens, the systematic affinities of archaic homodont odontocetes in the genera *Argyrocetus* and *Macrodelphinus* from the Early Miocene of the northeastern Pacific and southwestern Atlantic have remained poorly understood for a long time (Lydekker 1893; Kellogg 1932; Wilson 1935; Barnes 1976; Fordyce & Muizon 2001). The description of the new species *Chilcacetus cavirhinus*, based on two more complete specimens from the Early Miocene of the East Pisco Basin, provided some

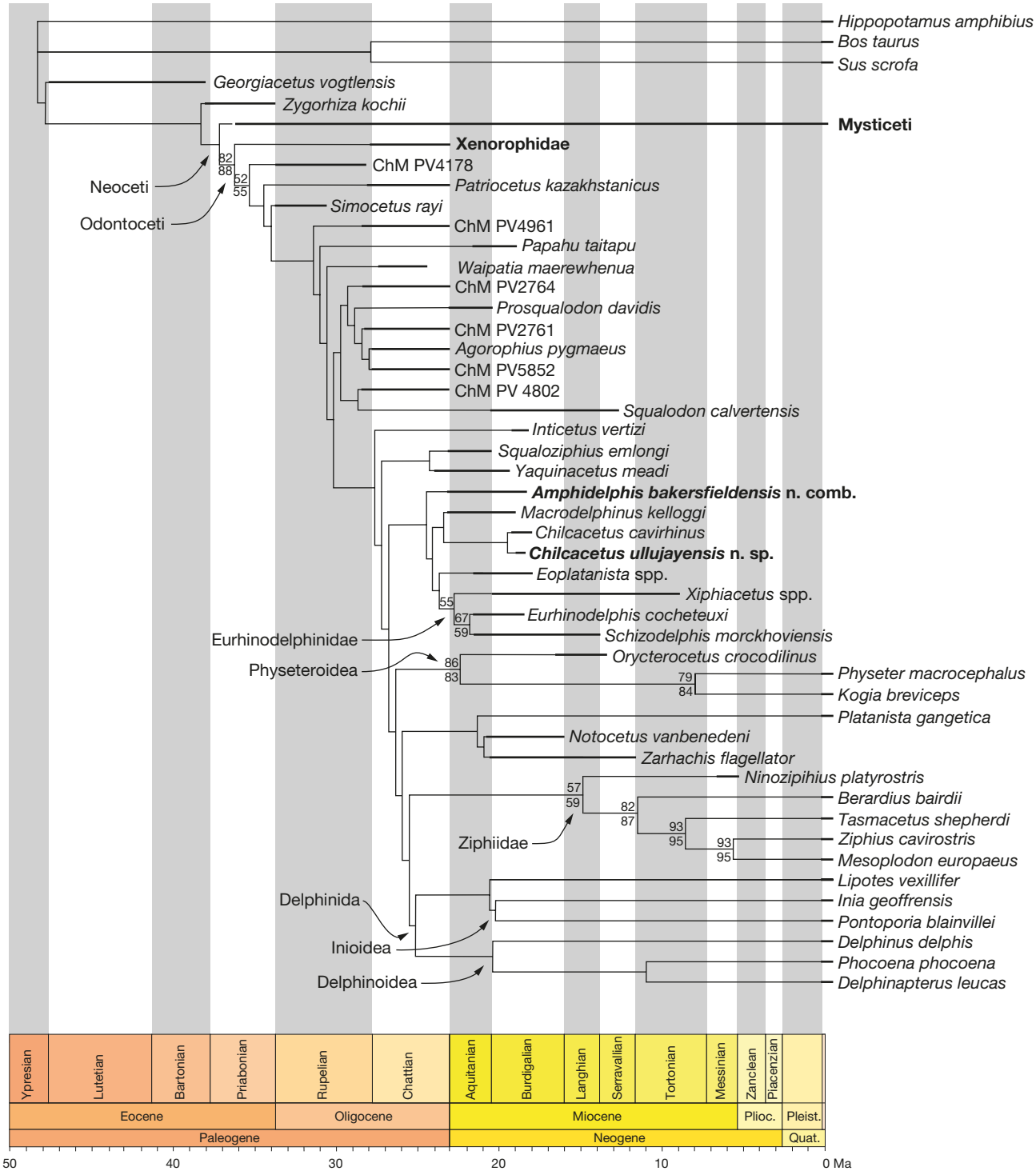

FIG. 26. — Time-calibrated single most parsimonious tree resulting from the heuristic search with implied weights (K = 12) and with a molecular constraint as a backbone, showing the phylogenetic relationships of *Amphidelphis bakersfieldensis* n. comb. and *Chilcacetus ullujayensis* n. sp. with other late-branching homodont stem odontocetes. Temporal ranges for taxa follow Bianucci & Landini (2002), Marx & Fordyce (2015), Lambert *et al.* (2017), Louwye *et al.* (2020), Lloyd & Slater (2021), Viglino *et al.* (2022), Boessenecker & Geisler (2023), Godfrey & Lambert (2023), Bianucci *et al.* (2024), and data presented in this work. Bootstrap and Jackknife support values > 50 are provided above and below nodes, respectively. Several clades (Mysticeti, Xenorophidae) were collapsed for clarity, while only a few extant delphinidan species were retained in this simplified tree (complete tree available with other trees in Appendix 9). Abbreviations: **Pleist.**, Pleistocene; **Plioc.**, Pliocene; **Quat.**, Quaternary.

clues about the existence of a clade of longirostrine dolphins, distinct from the Eurhinodelphinidae and Eoplatanistidae, in the eastern Pacific (Lambert *et al.* 2015). The description in this work of two new specimens of *Chilcacetus* from the same unit (the Chilcatay Formation) as the original material of *C. cavirhinus* leads to the diagnosis of a second, probably

geologically younger species, *Chilcacetus ullujayensis* n. sp. In addition to providing a higher-resolution chronostratigraphical setting for *Chilcacetus*, now firmly positioned in the Burdigalian (late Lower Miocene), this new material and recently prepared parts of the holotype of *C. cavirhinus* yield further anatomical information on this genus, especially for the tip of the rostrum and mandible, the postglenoid process of the squamosal, and the ear bones (including the periotic, tympanic, and malleus), all cranial regions that are critical to assess the systematics and phylogenetic relationships of early homodont odontocetes, as recently demonstrated for the squaloziphiid *Yaquinacetus meadi*, from the latest Oligocene to Early Miocene of the northeastern Pacific (Lambert *et al.* 2019).

Another smaller cranium from the Chilcatay Formation leads to the identification in the southeastern Pacific of a species previously only known from California, '*Argyrocetus*' *bakersfieldensis*, whereas two other specimens may either represent a new, closely related species, or indicate some degree of intraspecific variation. These new fossils reveal clear anatomical differences with the type species of *Argyrocetus*, *Argyrocetus patagonicus*, from the Early Miocene of the southwestern Atlantic (Lydekker 1893), especially at the level of the tip of the rostrum. These differences prompt the attribution of the Californian - Peruvian species in a new genus, making the new combination *Amphidelphis bakersfieldensis* n. comb., and confirm its exclusion from the family Eurhinodelphinidae. Furthermore, additional characters could be scored for *A. bakersfieldensis* n. comb. in our character-taxon matrix compared to a past analysis (Lambert *et al.* 2019).

As in the latter analysis, *Chilcacetus* and its relatives are recovered as stem odontocetes. The addition of two eurhinodelphinids in the character-taxon matrix results in a monophyletic Eurhinodelphinidae that is found to be closely related to *Chilcacetus*, together with *Eoplatanista* and *Macrodelphinus kelloggi*. However, the new scores for *A. bakersfieldensis* n. comb. place the latter outside the *Chilcacetus* clade sensu Lambert *et al.* (2019), sister to a larger clade also including *Eoplatanista* spp. and Eurhinodelphinidae. This result also differs from the first phylogenetic assessment of *Chilcacetus*, in which *A. bakersfieldensis* n. comb. was found as sister group to *C. cavirhinus*, but using a much smaller number of characters and taxa (Lambert *et al.* 2015). It can be noted that a sister group relationship between *Eoplatanista* and Eurhinodelphinidae has been proposed previously, in the superfamily Eurhinodelphinoidea Muizon, 1988 (Muizon 1988a, 1991 *contra* Lambert *et al.* 2015). While squaloziphiids form an earlier branching clade in our preferred tree (K = 12), in the equal weights tree they are more crownward, as in Lambert *et al.* (2019), but not making a clade as in the latter. Our analyses are more difficult to compare with the ones of Gaetán *et al.* (2023), as the latter did not use a molecular tree as a constraint. However, part of the analyses from this work (equal weights and K = 75) recover a clade containing *Chilcacetus cavirhinus*, the eurhinodelphinid *Xiphiacetus bossi*, and squaloziphiids (including *Crisocetus lydekkeri*, *S. emlongii*, and *Y. meadi*), a result that only partly matches our preferred tree.

Low support values (both bootstrap and Jackknife) for a majority of the nodes urge for remaining cautious with the interpretation of the obtained topologies. More complete specimens and/or a reassessment of the type material will be needed to analyze the relationships of *A. patagonicus* and of the third species previously attributed to the genus *Argyrocetus*, '*Argyrocetus*' *joaquinensis*. The addition in future phylogenetic analyses of the probable squaloziphiids *Crisocetus lydekkeri* and *Dolgopolis kinchikafiforo*, as well as of *Perditicetus yaconensis*, also sharing cranial similarities with the taxa described here, will also help to further test their relationships with *Chilcacetus* and its relatives. Finally, the systematic reassessment of poorly known taxa for which affinities with eurhinodelphinids have already been proposed, for example *Iniopsis caucasica* Lydekker, 1892, from the ?late Oligocene of Azerbaijan (Mchedlidze 1976; Muizon 1991; Lambert 2005a), could reveal early members of the clade which includes amongst others *Chilcacetus*, *Eoplatanista*, and Eurhinodelphinidae.

From a palaeobiogeographic viewpoint, similarities have been previously noted between odontocete assemblages from the Late Miocene of Baja California (Mexico) and California (United States) and assemblages from the East Pisco and Sacaco basins (Peru). An early delphinidan *Atocetus nasalis* (Barnes, 1985) and two phocoenids *Piscolithax boreios* Barnes, 1984 and *Piscolithax tedfordi* Barnes, 1984 from the northeastern Pacific are congeneric with southeastern Pacific species *Atocetus iquensis* Muizon, 1988 and *Piscolithax longirostris* Muizon, 1983 (Barnes 1984, 1985; Muizon 1984, 1988b; Velez-Juarbe & Valenzuela-Toro 2019; Parham *et al.* 2022), indicating several dispersal events across the equator during the Late Miocene. Similarities were also recently noted between odontocete assemblages from the Late Miocene of Panama and from Peru and Chile, with records of the phocoenid *Piscolithax* sp. and the physeteroids cf. *Acrophyseter* sp. and Scaphokogiinae indet. from the Chagres Formation in Panama, providing new clues for such dispersal events (Benites-Palomino *et al.* 2023). The record of *Amphidelphis bakersfieldensis* n. comb. in both California and Peru points to similar faunal exchanges, but much earlier, during the Early Miocene. Interestingly, recently described squaloziphiid-like odontocetes (*Crisocetus lydekkeri* and, more tentatively, *Dolgopolis kinchikafiforo*) from the Early Miocene of Patagonia (Viglino *et al.* 2021; Gaetán *et al.* 2023) also suggest faunal similarities between the northeastern Pacific (with *Squaloziphius emlongi* and *Yaquinacetus meadi*) and the southwestern Atlantic odontocete assemblages at that time. Further fossil discoveries and comparisons between these three fossil-rich regions may reveal additional faunal links (e.g., Lambert *et al.* 2023).

Combined with the recent description of multiple longirostrine to hyper-longirostrine species from various odontocete clades (Eurhinodelphinidae, Inticetidae, stem Physeteroidea Gray, 1821, and Platanidelphidi Bianucci, Muizon, Urbina & Lambert, 2020; Lambert *et al.* 2018, 2020, 2021; Bianucci *et al.* 2020) from the Chilcatay Formation, the new records of *A. bakersfieldensis* n. comb. and *Chilcacetus* spp. confirm the predominance of these long-snouted species in the East Pisco

Basin during the Burdigalian. The Chilcatay Formation was deposited in a marginal marine, warm to temperate, sheltered embayment connected with both riverine and open-ocean environments (Bianucci *et al.* 2018; Di Celma *et al.* 2018; Bianucci & Collareta 2022). Such a setting may have represented a favorable environment for these dolphins, as seen nowadays for the longirostrine dolphin *Pontoporia blainvillei* (Gervais & d'Orbigny, 1844) along the eastern coast of South America (Brownell 1989). A detailed comparison with other odontocete-rich Early Miocene units worldwide (e.g. the Libano Sandstone in Italy, the lower part of the Calvert Formation along the U.S. east coast, and the Gaiman and Monte Leon formations in Argentinian Patagonia; Pilleri 1985; Bianucci & Landini 2002; Viglino *et al.* 2019; Godfrey & Lambert 2023; Gaetán *et al.* 2023) could help identifying common traits and differences in toothed whale assemblages and local ecological/environmental settings.

Acknowledgements
We would like to thank Walter Aguirre, Joan Chauca-Luyo, Manuel Martínez-Cáceres, Rodolfo Salas-Gismondi, Julia Tejada, and Rafael Varas-Malca for their invaluable help during fieldwork, Walter Aguirre and Eusebio Diaz for the preparation of the studied fossil specimens, Giulia Bosio, Alberto Collareta, Claudio Di Celma, and Elisa Malinverno for the many stimulating discussions on the geological and chronostratigraphic context of the fossil localities from the East Pisco Basin, Advait M. Jukar (YPM) for generously providing photos of YPM 13406, Rachel A. Racicot for helping us contacting A. M. Jukar, Philippe Loubry and Lilian Cazes (MNHN) for taking new photos of MNHN.F.PRU11, and Ellen J. Coombs for kindly allowing us to use the 3D model of the cranium MUSM 1401. We also thank the following persons for providing access to the collections under their care and helping us in many ways during our visits: Ali J. Altamirano, Aldo Benites-Palomino, Rodolfo Salas-Gismondi, and Rafael Varas-Malca (MUSM), Larry G. Barnes and Vanessa R. Rhue (LACM), Dave J. Bohaska, James G. Mead, John J. Ososky, and Charles W. Potter (USNM), Mariagabriella Fornasiero and Letizia Del Favoro (MGP), Marcello A. Reguero (MLP), Sébastien Bruaux, Cecilia Cousin, Annelise Folie, and Olivier Pauwels (IRSNB), and the late R. Ewan Fordyce (OU). In addition to his many other contributions to cetacean palaeontology, Ewan will also be remembered for having rightly (and tactfully) pointed out at a conference the lack of precision of the stratigraphic framework in the initial description of *Chilcacetus*. Finally, we wish to thank the two reviewers, Toshiyuki Kimura and Jorge Velez-Juarbe, for their constructive comments and useful suggestions.

The research of GB in Peru has received financial support from the European Union – NextGenerationEU, Mission 4, Component 2 CUP I53D23002070 006. Project title: BIOVERTICES (BIOdiversity of VERTebrates in the Cenozoic Sea). The trip of RB to the MUSM in Lima was funded by the Stan Wood Award from the Palaeontological Association.

REFERENCES

Abel O. 1931. — Das skelett von *Eurhinodelphis cocheteuxi* aus dem Obermiozän von Antwerpen. *Mémoires du Musée Royal d'Histoire Naturelle de Belgique* 48: 191-334.

Barnes L. G. 1976. — Outline of eastern North Pacific fossil cetacean assemblages. *Systematic Zoology* 25 (4): 321-343. https://doi.org/10.2307/2412508

Barnes L. G. 1984. — Fossil odontocetes (Mammalia: Cetacea) from the Almejas Formation, Isla Cedros, Mexico. *PaleoBios* 42: 1-46.

Barnes L. G. 1985. — The Late Miocene dolphin *Pithanodelphis* Abel, 1905 (Cetacea, Kentriodontidae) from California. *Los Angeles County Museum Contributions in Science* 367: 1-27.

Benites-Palomino A., Vélez-Juarbe J., De Gracia C. & Jaramillo C. 2023. — Bridging two oceans: small toothed cetaceans (Odontoceti) from the Late Miocene Chagres Formation, eastern Caribbean (Colon, Panama). *Biology Letters* 19 (6): 20230124. https://doi.org/10.1098/rsbl.2023.0124

Bianucci G. & Collareta A. 2022. — An overview of the fossil record of cetaceans from the East Pisco Basin (Peru). *Bollettino della Società Paleontologica Italiana* 61 (1): 19-20. https://doi.org/10.4435/BSPI.2022.04

Bianucci G. & Landini W. 2002. — Change in diversity, ecological significance and biogeographical relationships of the Mediterranean Miocene toothed whale fauna. *Geobios* 35 (mémoire spécial 24): 19-28. https://doi.org/10.1016/S0016-6995(02)00045-1

Bianucci G., Lambert O. & Post K. 2007. — A high diversity in fossil beaked whales (Odontoceti, Ziphiidae) recovered by trawling from the sea floor off South Africa. *Geodiversitas* 29 (4): 5-62.

Bianucci G., Lambert O. & Post K. 2010. — High concentration of long-snouted beaked whales (genus *Messapicetus*) from the Miocene of Peru. *Palaeontology* 53 (5): 1077-1098. https://doi.org/10.1111/j.1475-4983.2010.00995.x

Bianucci G., Mijáin I., Lambert O., Post K. & Mateus O. 2013. — Bizarre fossil beaked whales (Odontoceti, Ziphiidae) fished from the Atlantic Ocean floor off the Iberian Peninsula. *Geodiversitas* 35 (1): 105-153. https://doi.org/10.5252/g2013n1a6

Bianucci G., Collareta A., Bosio G., Landini W., Gariboldi K., Gioncada A., Lambert O., Malinverno E., Muizon C. de, Varas-Malca R., Villa I. M., Coletti G., Urbina M. & Di Celma C. 2018. — Taphonomy and palaeoecology of the lower Miocene marine vertebrate assemblage of Ullujaya (Chilcatay Formation, East Pisco Basin, southern Peru). *Palaeogeography, Palaeoclimatology, Palaeoecology* 511: 256-279. https://doi.org/10.1016/j.palaeo.2018.08.013

Bianucci G., Muizon C. de, Urbina M. & Lambert O. 2020. — Extensive diversity and disparity of the Early Miocene platanistoids (Cetacea, Odontoceti) in the southeastern Pacific (Chilcatay Formation, Peru). *Life* 10 (3): 27. https://doi.org/10.3390/life10030027

Bianucci G., Benites-Palomino A., Collareta A., Bosio G., Muizon C. de, Merella M., Di Celma C., Malinverno E., Urbina M. & Lambert O. 2024. — A new Late Miocene beaked whale (Cetacea, Odontoceti) from the Pisco Formation, and a revised age for the fossil Ziphiidae of Peru. *Bollettino della Società Paleontologica Italiana* 63 (1): 21-43. https://doi.org/10.4435/BSPI.2024.10

Boessenecker R. W. & Geisler J. H. 2023. — New skeletons of the ancient dolphin *Xenorophus sloanii* and *Xenorophus simplicidens* sp. nov. (Mammalia, Cetacea) from the Oligocene of South Carolina and the ontogeny, functional anatomy, asymmetry, pathology, and evolution of the earliest Odontoceti. *Diversity* 15 (11): 1154. https://doi.org/10.3390/d15111154

Bosio G., Malinverno E., Collareta A., Di Celma C., Gioncada A., Parente M., Berra F., Marx F. G., Vertino A., Urbina M. & Bianucci G. 2020a. — Strontium Isotope Stratigraphy and the thermophilic fossil fauna from the middle Miocene of the East Pisco Basin (Peru). *Journal of South American Earth Sciences* 97: 102399. https://doi.org/10.1016/j.jsames.2019.102399

Bosio G., Malinverno E., Villa I. M., Di Celma C., Gariboldi K., Gioncada A., Barberini B., Urbina M. & Bianucci G. 2020b. — Tephrochronology and chronostratigraphy of the Miocene Chilcatay and Pisco formations (East Pisco Basin, Peru). *Newsletters on Stratigraphy* 53 (2): 213-247. https://doi.org/10.1127/nos/2019/0525

Bosio G., Bianucci G., Collareta A., Landini W., Urbina M. & Di Celma C. 2022. — Ultrastructure, composition, and $^{87}Sr/^{86}Sr$ dating of shark teeth from lower Miocene sediments of southwestern Peru. *Journal of South American Earth Sciences* 118: 103909. https://doi.org/10.1016/j.jsames.2022.103909

Brownell R. L. Jr 1989. — Franciscana *Pontoporia blainvillei* (Gervais and d'Orbigny, 1844), *in* Ridgway S. H. & Harrison R. (eds), *Handbook of marine mammals, vol. 4: River dolphins and the larger toothed whales*. Academic Press, London: 45-67.

Cabrera A. 1926. — Cetaceos fosiles del Museo de La Plata. *Revista del Museo de La Plata* 29: 363-411.

Di Celma C., Malinverno E., Collareta A., Bosio G., Gariboldi K., Lambert O., Landini W., Pierantoni P. P., Gioncada A. & Villa I. 2018. — Facies analysis, stratigraphy and marine vertebrate assemblage of the lower Miocene Chilcatay Formation at Ullujaya (Pisco basin, Peru). *Journal of Maps* 14 (2): 257-268. https://doi.org/10.1080/17445647.2018.1456490

Di Celma C., Pierantoni P. P., Malinverno E., Collareta A., Lambert O., Landini W., Bosio G., Gariboldi K., Gioncada A., De Muizon C., Molli G., Marx F. G., Varas-Malca R. M., Urbina M. & Bianucci G. 2019. — Allostratigraphy and paleontology of the lower Miocene Chilcatay Formation in the Zamaca area, East Pisco basin, southern Peru. *Journal of Maps* 15 (2): 393-405. https://doi.org/10.1080/17445647.2019.1604439

Evans H. E. & Lahunta A. de 2013. — *Miller's anatomy of the dog. Fourth edition*. Elsevier Saunders, St. Louis, 850 p.

Fordyce R. E. 1994. — *Waipatia maerewhenua*, new genus and new species (Waipatiidae, new family), an archaic late Oligocene dolphin from New Zealand, *in* Berta A. & Deméré T. A. (eds), Contributions in marine mammal paleontology honoring Frank C. Whitmore, Jr. *Proceedings of the San Diego Society of Natural History* 29: 147-178. https://www.biodiversitylibrary.org/page/2888017

Fordyce R. E. 2002. — *Simocetus rayi* (Odontoceti: Simocetidae) (new species, new genus, new family), a bizarre new archaic Oligocene dolphin from the eastern North Pacific. *Smithsonian Contributions to Paleobiology* 93: 185-222. https://doi.org/10.5479/si.00810266.93.185

Fordyce R. E. & Muizon C. de 2001. — Evolutionary history of cetaceans: a review, *in* Mazin J.-M. & Buffrénil V. de (eds), *Secondary adaptation of tetrapods to life in water*. Verlag Dr. Friedrich Pfeil, München: 169-233.

Gaetán C. M., Paolucci F. & Buono M. R. 2023. — A new squaloziphiid-like odontocete from the Early Miocene of Patagonia expands the cetacean diversity in the southwestern Atlantic Ocean. *Journal of Vertebrate Paleontology* 42 (6): e2232425. https://doi.org/10.1080/02724634.2023.2232425

Galatius A. & Kinze C. C. 2003. — Ankylosis patterns in the postcranial skeleton and hyoid bones of the harbour porpoise (*Phocoena phocoena*) in the Baltic and North Sea. *Canadian Journal of Zoology* 81 (11): 1851-1861. https://doi.org/10.1139/z03-181

Geisler J. H. & Sanders A. E. 2003. — Morphological evidence for the phylogeny of Cetacea. *Journal of Mammalian Evolution* 10 (1-2): 23-129. https://doi.org/10.1023/A:1025552007291

Geisler J. H., Mcgowen M. R., Yang G. & Gatesy J. 2011. — A supermatrix analysis of genomic, morphological, and paleontological data for crown Cetacea. *BMC Evolutionary Biology* 11 (112): 1-22. https://doi.org/10.1186/1471-2148-11-112

Godfrey S. J. & Lambert O. 2023. — Miocene toothed whales (Odontoceti) from Calvert Cliffs, Atlantic Coastal Plain, USA, *in* Godfrey S. J. (ed.), *The Geology and Vertebrate Paleontology of Calvert Cliffs, Maryland, USA*. Vol. 107. Smithsonian Contributions to Paleobiology, Washington, DC, USA: 49-186.

Kellogg R. 1925. — On the occurrence of remains of fossil porpoises of the genus *Eurhinodelphis* in North America. *Proceedings of the United States National Museum* 66 (26): 1-40.

Kellogg R. 1932. — A Miocene long-beaked porpoise from California. *Smithsonian Miscellaneous Collections* 87 (2): 1-11.

Kimura T. & Barnes L. G. 2016. — New Miocene fossil Allodelphinidae (Cetacea, Odontoceti, Platanistoidea) from the North Pacific Ocean. *Bulletin of the Gunma Museum of Natural History* 20: 1-58.

Lambert O. 2005a. — Review of the Miocene long-snouted dolphin *Priscodelphinus cristatus* du Bus, 1872 (Cetacea, Odontoceti) and phylogeny among eurhinodelphinids. *Bulletin de l'Institut royal des Sciences naturelles de Belgique, Sciences de la Terre* 75: 211-235.

Lambert O. 2005b. — Phylogenetic affinities of the long-snouted dolphin *Eurhinodelphis* (Cetacea, Odontoceti) from the Miocene of Antwerp. *Palaeontology* 48 (3): 653-679. https://doi.org/10.1111/j.1475-4983.2005.00472.x

Lambert O. & Goolaerts S. 2022. — Late Miocene survival of a hyper-longirostrine dolphin and the Neogene to Recent evolution of rostrum proportions among odontocetes. *Journal of Mammalian Evolution* 29: 99-111. https://doi.org/10.1007/s10914-021-09573-6

Lambert O., Muizon C. de & Bianucci G. 2013. — The most basal beaked whale *Ninoziphius platyrostris* Muizon, 1983: clues on the evolutionary history of the family Ziphiidae (Cetacea: Odontoceti). *Zoological Journal of the Linnean Society* 167 (4): 569-598. https://doi.org/10.1111/zoj.12018

Lambert O., Muizon C. de & Bianucci G. 2015. — A new archaic homodont toothed whale (Mammalia, Cetacea, Odontoceti) from the early Miocene of Peru. *Geodiversitas* 37 (1): 79-108. https://doi.org/10.5252/g2015n1a4

Lambert O., Martínez-Cáceres M., Bianucci G., Di Celma C., Salas-Gismondi R., Steurbaut E., Urbina M. & Muizon C. de 2017. — Earliest mysticete from the Late Eocene of Peru sheds new light on the origin of baleen whales. *Current Biology* 27 (10): 1535-1541. https://doi.org/10.1016/j.cub.2017.04.026

Lambert O., Muizon C. de, Malinverno E., Di Celma C., Urbina M. & Bianucci G. 2018. — A new odontocete (toothed cetacean) from the Early Miocene of Peru expands the morphological disparity of extinct heterodont dolphins. *Journal of Systematic Palaeontology* 16 (12): 981-1016. https://doi.org/10.1080/14772019.2017.1359689

Lambert O., Godfrey S. J. & Fitzgerald E. M. G. 2019. — *Yaquinacetus meadi*, a new latest Oligocene–early Miocene dolphin (Cetacea, Odontoceti, Squaloziphiidae, fam. nov.) from the Nye Mudstone (Oregon, USA). *Journal of Vertebrate Paleontology* 38 (6): e1559174. https://doi.org/10.1080/02724634.2018.1559174

Lambert O., Muizon C. de, Urbina M. & Bianucci G. 2020. — A new longirostrine sperm whale (Cetacea, Physeteroidea) from the lower Miocene of the Pisco Basin (southern coast of Peru). *Journal of Systematic Palaeontology* 18 (20): 1707-1742. https://doi.org/10.1080/14772019.2020.1805520

Lambert O., Muizon C. de, Varas-Malca R. M., Urbina M. & Bianucci G. 2021. — Eurhinodelphinids from the early Miocene of Peru: first unambiguous records of these hyper-longirostrine dolphins outside the North Atlantic realm. *Rivista Italiana di Paleontologia e Stratigrafia* 127 (1): 17-32. https://doi.org/10.13130/2039-4942/15124

Lambert O., Collareta A., Benites-Palomino A., Merella M., Muizon C. de, Bennion R., Urbina M. & Bianucci G. 2023. — A new platyrostrine sperm whale from the Early Miocene of the southeastern Pacific (East Pisco Basin, Peru) supports affinities with the southwestern Atlantic cetacean fauna. *Geodiversitas* 45 (22): 659-679. https://doi.org/10.5252/geodiversitas2023v45a22

Lloyd G. T. & Slater G. J. 2021. — A total-group phylogenetic metatree for Cetacea and the importance of fossil data in diversification analyses. *Systematic Biology* 70 (5): 922-939. https://doi.org/10.1093/sysbio/syab002

LOUWYE S., DECKERS J., VERHAEGEN J., ADRIAENS R. & VANDENBERGHE N. 2020. — A review of the lower and middle Miocene of northern Belgium. *Geologica Belgica* 23 (3-4): 137-156. https://doi.org/10.20341/gb.2020.010

LYDEKKER R. 1893. — Contribution to the knowledge of the fossil vertebrates of Argentina. Part II. Cetacean skulls from Patagonia. *Anales del Museo de La Plata* 1893: 1-14.

MARX F. G. & FORDYCE R. E. 2015. — Baleen boom and bust: a synthesis of mysticete phylogeny, diversity and disparity. *Royal Society Open Science* 2 (4): 140434. https://doi.org/10.1098/rsos.140434

MARX F. G., HOCKING D. P., PARK T., POLLOCK T. I., PARKER W. M., RULE J. P., FITZGERALD E. M. & EVANS A. R. 2023. — Suction causes novel tooth wear in marine mammals, with implications for feeding evolution in baleen whales. *Journal of Mammalian Evolution* 30: 1-13. https://doi.org/10.1007/s10914-022-09645-1

MCCURRY M. R. & PYENSON N. D. 2019. — Hyper-longirostry and kinematic disparity in extinct toothed whales. *Paleobiology* 45 (1): 21-29. https://doi.org/10.1017/pab.2018.33

MCGOWEN M. R., SPAULDING M. & GATESY J. 2009. — Divergence date estimation and a comprehensive molecular tree of extant cetaceans. *Molecular Phylogenetics and Evolution* 53 (3): 891-906. https://doi.org/10.1016/j.ympev.2009.08.018

MCGOWEN M. R., MONTGOMERY S. H., CLARK C. & GATESY J. 2011. — Phylogeny and adaptive evolution of the brain-development gene microcephalin (MCPH1) in cetaceans. *BMC Evolutionary Biology* 11 (1): 1. https://doi.org/10.1186/1471-2148-11-98

MCHEDLIDZE G. A. 1976. — *General features of the palaeobiological evolution of cetacea. {Osnovnye Cherty Paleobiologicheskoi Istorii Kitoobraznykh}*. Metsniereba Publishers, translated from Russian in 1984 by Amerind Publishing Co. Pvt. Ltd., New Delhi, Tbilisi, 139 p.

MEAD J. G. & FORDYCE R. E. 2009. — The therian skull: a lexicon with emphasis on the odontocetes. *Smithsonian Contributions to Zoology* 627: 1-248. https://doi.org/10.5479/si.00810282.627

MORAN M. M., BAJPAI S., GEORGE J. C., SUYDAM R., USIP S. & THEWISSEN J. G. M. 2015. — Intervertebral and epiphyseal fusion in the postnatal ontogeny of cetaceans and terrestrial mammals. *Journal of Mammalian Evolution* 22 (1): 93-109. https://doi.org/10.1007/s10914-014-9256-7

MUIZON C. DE 1984. — Les vertébrés de la Formation Pisco (Pérou). Deuxième partie: Les Odontocètes (Cetacea, Mammalia) du Pliocène inférieur de Sud-Sacaco. *Travaux de l'Institut Français d'Etudes Andines* 27: 1-188.

MUIZON C. DE 1988a. — Le polyphylétisme des Acrodelphidae, odontocètes longirostres du Miocène européen. *Bulletin du Muséum national d'Histoire naturelle, Paris* 10 (1): 31-88.

MUIZON C. DE 1988b. — Les vertébrés fossiles de la Formation Pisco (Pérou). Troisième partie: Les Odontocètes (Cetacea, Mammalia) du Miocène. *Travaux de l'Institut Français d'Etudes Andines* 42: 1-244.

MUIZON C. DE 1991. — A new Ziphiidae (Cetacea) from the Early Miocene of Washington State (USA) and phylogenetic analysis of the major groups of odontocetes. *Bulletin du Muséum national d'Histoire naturelle, Paris* 12: 279-326.

NELSON M. D. & UHEN M. D. 2020. — A new platanistoid, *Perditicetus yaconensis* gen. et sp. nov. (Cetacea, Odontoceti), from the Chattian–Aquitanian Nye Formation of Oregon. *Journal of Systematic Palaeontology* 18 (18): 1497-1517. https://doi.org/10.1080/14772019.2020.1783379

PARHAM J. F., BARRON J. A. & VELEZ-JUARBE J. 2022. — Middle and late Miocene marine mammal assemblages from the Monterey Formation of Orange County, California, *in* AIELLO I., BARRON J. & RAVELO C. (eds), Understanding the Monterey Formation and Similar Biosiliceous Units across Space and Time. *The Geological Society of America Special Paper* 556: 1-14. https://doi.org/10.1130/2021.2556(10)

PILLERI G. 1985. — The Miocene Cetacea of the Belluno sandstones (eastern southern Alps). *Memorie di Scienze Geologiche* 36: 1-87.

RAMASSAMY B., LAMBERT O., COLLARETA A., URBINA M. & BIANUCCI G. 2018. — Description of the skeleton of the fossil beaked whale *Messapicetus gregarius*: searching potential proxies for deep-diving abilities. *Fossil Record* 21 (1): 11-32. https://doi.org/10.5194/fr-21-11-2018

ROSTON R., BOESSENECKER R. & GEISLER J. 2023. — Evolution and development of the cetacean skull roof: a case study in novelty and homology. *Philosophical Transactions of the Royal Society B* 378 (1880): 20220086. https://doi.org/10.1098/rstb.2022.0086

SHIMADA K., WELTON B. J. & LONG D. J. 2014. — A new fossil megamouth shark (Lamniformes, Megachasmidae) from the Oligocene-Miocene of the western United States. *Journal of Vertebrate Paleontology* 34 (2): 281-290. https://doi.org/10.1080/02724634.2013.803975

SWOFFORD D. L. 2003. — *PAUP*. Phylogenetic analysis using parsimony (*and other methods). Version 4*. Sinauer Associates, Sunderland, Massachusetts.

TANAKA Y. & FORDYCE R. E. 2015. — A new Oligo-Miocene dolphin from New Zealand: *Otekaikea huata* expands diversity of the early Platanistoidea. *Palaeontologia Electronica* 18 (2): 1-71. https://doi.org/10.26879/518

VELEZ-JUARBE J. 2023. — New heterodont odontocetes from the Oligocene Pysht Formation in Washington State, USA, and a reevaluation of Simocetidae (Cetacea, Odontoceti). *PeerJ* 11: e15576. https://doi.org/10.7717/peerj.15576

VELEZ-JUARBE J. & VALENZUELA-TORO A. M. 2019. — Oldest record of monk seals from the North Pacific and biogeographic implications. *Biology Letters* 15 (5): 20190108. https://doi.org/10.1098/rsbl.2019.0108

VIGLINO M., BUONO M. R., FORDYCE R. E., CUITIÑO J. I. & FITZGERALD E. M. G. 2019. — Anatomy and phylogeny of the large shark-toothed dolphin *Phoberodon arctirostris* Cabrera, 1926 (Cetacea: Odontoceti) from the early Miocene of Patagonia (Argentina). *Zoological Journal of the Linnean Society* 185 (2): 511-542. https://doi.org/10.1093/zoolinnean/zly053

VIGLINO M., GAETÁN C. M., CUITIÑO J. I. & BUONO M. R. 2021. — First toothless platanistoid from the early Miocene of Patagonia: the golden age of diversification of the Odontoceti. *Journal of Mammalian Evolution* 28: 337-358. https://doi.org/10.1007/s10914-020-09505-w

VIGLINO M., BUONO M. R., TANAKA Y., CUITIÑO J. I. & FORDYCE R. E. 2022. — Unravelling the identity of the platanistoid *Notocetus vanbenedeni* Moreno, 1892 (Cetacea, Odontoceti) from the early Miocene of Patagonia (Argentina). *Journal of Systematic Palaeontology* 20 (1): 2082890. https://doi.org/10.1080/14772019.2022.2082890

WILSON L. E. 1935. — Miocene marine mammals from the Bakersfield region, California. *Bulletin of the Peabody Museum of Natural History* 4: 1-143.

Submitted on 22 April 2024;
accepted on 21 October 2024;
published on 5 June 2025.

APPENDICES

Appendix 1. — Textured 3D model of the cranium of *Chilcacetus cavirhinus* MUSM 4692, available at: https://doi.org/10.7934/P5641

Appendix 2. — Textured 3D model of the cranium of *Chilcacetus ullujayensis* n. sp. MUSM 2527, available at: https://doi.org/10.7934/P5641

APPENDIX 3. — 3D model of the cranium of Chilcacetus *ullujayensis* n. sp. MUSM 1401, available at: https://doi.org/10.7934/P5641

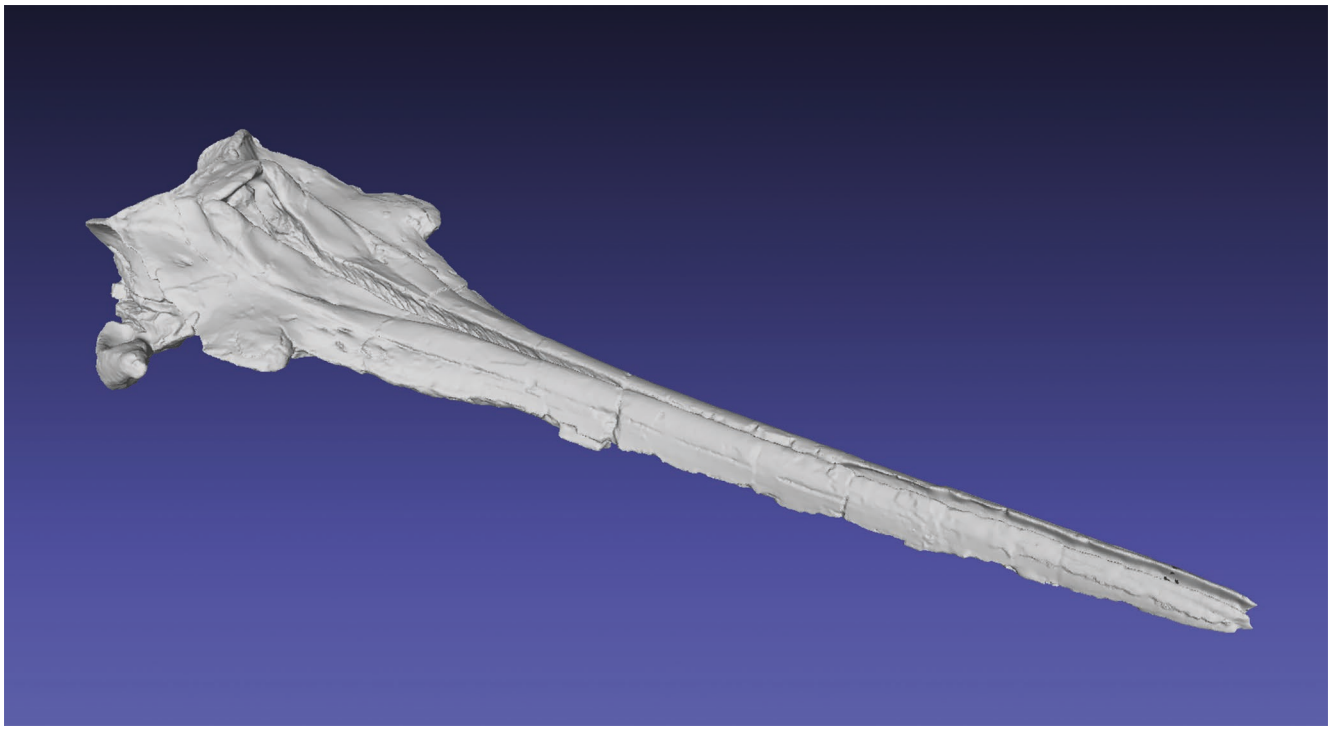

APPENDIX 4. — Textured 3D model of the cranium of *Amphidelphis bakersfieldensis* n. comb. MUSM 4691, available at: https://doi.org/10.7934/P5641

Appendix 5. — Textured 3D model of the cranium of Odontoceti aff. *Amphidelphis bakersfieldensis* MUSM 602, available at: https://doi.org/10.7934/P5641

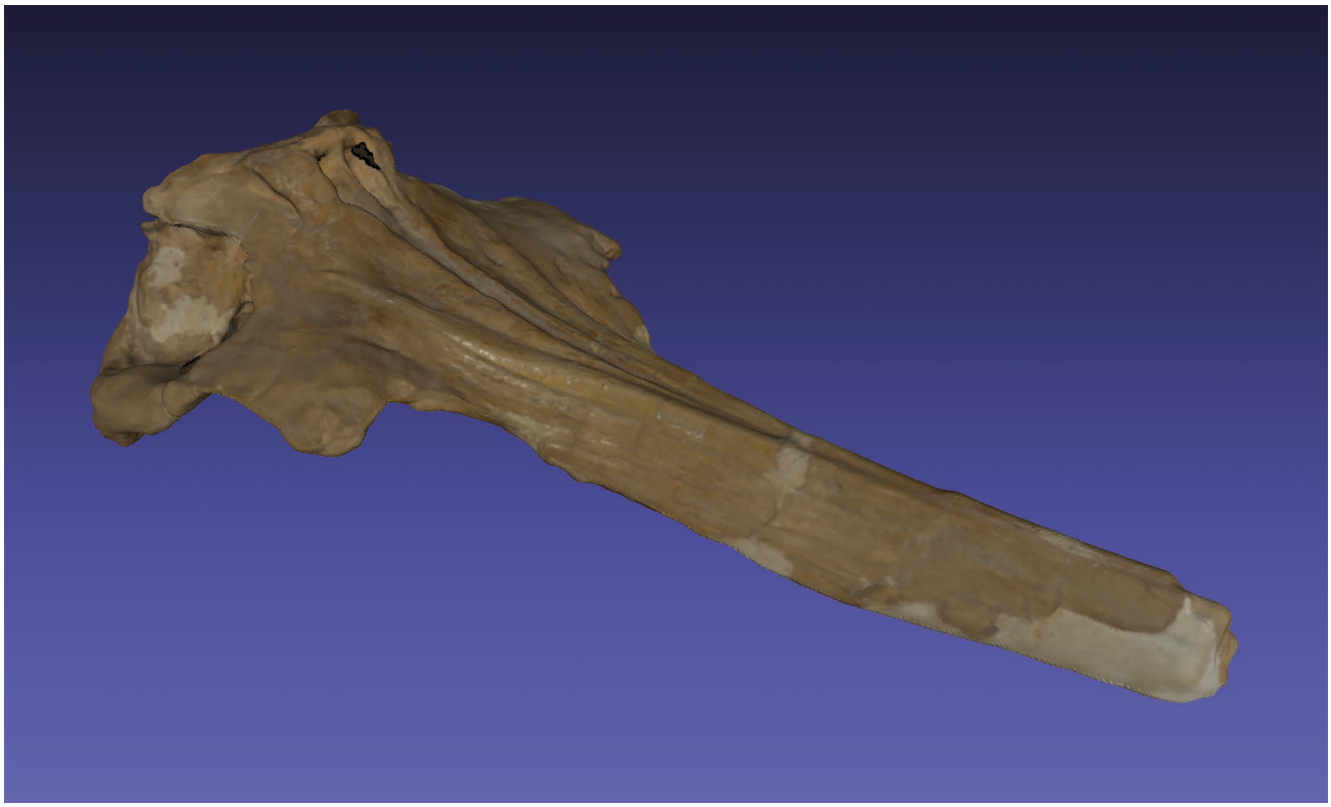

Appendix 6. — List of characters used in the phylogenetic analyses, modified from Lambert *et al.* (2019). Modified and new characters are **highlighted in yellow and red**, respectively, available at: https://doi.org/10.7934/P5641

Appendix 7. — Character-taxon matrix (nexus file), modified from Lambert *et al.* (2019). New taxa and taxa for which multiple scores were modified are **highlighted in red**, available on Morphobank (Project 5641): https://doi.org/10.7934/P5641

Appendix 8. — Constraint tree from Bayesian analysis of molecular data applied as a backbone for the phylogenetic analyses, based on (McGowen *et al.* 2009, 2011; Geisler *et al.* 2011), available at: https://doi.org/10.7934/P5641

Appendix 9. — Single most parsimonious tree or strict consensus tree resulting from the heuristic search with different settings, namely equal weights and implied weights with K = 3, 6, 9, and 12, available at: https://doi.org/10.7934/P5641